UNIVERSITY OF CALIFORNIA SAN DIEGO

Apoptotic DNase DFFB Mediates Cancer Acquired Drug Resistance

A Dissertation submitted in partial satisfaction of the requirements
for the degree Doctor of Philosophy

in

Biomedical Sciences

by

August Williams

Committee in charge:

Professor Matthew Hangauer, Chair
Professor Frank Furnari
Professor J. Silvio Gutkind
Professor Emily Wang
Professor Jean Wang

2023

The Dissertation of August Williams is approved, and it is acceptable in quality and form for publication on microfilm and electronically.

University of California San Diego

2023

DEDICATION

This dissertation is dedicated to all my current and previous mentors and peers. I am constantly inspired and motivated by your hard work and dedication.

TABLE OF CONTENTS

LIST OF FIGURES

LIST OF TABLES

LIST OF ABBREVIATIONS

6-TG	6-thioguanine
ATM	Ataxia-telangiectasia mutated
BET	Bromodomain and extraterminal [proteins]
CAD	Caspase-activated DNase
DDR	DNA damage response
DFFA	DNA fragmentation factor A
DFFB	DNA fragmentation factor B
DTEP	Drug-tolerant expanded persister
EMT	Epithelial-to-mesenchymal transition
H3K9me3	Tri-methylation of H3 lysine 9
HDAC	Histone deacetylase
HPRT	Hypoxanthine-guanine phosphoribosyltransferase
IAP	Inhibitor of apoptosis
ICAD	Inhibitor of CAD
IFNγ	Interferon gamma
KO	Knockout
MOMP	Mitochondrial outer membrane permeabilization
PRMT	Protein arginine methyltransferase
QVD	Quinoline-Val-Asp-Difluorophenoxymethylketone
scRNAseq	Single cell RNA sequencing
STING	Stimulator of interferon genes
TNF	Tumor necrosis factor

TRAIL	TNF-related apoptosis-inducing ligand
WES	Whole exome sequencing
WT	Wild type

ACKNOWLEDGEMENTS

I would first and foremost like to thank my thesis advisor, Dr. Matthew Hangauer, for all his guidance, advice, and patience during my graduate studies. I have greatly benefited from all the training he provided and would not be the scientist I am today without his mentorship. I appreciate the great example he set both inside and outside the lab, and I greatly look forward to any future collaborations. I would also like to thank my SPAC advisor and committee member Dr. Jean Wang for her continued advice through all stages of my graduate school training, including helpful meetings during my time on the Cancer Biology and Informatics and Omics training grant and during my many fellowship application attempts. I greatly appreciate all the support from my thesis committee, Dr. Jean Wang, Dr. J. Silvio Gutkind, Dr. Frank Furnari, and Dr. Shizhen Wang, for their useful insights, helpful discussions, assistance with fellowship applications, and letters of recommendation throughout the years. Your motivation and encouragement were extremely beneficial during my graduate studies. I would also like the many Hangauer lab members throughout the years who not only greatly contributed towards making this project a success, but also made spending time in lab enjoyable, exciting, and fun.

I would also like to thank my past mentors for believing in me, investing time and energy into my training, and for giving me a chance to work in your groups. Thank you for being upstanding people, and for setting a positive example in both life and science. Specifically, Dr. David Low, Dr. Zachary Ruhe, Dr. Cyril Benes, and Dr. Aaron Hata. I got the wonderful opportunity to attend and complete a Ph.D. due to your mentorship and support.

I would also like to thank all my friends, from both before and during graduate school, for providing encouragement, support, and fun during my Ph.D. I greatly appreciate all the

exciting adventures we had over the past several years that refreshed me during my studies. I also feel incredibly lucky for the talented group of scientists with me in my cohort. I am looking forward to all the incredible discoveries you will make.

My life is made infinitely better by my wife, Dr. Kelly Torosian, who I would like to thank for all the love and support during my Ph.D. Thank you for all the fun adventures and for matching at UCSD for both residency and fellowship. I am grateful we get to be together during these years of training and greatly look forward to all that is in store for our future together.

Finally, I would like to thank my parents and my sister for all their support throughout my entire life. I truly would not have made it this far without all your encouragement and love. Thank you for setting a great example and for being fun people who are always there for me. I hope you see this accomplishment as part of your own.

Chapter 2, in full, has been submitted for publication of the material in a research article with the title "Apoptotic DNase DFFB mediates cancer persister cell mutagenesis and acquired drug resistance." The authors are: Williams, August F.; Gervasio, David A.G.; Turkal, Claire E.; Stuhlfire, Anna E.; Wang, Michael X.; Mauch, Brandon E.; Nguyen, Ariel H.; Paw, Michelle H.; Hairani, Mehrshad; Lathrop, Cooper P.; Harris, Sophie H.; Page, Jennifer L.; Hangauer, Matthew J. The dissertation author was the primary researcher and author of this paper.

VITA

2015 Bachelor of Science in Biochemistry – Molecular Biology, University of California Santa Barbara

2023 Doctor of Philosophy in Biomedical Sciences, University of California San Diego

PUBLICATIONS

Williams AF, Gervasio DAG, Turkal CE, Hairani M, Wang MX, West AH, Stuhflire AE, Mauch B, Paw MH, Lathrop CP, Harris S, Page JL, Hangauer MJ. Apoptotic DNase DFFB mediates cancer persister cell mutagenesis and acquired drug resistance. (In Review).

Jensen SJ, Ruhe ZC, **Williams AF**, Nhan DQ, Garza-Sánchez F, Low DA, Hayes CS. Paradoxical activation of a type VI secretion system (T6SS) phospholipase effector by its cognate immunity protein. Journal of Bacteriology. (Accepted).

Hu H, Piotrowska Z, Hare PJ, Chen H, Mulvey HE, Mayfield A, Noeen S, Kattermann K, Greenberg M, **Williams A**, Riley AK, Wilson JJ, Mao YQ, Huang RP, Banwait MK, Ho J, Crowther GS, Hariri LP, Heist RS, Kodack DP, Pinello L, Shaw AT, Mino-Kenudson M, Hata AN, Sequist LV, Benes CH, Niederst MJ, Engelman JA. Three subtypes of lung cancer fibroblasts define distinct therapeutic paradigms. Cancer Cell. 2021 Nov 8;39(11):1531-1547.e10. doi: 10.1016/j.ccell.2021.09.003. Epub 2021 Oct 7. PMID: 34624218; PMCID: PMC8578451.

Raoof S, Mulford IJ, Frisco-Cabanos H, Nangia V, Timonina D, Labrot E, Hafeez N, Bilton SJ, Drier Y, Ji F, Greenberg M, **Williams A**, Kattermann K, Damon L, Sovath S, Rakiec DP, Korn JM, Ruddy DA, Benes CH, Hammerman PS, Piotrowska Z, Sequist LV, Niederst MJ, Barretina J, Engelman JA, Hata AN. Targeting FGFR overcomes EMT-mediated resistance in EGFR mutant non-small cell lung cancer. Oncogene. 2019 Sep;38(37):6399-6413. doi: 10.1038/s41388-019-0887-2. Epub 2019 Jul 19. PMID: 31324888; PMCID: PMC6742540.

Dastur A, Choi A, Costa C, Yin X, **Williams A**, McClanaghan J, Greenberg M, Roderick J, Patel NU, Boisvert J, McDermott U, Garnett MJ, Almenara J, Grant S, Rizzo K, Engelman JA, Kelliher M, Faber AC, Benes CH. NOTCH1 Represses MCL-1 Levels in GSI-resistant T-ALL, Making them Susceptible to ABT-263. Clin Cancer Res. 2019 Jan 1;25(1):312-324. doi: 10.1158/1078-0432.CCR-18-0867. Epub 2018 Sep 17. PMID: 30224339; PMCID: PMC6320296.

ABSTRACT OF THE DISSERTATION

Apoptotic DNase DFFB Mediates Cancer Acquired Drug Resistance

by

August Williams

Doctor of Philosophy in Biomedical Sciences

University of California San Diego, 2023

Professor Matthew Hangauer, Chair

The development of oncogene targeted therapies over the past few decades facilitated by cancer driver gene identification through next generation sequencing has resulted in impressive clinical responses against late-stage cancers. However, robust responses are hindered by acquired drug resistance. This is the scenario where a tumor initially responds to therapy, but then regrows even in the presence of continued drug treatment. Here, we investigate cancer persister cells as a model of acquired drug resistance to identify processes that allow tumors to overcome drug pressure. Single cell transcriptomic profiling revealed well-

characterized drug resistance processes occurring in persister cells such as epithelial-mesenchymal transition. Interestingly, it also revealed apoptotic signaling as a process shared across multiple persister cell models. We found that cancer persister cells survive caspase 3 activation and minority mitochondrial outermembrane permeabilization (MOMP). This sublethal apoptotic signaling activates the nuclease DFFB. DFFB causes mutagenic DNA damage resulting in persister regrowth through both genetic and nongenetic mechanisms. Inhibition of DFFB blocked persister cell regrowth both in cell culture and in vivo. Given the need for targets against stress adaptation mechanisms, DFFB represents a promising therapeutic target that could extend the efficacy of already available anti-cancer therapies.

CHAPTER 1

INTRODUCTION

Advances in next generation sequencing accelerated the development of oncogene targeted therapies with the goal of eliminating tumors while minimizing toxic side effects associated with traditional chemotherapy and radiation treatments. Despite impressive responses, drug resistance in cancer remains a barrier towards achieving robust responses especially for late-stage disease patients.[1] Acquired drug resistance, characterized by tumor regrowth after an initial therapy response, continues to frustrate clinical efforts towards increasing patient survival. This complex phenomenon involves multiple mechanisms including genetic alterations, epigenetic changes, altered drug metabolism, and influences from the tumor microenvironment.[2,3] Tackling acquired drug resistance is therapeutically challenging since these mechanisms can act in combination. Thus, understanding the underlying mechanisms of acquired drug resistance is critical for developing more effective therapies.

Persister cells are a subpopulation of tumor cells that survive continuous therapeutic pressure and lead to disease recurrence.[4] In patients, these cells may represent minimal residual disease during a therapeutic intervention. This is the point where tumor volume has decreased to a low or clinically undetectable level prior to relapse.[5–7] Thus, cancer persister cells represent a model system used to investigate acquired drug resistance in the laboratory. Experimentally, persister cells are the residual surviving cells following extended (>10 days) therapy exposure that is cytotoxic to the majority of the original, or parental, population.[4] Persister cells are characterized by their ability to enter a quiescent or slow proliferation state, allowing them to evade the cytotoxic effects of chemotherapy, oncogene targeted therapy, radiation therapy, and immunotherapy.[4,8,9] A fraction of persister cells eventually gain the ability to reenter the cell cycle and form growing

colonies even under drug pressure.[4,10] Despite their critical role in tumor recurrence, the underlying mechanisms governing persister cell formation, survival, and regrowth remain poorly understood.

The persister cell concept was originally described in bacteria from observations that repeated penicillin exposures could not sterilize the targeted streptococcal population.[11] Even though the majority of cells died, approximately 1% of the population survived. Preexisting dormant cells rather than cells containing heritable resistance mutations were proposed to explain the survival of this bacterial subpopulation,[12] and recent microscopy experiments confirmed this hypothesis.[13] Importantly, bacterial persister cells that regrow upon drug removal remain drug sensitive, suggesting that nongenetic survival mechanisms underly the persister phenotype.[13] Bacterial persistence may be mediated by various mechanisms including toxin-antitoxin systems as well as stochastic gene expression changes.[14,15] Stress responses including σ^S and SOS are activated in bacterial persister cells, which together mediate a stress-induced mutagenic state to facilitate adaptation through increased expression of DNA repair proteins and error-prone polymerases.[15–17] Given shared characteristics between both cancer and bacterial persister cells, this survival state may be evolutionarily conserved. Indeed, several recent reports also link persister cell characteristics with those involved in embryonic suspension at the blastocyst developmental stage termed diapause.[18–21] During diapause, cell division and metabolism are greatly reduced with embryos entering a reversible dormant state.[22] Thus, cancer persister cells enter an evolutionarily conserved survival state to escape drug stress.

One drug resistance scenario involves the Darwinian selection of cells with preexisting drug-resistance conferring mutations. However, cancer persister cells survive through nongenetic mechanisms like their bacterial counterparts. This is exemplified by the observation that removing drug to allow persister cell regrowth gives rise to daughter cells that are sensitive to treatment with

the same therapy.[4] Observations in the clinic of tumors responding to retreatment following a period of treatment withdrawal, known as a "drug holiday," is consistent with this persister cell characteristic.[23] While it remains unknown whether the majority of mutations in patients preexist or are acquired during therapy, cancer persister cells recapitulate key aspects of acquired drug resistance and represent useful models for discovery of fundamental resistance mechanisms. The emergence of acquired drug resistance therefore may not be a foregone conclusion and eliminating the residual cancer population through any acquired vulnerabilities may represent a strategy for increasing cures.

There are a variety of reports assessing persister cell origins using barcoding and microscopy approaches to determine whether these cells arise from preexisting parental cell subpopulations. Certain studies demonstrated that persister cells at least partially arise from defined preexisting populations.[24–26] These studies show that particular traits, such as high expression of aldehyde dehydrogenase,[24] histone demethylases,[25] growth factors,[26] or increased NOTCH signaling,[25] are present in the parental population and are selected for upon drug exposure. However, these traits appear stochastically upregulated, or "jackpotted," in the parental population suggesting that any cell has the ability to become drug tolerant.[26] Consistent with this theory, other studies utilizing DNA barcoding technology examined the diversity of barcodes remaining after cytotoxic drug exposure and found that persister cells are primarily induced by drug rather than preexisting.[19,20,27,28] Another barcoding study showed that this may depend on the treatment type, potentially explaining the various conflicting observations from others.[29] Thus, persister formation is generally mediated by heterogeneous, transient subclonal events that, whether preexisting or not, become selected for upon drug exposure.

Several survival mechanisms utilized by persister cells have been identified as potentially exploitable therapeutic vulnerabilities that could be taken advantage of to eliminate residual disease. These diverse mechanisms include growth factor signaling, chromatin remodeling, lipid peroxide reduction, apoptotic signaling, and DNA damage response.[4,9,24,30–32] In the seminal cancer persister cell report, a small screen of thirteen compounds revealed the IGF-1R inhibitor AEW541 as well as several histone deacetylase (HDAC) inhibitors as compounds that could eliminate persister cell formation.[4] IGF-1R inhibition was found to have a direct effect on histone demethylase KDM5A expression and the resulting chromatin state, suggesting a direct link between growth factor signaling and chromatin modification essential to persister formation. Further investigations are required to determine the link between IGF-1R and KDM5A in persister cells, which may reveal additional targets. Further evidence for the important role chromatin architecture plays in persister cell formation is the acquired sensitivity to epigenetic reader inhibition. Bromodomain and extraterminal (BET) proteins such as BRD4 facilitate persister cell chromatin remodeling and transcriptional changes required for survival. Inhibiting BET proteins with JQ1 prevented persister formation in targeted therapy-treated breast cancer models.[33,34] Another chemical screen identified ferroptosis, an iron-dependent cell death mechanism, as an acquired sensitivity in cells that enter the drug tolerant persister cell state.[30] Specifically, RSL3 and ML210, inhibitors of the lipid hydroperoxidase GPX4, selectively eliminated persister cells without affecting parental cell viability. GPX4 is the enzyme responsible for the reduction of phospholipid hydroperoxides.[35] The ferroptosis sensitivity in persister cells may be driven by the downregulation of antioxidant genes as well as the decreased levels of reducing cofactors NADPH and glutathione. This process may be mediated by the stress response transcription factor ATF4, but additional studies are required to determine the mechanism underlying this sensitivity.[36]

Persister cells also enter a mesenchymal state during epithelial-to-mesenchymal transition (EMT) which has been shown to increase sensitivity to ferroptosis.[37] Persister cells also rely on the upregulation of inhibitor of apoptosis (IAP) family proteins to avoid cell death from apoptosis signaling.[9,31] Inhibiting IAPs with SMAC-mimetics impaired persister cell formation from both immune therapy (PD-1 checkpoint blockade) and targeted therapy. Another vulnerability is the DNA damage response mediated by ataxia-telangiectasia mutated (ATM) kinase that is active in persister cells due to accumulated double strand DNA breaks. Co-treatment with an ATM inhibitor alongside targeted therapy was toxic to persister cells.[32] Caspase 3/7 activity culminating in activation of the apoptotic nuclease DNA fragmentation factor B (DFFB) was shown to mediate acute (24 hour) DNA damage from targeted therapy treatment, but whether this pathway continues to play a role during the longer treatment timepoint persister cell stage has not been elucidated. Persister cells are also susceptible to disulfiram potentially through inhibition of aldehyde dehydrogenase although additional studies are warranted.[24] In summary, diverse persister cell vulnerabilities have been reported, but more work is required to deduce the mechanisms underlying these vulnerabilities and determine if subpopulations of persisters can escape these stresses. Further, whether these treatment strategies will be effective in the clinic remains unknown.

Evidence suggests that the tumor microenvironment also influences drug tolerance and resistance. Cancer-associated fibroblasts can promote therapy resistance through both cell-cell contacts as well as secreted factors. Examples include integrin signaling through FAK in melanoma associated fibroblasts that confer sensitivity to BRAF inhibitors and HGF secretion reactivating the MET signaling pathway in non-small cell lung cancer.[38–40] Interestingly, HGF can also recruit immunosuppressive neutrophils to the tumor, facilitating survival from immune

effector cells.[41] Hypoxia, which is a common feature of solid tumors, can induce quiescence and therefore promote persister cell survival.[42–44] Low oxygen-induced factors such as MIG6 decrease sensitivity to tyrosine kinase inhibitor treatment by disrupting ERBB protein-protein interactions to favor pro-survival EGFR-HER3 signaling in a lung cancer model.[44] Several studies also show that inflammation, a characteristic feature of the tumor microenvironment, can promote persister survival through STAT3, NF-κB, and type I interferon responses.[45–48] Notably, the secreted factor TGF-β could promote several persister cell characteristics that include transitioning cell states through EMT as well as entering a mutagenic state through the downregulation of DNA repair factors.[45,49] A screen of fifty tumor microenvironment factors to identify pro- and anti-persistence factors further confirmed the importance interferon signaling plays in persister formation.[50] This study highlighted the intricate signaling balance persister cells must maintain to reap beneficial interferon-induced properties. While low concentrations of interferon-γ promoted persistence, higher concentrations hindered survival; both of which were mediated by STAT1.[50] This revealed an interesting sensitivity in STAT1 high cancer cells to a type I protein arginine methyltransferase (PRMT) inhibitor that disrupts RNA processing by blocking methylation of RNA binding proteins resulting indirectly in decreased STAT1 expression. These findings suggest that targeting tumor microenvironmental factors alongside cancer cell intrinsic mechanisms may offer synergistic therapeutic options against cancer persister cells.

After extended drug treatment, a fraction of persister cells reenter the cell cycle and grow into drug-tolerant expanded persister (DTEP) cell colonies. There are several explanations for how persister cells reenter the cell cycle. One study utilized cellular barcoding to show that cycling persister cells emerge from distinct lineages characterized by a metabolic shift to fatty acid oxidation as well as upregulation of antioxidant genes.[10] Another study described receptor driven

signals that "pulse" the MAP kinase pathway to stimulate entry into the cell cycle.[51] These signals arise from autocrine or paracrine signaling from nearby cells or from dying cells in a caspase-dependent process termed apoptosis-induced proliferation.[52] During this process related to wound healing, stem cell factors, proangiogenic factors, and prostaglandins are released from dying cells to stimulate growth and drug resistance in neighboring cells.[53–57] Recent literature investigating dormant metastatic cancer cells also shows that early cycling cells must overcome the STING pathway to emerge into disease relapse.[58] In this mechanism, chromatin remodeling and hypermethylation of the STING promoter and enhancer stimulated in part by TGF-β promote spontaneous outbreaks from disseminated cancer cells. As a result of escaping quiescence, these early cycling cells may activate stress survival signaling through the transcription factor ATF4 and incur DNA damage.[59] Therefore, both cell autonomous and non-cell autonomous mechanisms promote initial reentry into the cell cycle.

Several studies examined the transcriptional landscape at single cell resolution to determine persister subpopulations responsible for driving DTEP formation and tumor relapse. One study interrogated persister cells and DTEPs derived from patient xenograft models treated with BRAF and MEK inhibitors, and identified a nuclear receptor RXRG-driven neural crest stem cell state as the main relapse-driving subpopulation.[60] Other studies also confirmed that the majority of cell states driving relapse contain stem cell markers and characteristics that are potentially mediated by TGF-β.[61,62] These cell states, although nongenetic, appear heritable to daughter cells under drug pressure.[63] Importantly, intra- and inter-patient heterogeneity exists in the composition of minimal residual disease, indicating that several cell states have the capability to drive resistance. This poses significant therapy development and treatment challenges given the many ways drug resistance can develop.

Proliferating DTEP colonies at extended timepoints (>6 months) are more drug resistant than their early cycling progenitors. These cells are not as drug stressed, indicated by a decrease in DNA damage and by the presence of drug-resistance conferring mutations such as the EGFR gatekeeper mutation T790M in a non-small cell lung cancer model treated with EGFR inhibitors.[64–66] Importantly, these drug resistance mutations did not preexist in the starting population and each distinct DTEP colony contains unique mutations responsible for resistance, suggesting that they were acquired during the treatment period from a cell intrinsic mutagenic mechanism.[65,66] Recent studies demonstrated that, similar to bacterial persister cells, cancer persister cells also enter a stress induced mutagenic state characterized by the downregulation of accurate DNA repair enzymes and upregulation of error prone polymerases potentially mediated through TGF-β and MTOR signaling.[49,64,67] Targeted therapy induces a transient 7- to 50-fold increase of the mutagenic rate in persister cells that increases genetic diversity to promote escape from drug pressure.[27] Inhibiting error prone polymerases, such as REV1, could prevent or delay disease relapse in colorectal cancer models treated with targeted therapy.[27] However, these error prone polymerases may be involved in other undescribed processes that contribute to drug resistance since overexpression of the error prone polymerase POLκ increased drug resistance through an unknown mutagenesis-independent mechanism.[68] Therefore, cancer persister cells enter a stress induced mutagenic state mirroring that of bacterial persister cells as one strategy to escape drug pressure.

Other mutagenic processes in cancer persister cells have also been described. Several groups have investigated the role APOBEC3 enzymes play in persister cell mutagenesis. When foreign DNA is introduced into cells during viral or bacterial infections, APOBEC3 cytidine deaminases (APOBEC3A or APOBEC3B) hypermutate the foreign DNA, causing cytosine to

uracil to thymine mutations, to promote its degradation.[69] The APOBEC mutational signature has also been observed in patients, suggesting the enzyme as a potential source for acquired mutations.[70] Targeted therapy treatment in non-small cell lung cancer models induces APOBEC3A or APOBEC3B expression, increases DNA damage, and promotes the accumulation of APOBEC3-associated mutations.[71,72] Furthermore, genetic ablation of APOBEC3A delays drug resistant outgrowth while APOBEC3B overexpression accelerated tumor relapse.[71,72] APOBEC3 enzymes may also promote DTEP formation through deaminase-independent chromosomal instability mechanisms.[73] Thus, APOBEC3 enzymes represent an important novel therapeutic target that warrants additional studies as a potential strategy to combat persister cell mutagenesis and acquired drug resistance. Additional processes such as DNA damage from reactive oxygen species[67] or DNA replication errors[74] may also contribute to the persister cell mutagenesis phenotype, but the relevance of these mechanisms to different cell and cancer types requires further studies.

The motivating force driving the research in this thesis is identifying additional mutagenic and epigenetic mechanisms in persister cells that may promote DTEP formation. Specifically, I have focused on understanding if sublethal apoptotic signaling induced by drug stress contributes to mutagenesis, epigenetic changes, and DTEP formation and whether this pathway can be inhibited as a novel strategy to prevent the emergence of acquired drug resistance.

Apoptosis is a programmed form of cell death that plays an integral role in development, tissue homeostasis, and disease prevention.[75,76] Markers of apoptosis include membrane blebbing, cleavage of caspases, and DNA fragmentation. There are two apoptotic signaling pathways: intrinsic and extrinsic apoptosis. Intrinsic apoptosis is characterized by mitochondrial outer membrane permeabilization (MOMP) resulting in release of a variety of factors including

cytochrome c into the cytoplasm, apoptosome formation, and caspase 3 activation.[77] MOMP is mediated by the balance and activity of pro- and anti-apoptotic Bcl-2 family proteins. Extrinsic apoptosis is initiated by death receptors located in the cell membrane that respond to extracellular ligands. Once these receptors including Fas, tumor necrosis factor (TNF), and TNF-related apoptosis-inducing ligand (TRAIL) are activated they signal through caspases 8 and 10 leading to the cleavage of BID. BID then translocates to the mitochondria and contributes to MOMP through the pore-forming protein BAX, thus serving as a link between the extrinsic and intrinsic apoptotic pathways.[75] Ultimately, both pathways converge on cleavage and activation of the "executioner caspase," caspase 3.[77] Despite its well-known role in cell death, caspase 3 is also involved in death-independent cellular mechanisms. These include proliferation,[78,79] cell state changes,[80–83] and cancer initiation and progression.[84] Importantly, this implies that stressed cells can survive apoptotic signaling, even with caspase 3 activation.

Multiple studies have shown that cells can both recover from and survive during apoptotic signaling, generally referred to as sublethal apoptotic signaling. In a processes termed "anastasis" (Greek for "rising to life"), removing the toxic stimulus from cells allowed for recovery from caspase 3 cleavage but resulted in chromosomal abnormalities with important implications for carcinogenesis.[85] These recovering cells displayed elevated proangiogenic factors and switched from growth-arrested to proliferating to migratory cell states.[86] A recent report showed that directly inducing caspase 3 activation to lethal levels for some cells nonetheless allowed other cells in the population to live.[87] This supports that caspase 3 activation alone is insufficient to induce cell death, as the level of caspase activation could not distinguish between survival or death.[87] Cells can also survive "minority MOMP" where a minority of mitochondria outer membranes are permeabilized resulting in caspase activity and DNA damage.[88] In melanoma models, sublethal or

failed apoptosis led to the development of a more invasive phenotype both *in vitro* and *in vivo*.[89] Untreated cancer cells also undergo sublethal apoptosis-induced DNA breaks that confer stem cell-like properties through ATM, NF-κB, and STAT3 signaling.[90] Sublethal apoptosis may play a role in persister cell formation, since acutely (6 hours) inducing MOMP with BH3 mimetics conferred persister phenotypes.[36] This was mediated through activation of the integrated stress response and transcription factor ATF4 by cytochrome c release from the mitochondria. These studies all investigated untreated cancer cells or acute (<24 hours) cytotoxic treatments, but whether sublethal apoptosis occurs during chronic stress scenarios as experienced by cancer persister cells remains to be determined. Therefore, drug stress-induced sublethal apoptosis represents a potential pathway that could promote DNA damage and mutagenesis in persister cells.

During the final stages of apoptosis, the apoptotic nuclease DFFB (also known as Caspase activated DNase, CAD; or DFF40) is activated through proteolytic cleavage of its chaperone and inhibitor, DFFA (also known as Inhibitor of CAD, ICAD; or DFF35/45).[91] DFFB then dimerizes and creates double strand DNA breaks responsible for oligonucleosomal DNA fragmentation that is a hallmark of apoptosis.[92,93] DFFB activity can also induce single strand DNA nicks.[94,95] DFFB requires both Mg^{2+} and Zn^{2+} for catalytic activity and is composed of three domains: the CIDE-N domain mediating homodimerization and DFFA heterodimerization, the C2 domain, and the catalytic domain.[93,96,97] DFFA is required for proper DFFB protein stability following translation.[91,98] Thus, cells lacking DFFA also lose DFFB expression. Interestingly, DFFB is essential for mediating the majority of cell autonomous DNA fragmentation but is not required for cell death, as caspase activity is unaffected by loss of the nuclease.[91,99,100] Consistent with this, mice genetically modified for DFFA or DFFB deficiency can reproduce and are viable without

noticeable abnormalities.[99,100] DFFB therefore represents the main DNA damage effector during apoptotic signaling.

DFFB has been hypothesized to play a role both in tumor suppression and promotion. DFFB as a tumor suppressor has credence based on observations that radiation or chemical mutagen exposure to DFFB knockout (KO) mice have increased rates of tumorigenesis.[101,102] Specifically, 50 weeks following irradiation of C57BL/6 mice, 79% of wild type (WT) mice survived compared to 50% of DFFB KO mice.[101] While apoptosis was not affected, consistent with DFFB not being required for cell death, DFFB KO cells acutely acquired more chromosomal aberrations than WT cells. In the skin carcinogenesis model, DFFB KO mice had a four-fold (average of 1 papilloma per WT mouse and 4 papillomas per DFFB KO mouse) increase in papilloma development versus WT mice.[102] Analysis of DFFB expression levels in several cancer types suggest DFFB may be playing a tumor suppressor role. Poor prognosis in esophageal squamous cell carcinoma is correlated with lower DFFB expression.[103] A similar trend holds for studies involving colon cancer, renal cell carcinoma, and leiomyosarcoma.[104–106] Furthermore, glioblastoma cells display decreased DNA fragmentation and low nuclear DFFB localization while the human papillomavirus oncoprotein E6 can directly inhibit DFFB-mediated DNA fragmentation.[107,108] Although these studies suggest DFFB is a tumor suppressor, loss of DFFB or DFFA in cancers is rare, as observed through a comparison of normal and cancer tissues.[109] Indeed, other studies show that DFFB activity is correlated with carcinogenesis and tumor progression. Spontaneous DFFB activity through mitochondrial apoptosis promoted micronuclei formation and increased cancer metastasis.[110] A DFFB-mediated transcriptional signature derived from this study also correlated with poor prognosis across cancer types. In addition, high expression of DFFB or DFFA is correlated with worse prognosis in several cancer types in including serous ovarian cancer

and endometrial hyperplasias.[111,112] Interestingly, increased DFFB expression either caused therapy sensitivity or resistance depending on the treatment type, which may explain the conflicting results in clinical studies.[113] Specifically, loss of DFFB conferred resistance of cancerous T cells to the antimetabolites methotrexate, 6-mercaptopurine, and cytarabine but conferred sensitivity to the topoisomerase II inhibitors etoposide and teniposide.[113] Therefore, further investigation into the mechanism and regulation of DFFB activity during tumor initiation, progression, and drug resistance is warranted to determine favorable scenarios where targeting DFFB could provide a benefit to patients.

As previously discussed with caspase signaling, DFFB has also been implicated in roles outside of apoptosis and mutagenesis involved in cell state changes.[82,92,114] For example, BH3 mimetic exposure induced p53-dependent cellular senescence through DFFB-mediated DNA damage,[114] and DFFB-induced DNA nicks in the p21 promoter allowed for skeletal muscle cell differentiation.[82] A recent report also demonstrated that caspase-independent DFFB activity can promote cancer cell survival from radiation therapy.[115] After genotoxic stress introduced by radiation, DNA damage signaling from ATM and ATR directly phosphorylates DFFA to recruit the DFFA/DFFB heterodimer to chromatin. This “second wave” of DNA damage induced by DFFB promotes cell cycle checkpoint control between G2 and mitosis, whereas DFFB or DFFA deficient cells prematurely entered mitosis leading to increased genomic instability and toxicity. Thus, DFFB represents a potential targetable sublethal apoptosis or DNA damage response effector molecule that mediates cell cycle or cell state changes induced by drug stress.

DFFB also represents an attractive target against mutagenesis, as the nuclease was previously described to acutely induce mutations following exposure to diverse treatment modalities.[116] These studies all utilized the hypoxanthine-guanine phosphoribosyltransferase

(HPRT) with 6-thioguanine (6-TG) assay as a readout of mutagenesis. Cells containing a functional HPRT enzyme are killed by the purine analog 6-TG which is converted to a cytotoxic metabolite by HPRT. Therefore, any colonies that form after 6-TG exposure are presumed to be due to inactivating mutations in the HPRT gene, although other mechanisms of gene silencing are possible and direct genome sequencing is required to confirm HPRT assay results.[117] Therapies that caused HPRT disruption through DFFB activity include TRAIL, the topoisomerase inhibitors doxorubicin and SN38, the microtubule poison vincristine, and the proteasome inhibitors bortezomib, carfilzomib, ixazomib, and oprozomib.[118–120] As expected, directly genotoxic therapies such as the DNA cross-linking platinum compound cisplatin and DNA alkylating agent temozolomide caused DNA damage and HPRT gene disruption independent of DFFB.[118,119] Interestingly, necroptosis induction and the HDAC inhibitors vorinostat and romidepsin also caused DFFB-independent DNA damage and HPRT disruption through unknown mechanisms.[120,121] Despite BH-3 mimetics such as ABT-737 being previously shown to induce DFFB-dependent DNA damage,[88] neither BH3 mimetics nor SMAC mimetics alone at physiologically relevant levels were mutagenic based on the HPRT assay.[122] This may be because insufficient concentrations of BH3 mimetic or SMAC mimetic were used in the HPRT assays because higher BH3 mimetic as well as SMAC mimetic in combination with TNFα did cause DFFB-dependent HPRT disruption.[121] In summary, acute (<24 hour) activation of the apoptotic pathway with nongenotoxic agents causes DFFB-dependent DNA damage and HPRT inactivation. This DFFB activity was postulated to play a role in tumorigenesis or therapy-induced secondary tumors.[116] Whether DFFB is activated and causes mutations in surviving cells during chronic stress or treatments, such as in persister cells, has not been studied.

The research objective of this dissertation is to elucidate the role DFFB plays in cancer persister cell mutagenesis and regrowth. This is accomplished using several bioinformatic, molecular, and cellular biological techniques. Throughout the study, clinically relevant models for acquired drug resistance are used including *BRAF*-mutant melanoma treated with a BRAF and MEK inhibitor combination, *EGFR*-mutant non-small cell lung cancer treated with several generations of EGFR inhibitors, and HER2-positive breast cancer treated with a HER2 inhibitor. First, we investigate sublethal apoptotic signaling in persister cells followed by mechanistic studies to interrogate DFFB activation and activity. We then examine the genetic and nongenetic effects DFFB-induced DNA damage confers onto persister cells. Finally, we test whether DFFB ablation affects persister cell regrowth in cell culture and *in vivo* using mice xenograft models. Together, these data expand the sublethal apoptotic signaling mechanism to persister cells and reveal the critical role DFFB plays in mediating persister cell regrowth under drug stress.

CHAPTER 2

DFFB MEDIATES CANCER PERSISTER CELL DNA DAMAGE AND ACQUIRED DRUG RESISTANCE

Results

To discover how persister cells acquire drug resistance and seed tumour regrowth, we utilized models in which treatment with cytotoxic concentrations of targeted therapies results in death for the majority of cells subsequently revealing a residual population of primarily quiescent cancer persister cells (Figure 1a-d). Persister cells occupy a reversible pro-survival cell state such that upon drug removal and drug-free regrowth the cells become resensitized to drug.[4,30] This reversibility indicates an initial non-genetic mechanism of persister cell survival. However, upon prolonged drug treatment, a minority of persister cells regrow into drug-tolerant expanded persister (DTEP) cell colonies modeling the process of acquired resistance (Figure 1a-d). The mechanisms which promote the initial transition from persister cells into DTEP colonies are not known. However, it was previously shown that at later timepoints of treatment, expanded DTEP colonies possess resistance mutations which did not preexist and are not present in neighboring colonies.[65] Therefore, while it remains unknown whether the majority of resistance mutations in patients preexist or are acquired during therapy, these models recapitulate key aspects of acquired resistance including the clinical emergence of multiple parallel genetic resistance mechanisms and therefore are useful models for discovery of fundamental resistance mechanisms.[123–125]

To identify processes that confer drug resistance, we performed single cell RNA sequencing (scRNAseq) on targeted therapy-treated A375 melanoma and PC9 lung cancer persister cells and untreated parental cells. As previously seen in these and other persister cell types,[10,59,60,126] we observed heterogeneous persister cell subpopulations (Figure 2a,c, Table 1). To

discover pathways which are activated in persister cells, we analyzed the intersection of genes upregulated in both persister cells models (Figure 2e, Table 2). Consistent with previous observations that persister cells have an epithelial-mesenchymal transition (EMT) signature,[4,30,66] EMT was the most enriched gene set in persister cells. "UV response down" was also enriched, consistent with recently described downregulation of DNA repair genes in persister cells.[64,67,74] We also observed decreased cell cycle progression in the persister cell population in agreement with prior studies (Figure 2b,d).[4]

We then focused on the enriched "Apoptosis" Hallmark gene set signature (Figure 2e,f and Figure 3a) because recent reports have shown that mammalian cells can survive brief (< 24 hours) periods of apoptotic stress which, if removed before cell death occurs, can promote transient DNA damage and genomic alterations.[85,88,118–121,127] We hypothesized that sublethal apoptotic signaling could also occur in the chronic drug-induced stress setting of persister cells. Consistent with this, we observed that live persister cells exhibit partial mitochondrial cytochrome c release (Figure 3b, Figure 4) and partial loss of mitochondrial potential (Figure 5a, Figure 6) indicative of incomplete mitochondrial outermembrane permeabilization (MOMP). This observation of cytochrome c release in viable persister cells is consistent with a recent study which demonstrated that BH3 mimetic-induced cytochrome C mitochondrial release promotes persistence.[36] In addition, we found that persister cells have partially cleaved caspase 3 (Figure 3c, Figure 5b, Figure 7) and, using a fluorescent caspase 3/7 activity sensor, we observed a corresponding increase in caspase activity in live persister cells (Figure 3d, Figure 8). Sorted persister cells with intermediate elevated caspase 3/7 activity levels, but not lethally high levels, were capable of regrowth upon drug removal thereby confirming the viability of persister cells with sublethal levels of elevated caspase activity (Figure 3e, Figure 5c). This finding is consistent with a study showing that cells can

recover from intermediate, but not high, caspase activity.[87] While there is a small subpopulation of parental cells which have sublethal signaling in the absence of drug, consistent with a prior report,[90] we found that most sublethal apoptotic signaling is drug-induced because apoptotic signaling markers appear early during parental cell drug exposure and dissipate within 24 hours of drug removal from persister cells (Figure 5d,e). Taken together, these data indicate that persister cells undergo drug stress-induced sublethal apoptotic signaling.

Interestingly, we also found that persister cells from multiple tumour types treated with targeted therapies exhibit an increase in DNA damage signal γH2AX which is inhibited by treatment with the pan-caspase inhibitor Quinoline-Val-Asp-Difluorophenoxymethylketone (QVD) indicating that caspase signaling is required for persister cell DNA damage (Figure 3f, Figure 5f-i, Figure 9). We then sought to address how apoptotic signaling promotes DNA damage in persister cells. We hypothesized that an apoptotic DNase could transmit sublethal apoptotic signaling into DNA strand breaks without persister cell death. During apoptosis, DNase DFFB (also known as DFF40 and Caspase-Activated DNase, CAD) is activated by caspase 3-mediated proteolytic cleavage of chaperone and inhibitor protein DFFA (also known as DFF45 and ICAD). Activated DFFB then dimerizes and induces DNA single and double strand breaks resulting in fragmentation of chromosomal DNA during apoptotic cell death.[92,94,128] In addition, it was previously reported that short term (< 24 hours) minority MOMP can cause DFFB-dependent DNA damage.[88] Based on this precedent, we sought to determine whether DFFB activation occurs within persister cells and mediates DNA damage. Consistent with sublethal activation of DFFB, we observed low but detectable levels of caspase-dependent cleavage of DFFA in persister cells (Figure 5j, Figure 10a). To test whether DFFB has a functional role, we then generated multiple CRISPR-mediated DFFB knockout (KO) clones for each persister cell model (Figure 11a-f). Using

these DFFB KO cells, which proliferate similarly to DFFB WT cells in the absence of drug both in cell culture and *in vivo* (Figure 12a-e), we first tested whether DFFB is required for initial drug response. This is an important question because the canonical DNA fragmentation role for DFFB is associated with apoptotic cell death and it is possible that DFFB KO cells are less sensitive to targeted therapy.[92] However, consistent with prior reports demonstrating that DFFB is not required for apoptotic death,[91,99] we found that DFFB KO and WT cells respond similarly to targeted therapy treatment (Figure 13a-d). We also found that DFFB KO cells form persister cells and minimal residual disease *in vivo* at similar levels to WT cells (Figure 13e-i). While there is clonal variability in each of these assays, this variation is independent of DFFB status when considered across cell lines. Therefore, these data indicate that DFFB is not required for cancer cell proliferation, drug response or persister cell formation.

We then tested whether persister cell DNA damage is induced by DFFB. We found that drug-induced DNA damage was absent in DFFB KO persister cells across all tested tumour types (Figure 10b, Figure 14a-c) and re-expression of WT DFFB, but not nuclease activity deficient mutant DFFB,[129] restored drug-induced DNA damage in DFFB KO persister cells (Figure 10c). Therefore, DFFB DNase activity is the primary source of drug-stress induced DNA damage in persister cells. We then sought to determine whether DFFB-induced DNA damage in persister cells results in mutagenesis, a potential source of drug resistance. To determine this, we performed whole exome sequencing (WES) of single cell bottlenecked DFFB WT and KO A375 cells subjected to 7 weeks of drug treatment with dabrafenib and trametinib. Analysis of WES data from multiple replicate populations revealed that DFFB WT DTEP cells acquired a variety of mutations distinct to each DTEP cell, consistent with a previous report which analyzed EGFR mutant lung cancer DTEP cell mutations.[65] However, we found that DFFB KO cells had fewer than half as

many acquired mutations as WT cells (Figure 10d). These observations indicate that DFFB promotes mutagenesis during prolonged drug treatment.

It was previously reported that cancer stress-induced mutagenesis is facilitated by downregulation of DNA repair genes and upregulation of error prone polymerases.[27,64,67,74] We considered whether DFFB may affect expression of these genes, potentially facilitating error prone repair of DFFB-induced DNA damage. However, scRNAseq analysis revealed that both WT and KO persister cells possess this same pattern of differentially expressed genes, indicating that DFFB promotes mutagenesis independent of indirect effects on DNA repair gene expression (Figure 15).

We next investigated the WES data to determine if drug resistance-conferring mutations were acquired in DFFB WT DTEP cells. A previous report found that the emergence of the EGFR T790M gatekeeper mutation in lung adenocarcinoma persister cells in cell culture was not detectable until at least 5 months of EGFR inhibitor drug exposure.[66] In patients, BRAF inhibitor and MEK inhibitor combination treatment resistance-conferring mutations in *BRAF* mutant melanoma have been detected at relapse in the clinic between 3-18 months including MAPK pathway *MEK1/2* mutations, *BRAF* amplification, *BRAF* alternative splicing, and *NRAS* mutations.[124,125] Notably, these melanoma clinical studies each also reported several patients with acquired drug resistance without identifiable resistance mutations indicating that either unknown resistance mutations or non-genetic mechanisms can also mediate resistance. In our WES data, which was acquired early when DFFB WT DTEP colonies first emerged at 7 weeks of drug treatment, we identified in WT but not DFFB KO cells several mutations that could potentially play a role in resistance. These include genes in the MAPK (*BRAF*) and interferon-γ (IFNγ) pathways (*IFNGR1*, *JAK1*) among others. Specifically, one of the sequenced DFFB WT DTEP cell-derived samples contained a *BRAF* p.R252* nonsense mutation that was previously observed

in skin basal cell carcinoma and non-small cell lung cancer patients.[130,131] We found that these *BRAF* p.R252* DTEP cells are less sensitive than parental cells to BRAF inhibitor dabrafenib treatment alone, resistant to additional ERK inhibition, and recover phosphorylated ERK signal more robustly than parental cells during treatment (Figure 16). Therefore, this acquired *BRAF* mutation may contribute to persister cell resistance and regrowth into a DTEP colony by promoting MAPK signaling during treatment.

We also identified a variety of other mutations in DFFB WT DTEP cells which could potentially contribute to resistance including mutations in HER3 ligand *NRG1*,[132] *YAP*,[133] cell cycle genes (*PPP2CB, CDK11B*),[134,135] and alterations affecting the p53 pathway (*MDM2*).[136] Taken together, these data suggest that DFFB-mediated mutagenesis may directly promote acquired resistance in some persister cells.

Given that DTEP colonies exhibit very slow proliferation consistent with partial resistance, and that it is difficult to reconcile a mere two-fold decrease in DFFB KO cell acquired mutations with the observed 10-fold decrease in DFFB KO DTEP colony formation, we reasoned that early acquired mutations alone may not be sufficient to promote initial DTEP formation aside from rare cases. We therefore considered whether there are DFFB-dependent signaling changes which promote DTEP formation. To investigate DFFB-mediated signaling pathways, we assessed Hallmarks gene sets in WT versus DFFB KO persister cells. We found that all enriched pathways were depleted in WT cells compared to DFFB KO cells, suggesting that DFFB-induced DNA damage is involved in gene silencing (Figure 17a). We focused on the "Interferon gamma response" signature due to the known association of the IFNγ pathway with growth arrest and persister cell formation.[48,50,137] This signature was evenly distributed across DFFB KO subpopulations, consistent with this process occurring in a majority of DFFB KO persister cells

(Figure 17b). The "Interferon gamma response" signature remained enriched between WT and DFFB KO populations at the later DTEP timepoint as well, suggesting that IFNγ signaling may be a chronic growth suppressive process in cells lacking DFFB (Figure 17c-d). To determine possible IFNγ signature-promoting mechanisms, we investigated the individual genes responsible for driving the signature in DFFB KO cells and identified genes such as *CCL2*, *IFITM2*, *IFITM3*, and *IL18* which are downstream of DNA-sensing receptors (Figure 17e).[138] We reasoned that stimulator of interferon genes (STING) protein activation from cytosolic DNA released from mitochondria during sublethal apoptotic signaling could explain the upregulation of these genes. Consistent with this, we observed increased STING levels across multiple persister cell models versus parental cells (Figure 17f-g).[139–142] Interestingly, DFFB KO have higher STING levels than WT cells overall, potentially indicating that DFFB may regulate STING. Downstream of STING, we investigated STAT1 levels given recent literature describing the importance this factor plays in modulating persistence.[50] Importantly, the level of STAT1 influences how the persistence phenotype is affected, as low levels promote while high levels block persistence. While we observed a modest increase in STAT1 levels in WT persister cells, DFFB KO persister cells had a larger increase (Figure 17h-i). Furthermore, caspase inhibition in WT cells also increased STAT1 levels indicating that caspase-mediated DFFB activation suppresses STAT1 in DFFB WT persister cells (Figure 17j-k). This data is consistent with previous reports in hematopoietic stem cell development and viral infection models showing that apoptotic caspases block interferon gene activation downstream of STING activated by mitochondrial DNA.[140,141] Importantly, our data show that the caspase-mediated downregulation of interferon genes is driven by DFFB whereas the link between caspase signaling and decreased interferon signaling was previously speculative. We then tested whether this interferon pathway affects DTEP colony formation, and indeed found

that JAK inhibitor treatment rescued the ability of DFFB KO persister cells to form DTEP colonies (Figure 17l). This finding is consistent with a previous report showing that JAK inhibition blocks anti-persistence effects from IFNγ without interfering with the pro-persistence effects.[50] Together, this data shows that DFFB suppresses growth-inhibiting interferon signaling stimulated by STING and STAT1 activation to promote persister regrowth. Furthermore, the observation of interferon pathway modulation, which is central to immune-mediated tumour control, raises the possibility that DFFB activity could affect tumour-immune interactions.[139,143]

DFFB-induced DNA damage may hinder interferon gene expression through multiple mechanisms. One possibility is through mutations. Interestingly, three unique WT DTEP samples from the WES experiment contained mutations in *IFNGR1*, *JAK1*, and *IFNAR2* suggesting potential genetic modulation of the pathway. However, exposing the *IFNGR1* mutant sample and the *JAK1* mutant sample to IFNγ did not appear to disrupt phosphorylated STAT1 or STAT1 signal indicating that these specific novel mutations do not directly interfere with canonical interferon signaling (Figure 18a). Another possibility is that DNA damage interferes with gene expression. DNA damage directly interferes with gene transcription through transcriptional interference wherein transcriptional machinery stalls due to the presence of DNA damage within gene bodies.[144] To determine if DFFB-induced DNA damage downregulates genes through transcriptional interference, we investigated the length of downregulated genes in WT and DFFB KO persister cells compared to parental cells because longer length genes are preferentially downregulated by stochastically distributed DNA damage during transcriptional interference.[145] Indeed, consistent with DFFB-induced DNA damage-mediated transcriptional interference, we observed genes of longer lengths are preferentially downregulated in DFFB WT cells versus DFFB KO cells (Figure 18b). We also found this phenotype present in a comparison of DTEP-timepoint

cells to persister cells, indicating transcriptional interference as an ongoing chronic process throughout drug treatment including at relapse phase (Figure 18c). Along with transcriptional interference, DNA damage can also modulate gene expression through promoter methylation or repressor relocalization[117,146] and DFFB has been specifically reported to affect cell state through DNA damage-mediated gene expression changes.[82] A previous study reported that persister cells accumulate tri-methylation of H3 lysine 9 (H3K9me3) at LINE-1 elements that dampens interferon response genes to promote survival.[147] H3K9me3 serves as a mark that promotes DNMT1-mediated maintenance of DNA methylation that could silence gene expression.[148] Consistent with the hypothesis that DFFB mediates interferon gene silencing, we observed a global decrease in H3K9me3 levels in DFFB KO persister cells (Figure 18d). Furthermore, while the identified interferon-related mutations in DFFB WT DTEP colonies did not directly impact interferon signaling, their presence provides evidence of DNA damage within these genes which may be silenced through transcriptional interference and gene methylation induced by DFFB activity. It is also possible that DFFB modulates STING signaling by directly degrading cytoplasmic DNA since STING levels are higher across multiple models of DFFB KO cells (Figure 17f-g). Therefore, by one or more mechanisms, DFFB activity allows persister cells to overcome the growth inhibiting effects of interferon signaling.

We also considered whether DFFB could contribute to resistance through other non-mutational mechanisms. We investigated DNA damage response (DDR) signaling that could result from persister cell DFFB-induced DNA damage which is not present in DFFB KO cells (Figure 14). Previous studies have reported that DFFB-induced DNA damage results in context-dependent activation of ATM,[32] ATR,[115] DNA-PK[149] or JNK[88] including a report which showed that spontaneous DNA damage in parental cells results in ATM-mediated activation of NF-κB and

phosphorylated STAT3 to promote tumourigenicity and stemness.[90] However, we did not observe any of these signals in A375 melanoma persister cells (Figure 19a-f) and ATM or DNA-PK inhibition did not decrease A375 DTEP colony formation (Figure 19g-i). DFFB-induced micronuclei was also reported, but we did not observe a significant increase in WT persister cells (Figure 19j).[110] It is also possible that DFFB-induced DNA damage promotes persister cell cycle arrest to preserve cell viability, analogous to a recent report demonstrating that within 24 hours of acute radiation-induced DNA damage, DFFB further amplifies DNA damage resulting in prolonged G2 cell cycle arrest to prevent lethal premature mitotic entry.[115] DFFB-mediated cell cycle arrest might similarly promote cell viability during initial slow DTEP colony formation. However, we found DFFB-induced DNA damage is not necessary for persister cell cycle arrest because both DFFB WT and KO persister cells are similarly G1 cell cycle arrested, including low expression of the proliferation marker *Ki-67*, despite DFFB KO cells lacking DNA damage (Figure 2b, Figure 20a,b, Figure 14). It is likely that cell cycle arrest is instead mediated directly by dabrafenib- and trametinib-inhibition of MAPK signaling independent of DNA damage in A375 persister cells. In addition, multiple studies have reported that apoptotic cells can promote survival and drug resistance of neighboring cells through secreted factors.[52] However, we found that DFFB KO persister cell failure to transition into DTEP colonies (see Figure 21) is not rescued by supplementation with DFFB WT persister cell conditioned media indicating secreted factors are not sufficient to promote DTEP colony formation (Figure 20e).

We next tested whether DFFB is required for persister cells to regrow into DTEP colonies. Strikingly, we found that all DFFB KO persister cell clones were severely hindered in their ability to form DTEP colonies across all tested tumour types and targeted therapies (Figure 21a-c). The role of DFFB in DTEP colony formation is independent of cell viability because DFFB loss does

not result in decreased viability in our tested parental or persister cells (Figure 12a-d, Figure 13) or a wide array of other parental cancer cell types (Figure 12e), and DFFB does not promote clonogenic growth under drug stress (Figure 20c,d).[150,151] We then tested whether DFFB is required for acquired resistance in vivo. A375 DFFB WT or KO melanoma tumours were formed on opposing flanks of mice which were then treated with dabrafenib and trametinib. Consistent with cell culture findings showing that DFFB status does not affect initial treatment response or persister cell formation (Figure 13), treatment initially shrunk both DFFB WT and DFFB KO tumours to a minimal residual volume (Figure 13i). However, only DFFB WT tumours regrew during further treatment (Figure 21d). Together, these data point toward an essential functional role for DFFB in acquired resistance to targeted therapy.

Discussion

Drug stress-induced DNA damage and mutagenesis were recently observed in cancer but the mutagenic mechanism remains poorly understood.[27,64,67,74] We reasoned that if the mutagenic process is gene-driven, it could be inhibited. Based on prior reports showing that cells which recover from brief periods (< 24 hours) of certain cytotoxic treatments can acquire DFFB-mediated mutations, we hypothesized that chronically drug-stressed persister cells may undergo drug stress-induced apoptotic signaling without death resulting in DFFB-mediated mutagenesis.[85,88,118–121,127,152] Indeed, our findings reveal that, during long term drug treatment on a timescale relevant for the initiation of cancer acquired drug resistance, surviving persister cells from multiple tumour types and targeted therapy treatments exhibit sublethal apoptotic signaling and undergo DFFB-mediated DNA damage and mutagenesis. However, DFFB is not the sole source of acquired mutations because DFFB KO cells do acquire some mutations during treatment (Figure 10d)

consistent with additional mutagenic mechanisms potentially mediated by reactive oxygen species, APOBEC3A/B, other nucleases such as ENDOG, or DNA replication errors in rare cycling persister cells.[10,27,67,71,72,74,90] Most importantly, we also found that DFFB is required for persister cell regrowth into DTEP colonies and tumour relapse. While early DTEP formation is likely due to DFFB-mediated suppression of interferon genes, continued DFFB activity in these colonies may allow cells to acquire robust drug resistance through both genetic and nongenetic factors. Given that DFFB is nonessential for mouse development,[99,101] is a potentially therapeutically targetable enzyme,[153] and that, beyond our persister cell findings which do not depend on elevated DFFB expression (Figure 11a-c), high DFFB and DFFA expression in primary tumours nonetheless correlates with worse patient outcomes (Figure 22), DFFB has the characteristics of a promising therapeutic target.

More broadly, sublethal apoptotic caspase signaling has been reported to occur in other contexts.[82,92,154,155] Therefore, DFFB may also induce DNA damage and mutagenesis in normal human tissues under physiological stress. Recent data revealed that nondividing and dividing human tissues acquire somatic mutations at a similar rate indicating that unknown mechanisms of DNA replication-independent mutagenesis are the major sources of somatic mutations in humans.[156] Our findings raise the possibility that, in addition to a role in cancer acquired drug resistance, DFFB may also promote DNA damage and mutagenesis in other scenarios.

Methods

Cell lines and culture

A375 (CRL-1619) and BT474 (HTB-20) cells were purchased from the ATCC. PC9 cells were provided by the Altschuler and Wu Lab at UC San Francisco. A375 cells were cultured in DMEM

(Thermo Fisher Scientific) supplemented with 10% fetal bovine serum (FBS) and 1% Antimycotic/Antibiotic (AA) (Thermo Fisher Scientific). PC9 cells were cultured in RPMI-1640 medium (Thermo Fisher Scientific) supplemented with 5% FBS and 1% AA. BT474 cells were cultured in RPMI-1640 medium supplemented with 10% FBS and 1% AA. All cell lines were maintained in 5% CO2 atmosphere at 37 °C. Cell lines were split with 0.25% trypsin-EDTA (Thermo Fisher Scientific). Cell line identities were confirmed with STR profiling at the UC Berkeley Cell Culture Facility. All cell lines regularly tested negative for mycoplasma throughout these investigations using the Lonza Mycoalert Mycoplasma Detection Kit.

Chemicals and drugs

Dabrafenib (S2807), trametinib (S2673), erlotinib (S7786), osimertinib (S7297), lapatinib (S2111), staurosporine (S1421), ERK inhibitor SCH772984 (S7101), ATM inhibitor KU-55933 (S1092), DNA-PK inhibitor NU7441 (S2638), puromycin (S9631), doxycycline hyclate (S4163), and Quinoline-Val-Asp-Difluorophenoxymethylketone (QVD) (S7311) were purchased from Selleck Chemicals. Etoposide (E55500) was purchased from Research Products International. JC-1 dye (T3168) and digitonin (AC407565000) were purchased from Thermo Fisher Scientific. Ghost Dyes Violet 510 (13-0870-T100) and Red 780 (13-0865-T100) were purchased from Tonbo Biosciences. Carbonyl cyanide m-chlorophenyl hydrazone (CCCP) was purchased from Abcam (ab141229). BioTracker NucView 530 Red Caspase-3 Dye (PBS) (SCT105) and cytochalasin B (C2743) were purchased from Sigma-Aldrich. Recombinant human TNFα (300-01A) was purchased from Peprotech. JAK inhibitor ruxolitinib was purchased from MedChemExpress (HY-50856).

Persister cell derivation

Previously described protocols were utilized.[4,30] Briefly, A375 cells were treated with 250 nM dabrafenib and 25 nM trametinib for 14 days, PC9 cells were treated with 2.5 μM erlotinib for 10 days, or with 300 nM or 500 nM osimertinib for 9 days, and BT474 cells were treated with 500 nM or 2 μM lapatinib for 10 days to generate persister cells. Pre-derived persister cells were assayed while still in drug unless otherwise noted. In experiments utilizing caspase inhibitor QVD, 10 μM QVD was added together with the respective targeted therapy treatment for the duration of the experiment. Media and drug were replenished every 3-4 days.

DTEP colony formation

Cells were plated at low starting densities to avoid outgrowth of overlapping DTEP colonies. Specifically, A375 cells were seeded at 4,000 cells per 10 cm dish, and 250 nM dabrafenib and 25 nM trametinib media was added the next day. PC9 cells were seeded at 5,000 cells per 10 cm dish, and 2.5 μM erlotinib or 300 nM osimertinib media was added the next day. BT474 cells were seeded at 500,000 cells per 10 cm dish, and 2 μM lapatinib was added 72 hours later. Drug media was refreshed every 3-4 days. At 7 weeks in drug for A375 cells, 5 weeks in drug for PC9 cells, and 11 weeks in drug for BT474 cells, plates were fixed with 90% methanol and stained with crystal violet. The plates were then blinded by a separate laboratory member prior to colony counting by microscopy. Colonies with greater than 25 cells were considered DTEP colonies. To calculate the fraction of cells that regrew into DTEP colonies ("DTEP fraction"), the number of DTEP colonies per plate was divided by the sum of the number of isolated single cells plus colonies of any size. For experiments utilizing whole exome sequenced DFFB WT DTEP colony-derived cells, these single cell bottlenecked populations were maintained in drug-free media for further analysis unless otherwise noted.

Clonogenic assay

The clonogenic growth assay was performed according to a previously reported protocol with some modifications.[157] Specifically, A375 WT and DFFB KO #1 cells were seeded at 100 cells per plate in the indicated concentration of dabrafenib and trametinib. The respective media was replenished every 3-4 days. Control cells and cells treated with 1 nM dabrafenib and 0.1 nM trametinib were fixed with 90% methanol and stained with 0.5% crystal violet on day 9. Cells treated with 10 nM dabrafenib and 1 nM trametinib were fixed and stained at week 4. The plates were then blinded and quantification was performed by counting visible colonies.

Microscopy

Brightfield photos were captured with the EVOS XL Core microscope using the 4X LPlan PH2 objective and micronuclei were quantified with the EVOS M5000 and 60X PlanApo N objective.

Cell viability

Cell viability was assessed with CellTiter Glo (CTG) 2.0 Cell Viability assay (Promega, #G7571). Luminescence was read with a Molecular Devices SpectraMax iD3 plate reader with SoftMax Pro 7 software.

Single cell RNA sequencing

A375 cells were cultured with 250 nM dabrafenib and 25 nM trametinib and PC9 cells were treated with 2.5 μM erlotinib for 2 weeks to establish persister cells. A375 WT and DFFB KO cells were cultured with 250 nM dabrafenib and 25 nM trametinib for 9 weeks during which WT cells formed DTEP colonies but KO cells did not. For all conditions, an untreated parental control was cultured alongside the drug-treated conditions. At the time of analysis, cells were lifted with trypsin and libraries were generated using the 10X Chromium Single Cell 3' v3 kit (10X Genomics). Quality control of the libraries was conducted with the High Sensitivity D1000 ScreenTape kit with the

Agilent TapeStation and then sequenced using a NovaSeq S4 flowcell on an Illumina NovaSeq 6000 sequencer at the UCSD Institute for Genomic Medicine.

Read alignment and data processing

Fastq files were aligned to the human "refdata-cellranger-GRCh38-3.0.0" genome with 10X Genomics Cell Ranger 3.1.0 using the "cellranger count" command to generate single cell feature counts for each library.[158] The "filtered_feature_bc_matrix" generated for each population was used to create a "Seurat object" in the Seurat R package version 4.0.3.[159–161] Cells containing greater than 1,000 and less then 7,500 features, and with less than 20% mitochondrial reads were included in downstream analyses. A cell cycle score was calculated for each cell using the default Seurat method with a published list of cell cycle genes,[162] and this score was used to regress cell cycle during normalization and scaling with the "SCTransform" command.

Determining variable features and mapping

The commands "RunPCA," "RunUMAP," "FindNeighbors," and "FindClusters" were performed with default settings, with 30 dimensions used for "RunUMAP" and "FindNeighbors." In the "FindClusters" command, the resolution for A375 and PC9 was set to 1.0, and 0.15, respectfully, based on visualization of graphed clusters. For cluster analyses within the persister cell populations only, the resolution was set to 0.2 for A375 and 0.05 for PC9. The Seurat command "FindMarkerGenes" was used with default parameters to identify differentially expressed genes between specified populations or clusters of cells.

Persister cell gene signature analysis

Differentially expressed genes between persister cell and parental populations that were shared between A375 and PC9 with consistent direction were selected for analysis. From the intersected 1,051 genes, the 330 upregulated genes were input into the Molecular Signatures Database to

discover Hallmark gene set enrichments using a hypergeometric test. This identified 17 gene sets with a false discovery rate q value less than 0.001 (Table 2). The apoptosis gene set was assessed with the AUCell package version 1.12.0 which calculated gene set scores per cell.[163] Briefly, genes are ranked from highest to lowest expression in each cell before determining a gene set score based on the top 5% of the ranked genes for each "Hallmarks" gene set in each cell. These were then visualized on a UMAP with Seurat. Single gene scaled expression was visualized with the Seurat "FeaturePlot" command. For individual persister cell clusters and DTEP-timepoint comparisons, GSEA was conducted with the ClusterProfiler R package (version 3.18.0) which calculated a normalized enrichment score (NES) for each gene set in the specified cluster.[164] The minimum gene set size for analysis was set to five and the Benjamini-Hochberg method was used for false discovery rate correction. Statistically significant pathways are presented in Table 2.

JC-1 mitochondrial membrane potential assay

A375 persister cells were derived with 250 nM dabrafenib and 25 nM trametinib for 2 weeks and untreated parental cells were cultured alongside. After 2 weeks of culture, cells were lifted with trypsin for JC-1 staining. As a positive control, cells were treated with 50 μM carbonyl cyanide m-chlorophenyl hydrazone (CCCP) for 5 minutes. JC-1 was dissolved in DMSO (Thermo Fisher Scientific, #D12345) at a final concentration of 150 μM and cells were stained for 30 minutes away from light at 37 °C. Cells were then stained with Ghost Dye Red 780 (Tonbo Biosciences, #13-0865-T100) diluted 1:1000 in PBS (Gibco, #10010023) for 15 minutes away from light at room temperature. Cells were washed in PBS and analyzed on a BD FACSCanto RUO flow cytometer using 488 nm and 640 nm lasers for green and red fluorescence respectively. At least 30,000 live cell events were collected per sample. The flow cytometry results were analyzed using FlowJo Software (BD Life Sciences) version 10.7.1.

Immunoblotting

Cancer persister cells were derived with drug treatment in 10 or 15 cm plates. Cells were then washed with PBS and lysed using RIPA buffer (Thermo Fisher Scientific, #89900) supplemented with Phosphatase inhibitor (Thermo Fisher Scientific, #78420) and protease inhibitor (Thermo Fisher Scientific, #78430). Lysates were centrifuged at 14,000 g at 4 °C for 15 min, and the protein concentration of the supernatant was determined using the Pierce BCA Protein Assay Kit (Thermo Fisher Scientific, #23225). Lysates were mixed with sample buffer (Thermo Fisher Scientific, NP0007) and denatured at 70 °C for 10 min. Samples were separated by SDS–PAGE (Bolt 4–12% Bis-Tris Gel, Life Technologies, NW04120BOX), run with Chameleon Duo Pre-stained Protein Ladder (LICOR, #928-60000, and transferred to a nitrocellulose membrane using the iBLOT 2 Dry Blotting System (Life Technologies, IB21001). Membranes were blocked with 5% BSA for 1 h at room temperature, and then incubated with primary antibody at 4 °C overnight. LICOR secondary antibodies were then incubated with the membrane for 1 h at room temperature, and the membrane was imaged using the LICOR Odyssey Imaging System and Image Studio version 5.2. β-Tubulin or Vinculin levels were measured as a loading control. Antibody commercial sources were: β-Tubulin (Invitrogen, MA5-16308); γH2AX (Cell Signaling Technology, #9718); Cleaved caspase 3 (Cell Signaling Technology, #9664); ATM (Cell Signaling Technology, #2873); phosphorylated ATM (Abcam, ab81292); ATR (Cell Signaling Technology, #2790); phosphorylated ATR (Cell Signaling Technology, #2853); DNA-PKcs (Cell Signaling Technology, #38168); phosphorylated DNA-PKcs (Cell Signaling Technology, #68716); JNK (Cell Signaling Technology, #9252); phosphorylated JNK (Cell Signaling Technology, #4668); NF-κB (Cell Signaling Technology, #8242; phosphorylated NF-κB (Cell Signaling Technology, #3033); STAT3 (Cell Signaling Technology, #9139; phosphorylated STAT3 (Y705) (Cell

Signaling Technology, #9145); STING (Cell Signaling Technology, #13647); phosphorylated STING (Cell Signaling Technology, #19781); Cytochrome c (BioLegend, #612310); DFFB (Santa Cruz Biotechnology, SC-374067); DFFA (Abcam, ab108521); IRDye 680RD Goat anti-Mouse IgG secondary antibody (LICOR, #926-68070); IRDye 800CW Goat anti-Mouse IgG secondary antibody (LICOR, #926-32210); IRDye 680RD Goat anti-Rabbit IgG secondary antibody (LICOR, #926-68071); IRDye 800CW Goat anti-Rabbit IgG secondary antibody (LICOR, #926-32211); Vinculin (Cell Signaling Technology, #4650).

DNA damage, cleaved caspase 3, and cytochrome c flow cytometry

A375 persister cells were derived with 250 nM dabrafenib and 25 nM trametinib for 2 weeks and untreated parental cells were cultured alongside. For γH2AX experiments, A375 persister cells treated with 10 μM QVD for the duration of drug treatment were also prepared. After 2 weeks of culture, cells were trypsinized and collected for staining. Cells were stained with viability dye Ghost Dye Red 510 or 780 diluted 1:1000 in PBS for 15 minutes away from light at room temperature. For cytochrome c staining, incubation in 50 μg/mL digitonin in PBS for 10 minutes on ice was used to selectively permeabilize the cell membrane.[165] Cells were fixed with 4% Paraformaldehyde for 10 minutes at room temperature. For γH2AX and cleaved caspase 3 staining, cells were permeabilized with 0.3% Triton X-100 in PBS for 10 minutes at room temperature. Cells were stained for proteins of interest using primary conjugated antibodies at manufacturer recommended dilutions in PBS for 30 minutes to 1 hour at room temperature. Cells were washed in PBS and analyzed on a BD FACSCanto RUO flow cytometer using 405 nm and 640 nm lasers for blue and red fluorescence respectively. At least 30,000 live cell events were collected per sample. The flow cytometry results were analyzed using FlowJo Software (BD Life Sciences) version 10.7.1.

Caspase 3/7 activity reporter assay

Caspase activity was measured using NucView 530 Caspase-3 Substrate (Biotium #10408). A375 persister cells were pre-derived from 2 week treatment with 250 nM dabrafenib with 25 nM trametinib while parental cells were cultured alongside. Positive control cells were derived from 4-hour parental cell treatment with 1 μM staurosporine and these pre-apoptotic cells were assayed by flow cytometry prior to death. Adherent tumour cells were collected by trypsinization (~1 million cells/sample), washed in PBS, and incubated with Ghost Dye Violet 510 cell viability dye following the manufacturer's instructions. Cells were washed with PBS + 1% FBS and subsequently incubated with 5 μM NucView 530 Caspase-3 Substrate for 30 minutes (in PBS + 1% FBS) and analyzed by flow cytometry using a BD FACSAria II sorter. Cells not treated with NucView 530 Caspase-3 Substrate were used as unstained controls. Fluorescence was measured as follows: Ghost Dye Violet 510 (405 nm laser, 525/50 filter), NucView 530 Caspase-3 Substrate (488 laser, 530/30 filter). Sorted live cells were collected in PBS + 10% FBS and used for downstream viability assays. For testing caspase 3/7 activity-positive persister cell regrowth, cells were sorted and plated at 1,000 cells per well in 12-well plates in drug-free media. 24 hours later, CTG was performed to measure cell viability. To assess regrowth ability, drug-free media refreshed on day 3 and CTG was performed on day 6.

CRISPR editing

CRISPR editing was performed at the UC San Francisco Cell and Genome Engineering Core. Human DFFB sgRNA g1 was previously reported.[88] Additional guide RNAs targeting the first (g4) or second (g2r) exon of human DFFB were designed using the UCSC Genome Browser and cloned into the eSpCas9(1.1) vector. eSpCas9(1.1) vector is from the Feng Zhang laboratory at MIT (Addgene plasmid #71814; RRID:Addgene_71814). A375 DFFB KO clone #1 was

constructed with sgRNA g1, A375 DFFB KO clone #2 was constructed with g4, PC9 DFFB KO clones were both constructed with g2r, and BT474 DFFB KO clones were both constructed with g4.

DFFB sgRNA	Sequence
g1	5'-CAGCCCGAGGAAGTTCGGCG-3'
g2r	5'-GCTCCGTGCCATCCTCGTAC-3'
g4	5'-TGCCAGGAGGTGCTGCGCAA-3'

Following sequence verification, the guide constructs were introduced individually either by transfection or electroporation. For transfection, guide constructs were co-transfected with a vector expressing mCherry and puromycin resistance using Lipofectamine 3000. Transfected cells were selected with 1 μg/mL puromycin for 3-4 days. For electroporation, cells were electroporated with the CRISPR/Cas9 RNP (gRNAs and high-fidelity Cas9p from IDT, Coralville IA) using the Lonza 4D Nucleofector kit SF with program FF-120. After cell expansion, genomic DNA was extracted from a portion of the cell pool (Nucleospin Blood gDNA extraction kit, Takara Bio) and the target sites were amplified (Phusion DNA polymerase, NEB) and sequenced using the primers indicated in the table below (Sanger sequencing by GeneWiz, South San Francisco, CA; primers and sgRNA cloning oligonucleotides from IDT, Coralville IA). CRISPR/Cas9 efficiency was determined by TIDE analysis (tide.deskgen.com). Clones which showed only frameshift-causing indels in all alleles were further analyzed by TOPO cloning (Life Technologies) and Sanger sequencing and with the ICE analysis tool (Synthego). Clones with a DFFB KO genotype were subsequently confirmed to lack DFFB protein expression by western blot.

DFFB sgRNA	Primer
g1 and g4	Amplification primer, Forward 5'-TCTGAGTAAGGTAATGTGGTGTCC-3'

	Amplification primer, Reverse 5'-CCGGGTCTCCTAGCTCTGAT-3'
	Sequencing Primer 5'-GAGAGGTGGGAAGAGGGAAGG-3'
g2r	Amplification primer, Forward 5'-AAAGACAGGCTCTATTTGAAGCG-3'
	Amplification primer, Reverse 5'-GGACACCTCAAATGAACGCAAATA-3'
	Sequencing Primer 5'-AAAAGACGACCAATTGAACAGCTG-3'

Lentivirus production

E. coli cultures with lentiviral vectors purchased from VectorBuilder were grown on LB Agar Ampicillin-100 plates (Sigma-Aldrich, #L5667). A colony was picked and grown overnight in LB-amp and plasmid DNA was isolated using the Qiagen HiSpeed Plasmid Midi Kit (Qiagen #12643) and quantified with a Nanodrop. HEK293T cells were transfected with packaging plasmids psPAX2 (Addgene, #12260) and pMD2G (Addgene, #12259) in Opti-MEM (Thermo Fisher Scientific, #31985062) and polyethylenimine (Sigma-Aldrich, #764604). Virus-containing supernatant was collected, centrifuged, then filtered with a 0.45 μM filter (Sigma-Aldrich, #SE1M003M00).

Doxycycline-induced DFFB re-expression

Doxycycline-inducible DFFB expression vectors were obtained from VectorBuilder. Lentivirus was produced as described above. The WT DFFB [NM_004402.4] or nuclease-deficient DFFB (H260N) lentivirus was then transduced into A375 DFFB KO cells.[129] Cells were selected with 2 μg/mL puromycin for 3 days. After expansion, cells were seeded and 1.0 μg/mL doxycycline was

added the following day. Media with doxycycline was refreshed every 3-4 days for the duration of the experiment.

Whole exome sequencing and analysis

To eliminate preexisting genetic heterogeneity, a single A375 WT or DFFB KO cell was used to start the experiment. Following initial expansion for 3 weeks, a portion of the cell population was frozen for the reference sequence and the remaining cells were plated onto 10 cm dishes at 4,000 cells per dish. 250 nM dabrafenib plus 25 nM trametinib was added the following day, and drug media was refreshed every 3-4 days. Following 7 weeks of drug treatment, the DFFB WT plates were composed of primarily DTEP colonies while the DFFB KO plates were almost exclusively isolated cells or small clumps of surviving persister cells which had not regrown (see Fig. 3a). Then, each plate was allowed to regrow without drug for 10 days, cells were lifted with trypsin, and multiple individual cells were isolated through single cell bottlenecks in 384 well plate wells to purify their genotypes. The isolated single cells were subsequently expanded for 5 weeks in drug-free media in increasing well sizes up to a 10 cm plate to accumulate adequate genomic DNA content for genomic sequencing. Frozen cell pellets were sent to Novogene for DNA extraction, library preparation for whole exome sequencing (all drug treated samples, Agilent SureSelect V6 58M) or whole genome sequencing (pre-treatment reference sample, NEB Ultra II), and sequenced on an Illumina NovaSeq 6000 PE150.

Single nucleotide variant analysis

Each sample was analyzed according to the GATK best practices workflow for data preprocessing for variant discovery followed by the somatic short variant discovery workflow.[166–168] GATK version 4.2.4.0 pipelines were used. Fastq files were mapped to the hg38 reference genome provided in the GATK shared resource bucket with BWA.[169] Duplicate reads were marked with

Picard, and base scores were recalibrated with the GATK tool "BaseRecalibrator." Mutect2 was used to call mutations between the drug treated sample and the respective starting population reference sample. Sequencing errors and contamination were estimated with "GetPileUpSummaries", "CalculateContamination", and "FilterMutectCalls". Variants were annotated with "Funcotator". Low frequency (frequency < 0.3) mutations, which could arise post-treatment during expansion from isolated single cells prior to sequencing, were excluded from the analysis. Output files were analyzed with the Maftools R Bioconductor package version 2.6.05.[170]

In vivo tumour acquired resistance

The University of California San Francisco Institutional Animal Care and Use Committee (IACUC) approved the xenograft studies which were performed at the UCSF Preclinical Therapeutics Core in protocol #AN179937. Sample size was determined based on prior experience with this model.[30] A375 cells were cultured in DMEM with 10% FBS prior to implantation. Cells were suspended in a 1:1 mixture of PBS:matrigel to a final concentration of 1 x 10^8 cells/mL. 10 million DFFB WT and KO A375 cells were subcutaneously injected into opposing flanks of 6-8 week old female NSG mice (Jackson Laboratory, #005557). When tumour volumes reached 100-200 mm^3, drug dosing was started via once daily oral gavage with 100 mg/kg dabrafenib and 1 mg/kg trametinib. Tumour volumes were measured 1-2 times per week by blinded observers. Tumour volumes were normalized to the minimum volume of each tumour during treatment and fold change of tumour regrowth from this minimum volume was calculated. To focus analysis on acquired resistance, only mice with at least one relapsed tumour (WT or KO), defined by 10-fold regrowth from the minimal volume during treatment, were included in Fig. 3d. Additional mice which did not exhibit tumour relapse of either WT or KO tumours were excluded from Fig. 3d but are included in the Fig. 3 source data.

Micronuclei quantification

We followed the cytokinesis-block micronucleus cytome assay to investigate micronuclei in drug-treated cells.[171] Twelve thousand A375 cells were plated onto each chamber of NUNC Lab-Tek II 4-well chamber slides (154526PK) and treated with 250 nM dabrafenib and 25 nM trametinib for 15 days to generate persister cells, with media being refreshed every 3 days. Because persister cells are quiescent and the micronuclei assay requires cell division to identify bi-nucleated cells, at day 15 of drug treatment, persister cells were given a 48-hour holiday in drug-free media to facilitate initiation of cell division before being treated for 48 hours with cytochalasin B in media at a final concentration of 3 μg/mL. Therefore, by necessity, this assay measured early drug-free regrowing cells rather than persister cells. For the parental cell control, 12,000 control A375 parental cells were plated onto each chamber of the slides and allowed to grow for 24 hours in drug-free media before being treated with cytochalasin B. Following cytochalasin B treatment, cells were fixed in paraformaldehyde at 4% in PBS at room temperature for 10 minutes. Cells were then washed three times in PBS before being mounted with DAPI-containing Fluoroshield (ab104139). Slides were blinded prior to quantification. A minimum of 200 bi-nucleated cells were counted per condition, and four replicates were performed each for the untreated control and drug-treated groups.

Patient survival data analysis

Disease free survival and overall survival Kaplan-Meir curves for DFFB and DFFA expression were analyzed and plotted with GEPIA2.[172] The median was used for the "Group Cutoff." All cancer types were included in the analysis.

CRISPR screen DFFB gene essentiality analysis

The PICKLES database was used to investigate DFFB essentiality.[151,173] Cell lines were sorted by cancer type and analyzed with the Score/Sanger dataset.[150] Negative Bayes factor values are considered non-essential.[174]

DFFB WT conditioned media rescue of DFFB KO DTEP colony formation

Cells were plated and drug treated as described above to form DTEP colonies. WT and DFFB KO cells were cultured simultaneously with matching drug concentrations. Once persister cells were formed at week 2, media from the respective WT or DFFB KO conditioned media source plates were mixed 1:1 with fresh drug media, filtered through a 0.45 μm filter (Sigma-Aldrich, #SE1M003M00), and added to the respective experimental plates. DTEP colony formation was assessed as described above.

Data availability

Single cell RNA sequencing data have been deposited in NCBI's Gene Expression Omnibus (accession number: GSE196018). Whole exome sequencing and whole genome sequencing data have been deposited in the NCBI Sequence Read Archive (PRJNA800470). DFFB essentiality scores from the PICKLES database is available from the Hart laboratory (https://pickles.hart-lab.org/). Survival data analysis from the TCGA and GTEx projects are available from the Zhang laboratory (http://gepia2.cancer-pku.cn). Expression data for GEPIA2 is available from UCSC Xena project (UCSC Toil RNA-seq Recompute) (https://xenabrowser.net/datapages/) and clinical data is available from the Genomic Data Commons Data Portal (https://portal.gdc.cancer.gov/). Source data are provided with this paper.

Statistical analyses

All statistical tests were performed with GraphPad Prism version 9.0.0 (86), R version 4.0.3, or RStudio version 1.2.5033. Unless otherwise noted, mean with standard deviation are plotted on graphs with P values calculated using unpaired, two-tailed Student's t-tests. Differentially expressed genes from scRNAseq were calculated using the Wilcoxon Rank Sum test. Gene set enrichment was calculated with hypergeometric test. Results from statistical tests are stated or represented by the following: ns indicates $P>0.05$, *$P<0.05$, **$P<0.01$, ***$P<0.001$, ****$P<0.0001$. All statistical analysis was performed on data from at least three biological replicates.

Acknowledgements

We thank the UCSF Cell and Genome Engineering Core for generating CRISPR-mediated knockout cell lines and UCSF Preclinical Therapeutics Core for performing mouse experiments. This chapter includes data generated at the UC San Diego Institute for Genomic Medicine Genomics Center utilizing an Illumina NovaSeq 6000 that was purchased with funding from a National Institutes of Health SIG grant (#S10 OD026929). This work was performed with the support of the Flow Cytometry Core at the San Diego Center for AIDS Research (P30 AI036214), the VA San Diego Health Care System, and the San Diego Veterans Medical Research Foundation. We also acknowledge discussions with other members of the UCSD Cancer Target Discovery and Development (CTD^2) Center (U01CA217885) and Jean Y. J. Wang (UCSD) for comments on this work. This research was supported by the UCSD Cancer Biology, Informatics & Omics T32 training grant T32CA067754 (A.F.W.), UCSD Moores Cancer Center American Cancer Society Institutional Research Grant IRG-15-172-45, NIH/NCI R01CA212767, V Foundation for Cancer Research V Scholar Award V2021-035, Bristol-Myers

Squibb – Melanoma Research Alliance Young Investigator Award 689282, University of California Cancer Research Coordinating Committee Award C23CR5537, University of California Academic Senate Bridge Grant BG104446 and Tower Cancer Research Foundation Career Development Award (M.J.H.).

Chapter 2, in full, has been submitted for publication of the material in a research article with the title "Apoptotic DNase DFFB mediates cancer persister cell mutagenesis and acquired drug resistance." The authors are: Williams, August F.; Gervasio, David A.G.; Turkal, Claire E.; Stuhlfire, Anna E.; Wang, Michael X.; Mauch, Brandon E.; Nguyen, Ariel H.; Paw, Michelle H.; Hairani, Mehrshad; Lathrop, Cooper P.; Harris, Sophie H.; Page, Jennifer L.; Hangauer, Matthew J. The dissertation author was the primary researcher and author of this paper.

Figures

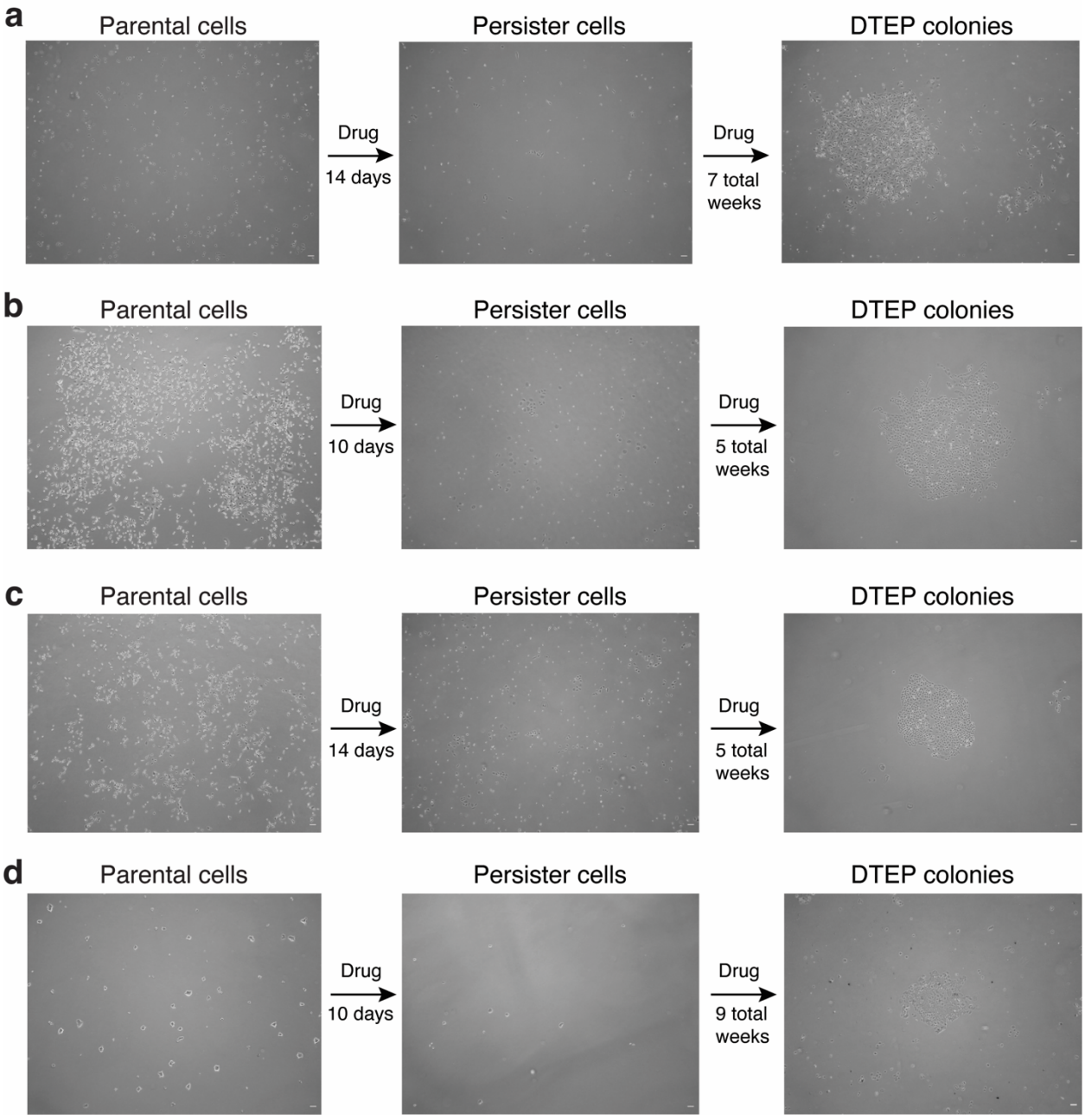

Figure 1: Persister cell and DTEP colony formation models. a, A375 BRAF V600E melanoma cells treated with 250 nM dabrafenib and 25 nM trametinib. **b,** PC9 EGFR mutant lung adenocarcinoma cells treated with 2.5 μM erlotinib. **c,** PC9 cells treated with 500 nM osimertinib. **d,** BT474 HER2+ breast cancer cells treated with 2 μM lapatinib. Time shown to DTEP colony formation includes initial persister cell formation treatment period. Scale bar = 100 μm.

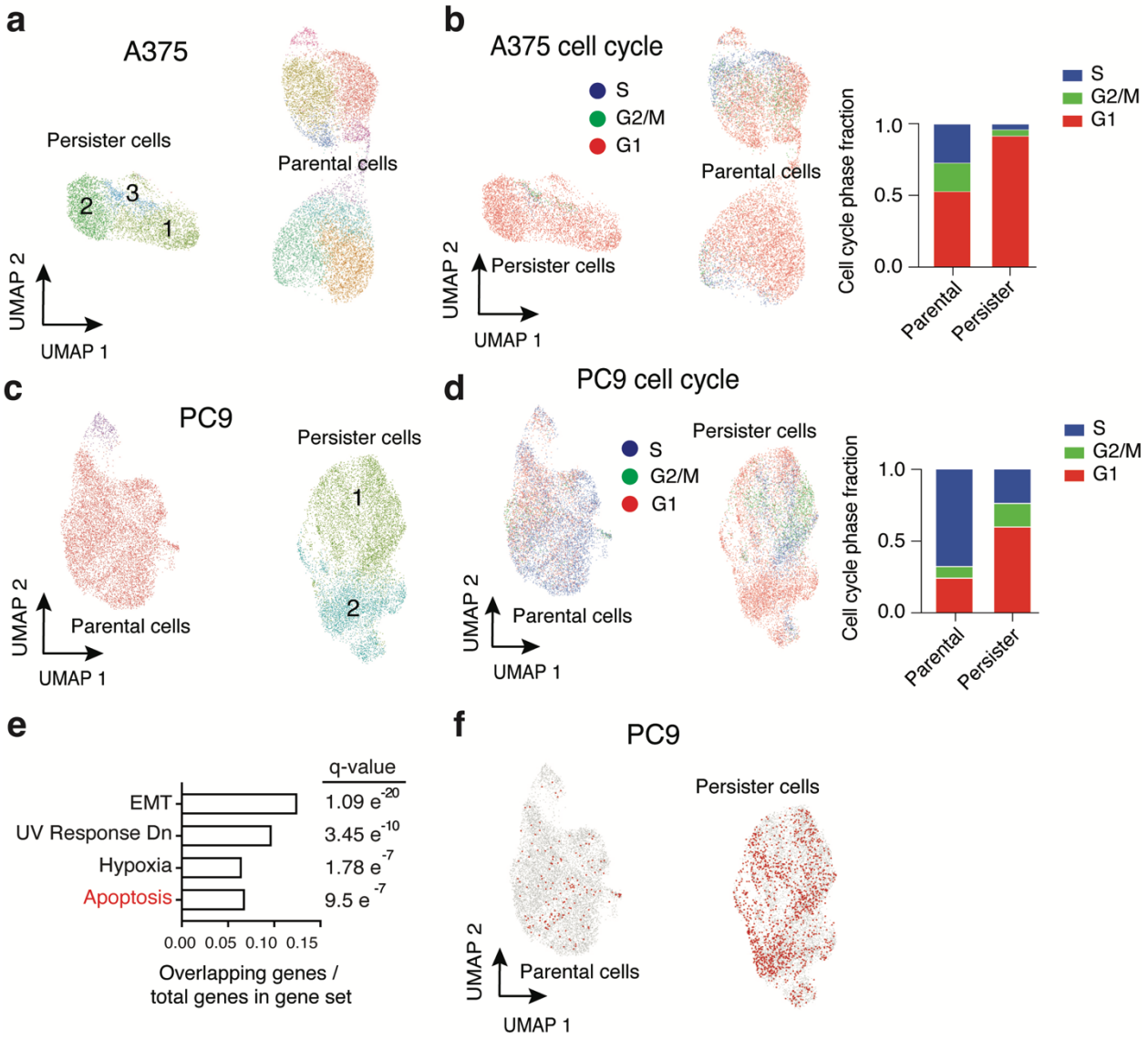

Figure 2: ScRNAseq of parental and persister cells. a-b, ScRNAseq of A375 persister cells treated with 250 nM dabrafenib and 25 nM trametinib compared to untreated parental cells. **a,** A375 UMAP showing clusters within persister and parental populations. See Table 2 for enriched gene sets between persister cell clusters. **b,** A375 UMAP colored by cell cycle stage. Bar graph shows fraction of cells in each cell cycle stage. **c,d** ScRNAseq of PC9 persister cells treated with 2.5 μM erlotinib compared to untreated parental cells. **c,** PC9 UMAP showing clusters within persister and parental populations. See Table 2 for enriched gene sets between persister cell clusters. **d**, PC9 UMAP colored by cell cycle stage. Bar graph shows fraction of cells in each cell cycle stage. **e,** Top enriched Hallmarks gene sets composed of genes upregulated in both A375 and PC9 persister cells versus parental cells. False discovery rate q value represents the Benjamini-Hochberg corrected hypergeometric P value. See Table 2 for all enriched pathways. **f,** PC9 cells with high Hallmarks Apoptosis gene set scores highlighted in red.

Table 1: Gene sets enriched in the scRNAseq persister cell clusters. See methods for cluster differentiation. Clusters are labeled in figure 2a,c.

Cell line	Cluster comparison	Hallmark gene set	NES	q-values
A375	1 vs 2	HALLMARK_EPITHELIAL_MESENCHYMAL_TRANSITION	-2.357825	6.07E-05
	1 vs 2,3	HALLMARK_EPITHELIAL_MESENCHYMAL_TRANSITION	-2.278528	7.66E-05
	2 vs 3	HALLMARK_EPITHELIAL_MESENCHYMAL_TRANSITION	3.054053	3.11E-09
		HALLMARK_UV_RESPONSE_DN	2.439939	1.56E-03
		HALLMARK_APICAL_JUNCTION	2.29862	2.38E-03
		HALLMARK_COAGULATION	2.246135	4.25E-03
		HALLMARK_KRAS_SIGNALING_UP	2.184649	3.15E-03
		HALLMARK_TNFA_SIGNALING_VIA_NFKB	1.977507	1.55E-02
		HALLMARK_KRAS_SIGNALING_DN	1.924557	3.24E-02
		HALLMARK_MTORC1_SIGNALING	-1.826659	1.74E-02
		HALLMARK_MYC_TARGETS_V2	-1.887261	1.55E-02
		HALLMARK_MITOTIC_SPINDLE	-2.549494	5.49E-06
		HALLMARK_MYC_TARGETS_V1	-3.124477	1.05E-09
		HALLMARK_G2M_CHECKPOINT	-3.780707	1.05E-09
		HALLMARK_E2F_TARGETS	-3.800463	1.05E-09
	2 vs 1,3	HALLMARK_EPITHELIAL_MESENCHYMAL_TRANSITION	2.312552	3.70E-05
		HALLMARK_APICAL_JUNCTION	1.900918	1.18E-02
		HALLMARK_CHOLESTEROL_HOMEOSTASIS	-2.055603	1.18E-02
		HALLMARK_MYC_TARGETS_V1	-2.18743	1.18E-02
	3 vs 1	HALLMARK_G2M_CHECKPOINT	3.60733	1.68E-09
		HALLMARK_E2F_TARGETS	3.404151	1.68E-09
		HALLMARK_MITOTIC_SPINDLE	2.770806	5.11E-09
		HALLMARK_MYC_TARGETS_V1	2.355594	8.82E-06
		HALLMARK_GLYCOLYSIS	1.769715	2.21E-02
		HALLMARK_IL2_STAT5_SIGNALING	-1.888872	2.34E-02
		HALLMARK_KRAS_SIGNALING_UP	-1.934763	2.34E-02
		HALLMARK_TNFA_SIGNALING_VIA_NFKB	-2.105538	4.41E-03
		HALLMARK_MYOGENESIS	-2.181728	2.64E-03
		HALLMARK_COAGULATION	-2.363269	1.52E-03
	3 vs 1,2	HALLMARK_G2M_CHECKPOINT	3.582719	1.02E-09
		HALLMARK_E2F_TARGETS	3.396161	1.02E-09
		HALLMARK_MITOTIC_SPINDLE	2.695764	1.26E-07
		HALLMARK_MYC_TARGETS_V1	2.561328	1.58E-07
		HALLMARK_ANGIOGENESIS	-1.919886	1.98E-02
		HALLMARK_UV_RESPONSE_DN	-1.978699	1.04E-02
		HALLMARK_IL2_STAT5_SIGNALING	-2.090516	4.28E-03
		HALLMARK_MYOGENESIS	-2.310895	1.95E-03
		HALLMARK_TNFA_SIGNALING_VIA_NFKB	-2.506182	6.76E-04
		HALLMARK_KRAS_SIGNALING_UP	-2.610102	9.67E-05
		HALLMARK_COAGULATION	-2.777507	8.93E-06
		HALLMARK_EPITHELIAL_MESENCHYMAL_TRANSITION	-3.373715	1.02E-09
PC9	1 vs 2	HALLMARK_G2M_CHECKPOINT	3.427198	1.47E-09
		HALLMARK_E2F_TARGETS	2.915845	1.47E-09
		HALLMARK_MITOTIC_SPINDLE	2.525483	4.80E-06
		HALLMARK_SPERMATOGENESIS	2.052184	4.50E-03
		HALLMARK_MYC_TARGETS_V1	2.030689	2.70E-03
		HALLMARK_FATTY_ACID_METABOLISM	1.84044	1.48E-02
		HALLMARK_EPITHELIAL_MESENCHYMAL_TRANSITION	-1.812951	3.05E-02
		HALLMARK_MYOGENESIS	-1.968918	9.58E-03
		HALLMARK_COMPLEMENT	-2.128217	7.32E-03
		HALLMARK_HYPOXIA	-2.166671	5.62E-03
		HALLMARK_UV_RESPONSE_DN	-2.238077	5.55E-03

Table 2: Enriched Hallmark gene sets from persister cell upregulated genes. Differentially expressed genes shared between A375 and PC9 were investigated with a hypergeometric test to identify enriched pathways.

Gene Set Name [# Genes (K)]	# Genes in Overlap (k)	k/K	p-value	FDR q-value
HALLMARK_EPITHELIAL_MESENCHYMAL_TRANSITION [200]	25	0.125	$2.18\ e^{-22}$	$1.09\ e^{-20}$
HALLMARK_UV_RESPONSE_DN [144]	14	0.097222222	$1.38\ e^{-11}$	$3.45\ e^{-10}$
HALLMARK_HYPOXIA [200]	13	0.065	$1.07\ e^{-8}$	$1.78\ e^{-7}$
HALLMARK_APOPTOSIS [161]	11	0.068322981	$8.78\ e^{-8}$	$9.5\ e^{-7}$
HALLMARK_TNFA_SIGNALING_VIA_NFKB [200]	12	0.06	$9.5\ e^{-8}$	$9.5\ e^{-7}$
HALLMARK_MITOTIC_SPINDLE [199]	11	0.055276382	$7.37\ e^{-7}$	$5.53\ e^{-6}$
HALLMARK_APICAL_JUNCTION [200]	11	0.055	$7.75\ e^{-7}$	$5.53\ e^{-6}$
HALLMARK_ANDROGEN_RESPONSE [100]	8	0.08	$1.57\ e^{-6}$	$9.83\ e^{-6}$
HALLMARK_MYOGENESIS [200]	10	0.05	$5.76\ e^{-6}$	$3.2\ e^{-5}$
HALLMARK_ESTROGEN_RESPONSE_EARLY [200]	9	0.045	$3.87\ e^{-5}$	$1.49\ e^{-4}$
HALLMARK_ESTROGEN_RESPONSE_LATE [200]	9	0.045	$3.87\ e^{-5}$	$1.49\ e^{-4}$
HALLMARK_HEME_METABOLISM [200]	9	0.045	$3.87\ e^{-5}$	$1.49\ e^{-4}$
HALLMARK_OXIDATIVE_PHOSPHORYLATION [200]	9	0.045	$3.87\ e^{-5}$	$1.49\ e^{-4}$
HALLMARK_PROTEIN_SECRETION [96]	6	0.0625	$1.3\ e^{-4}$	$4.48\ e^{-4}$
HALLMARK_COAGULATION [138]	7	0.050724638	$1.34\ e^{-4}$	$4.48\ e^{-4}$
HALLMARK_GLYCOLYSIS [200]	8	0.04	$2.33\ e^{-4}$	$6.85\ e^{-4}$
HALLMARK_INTERFERON_GAMMA_RESPONSE [200]	8	0.04	$2.33\ e^{-4}$	$6.85\ e^{-4}$

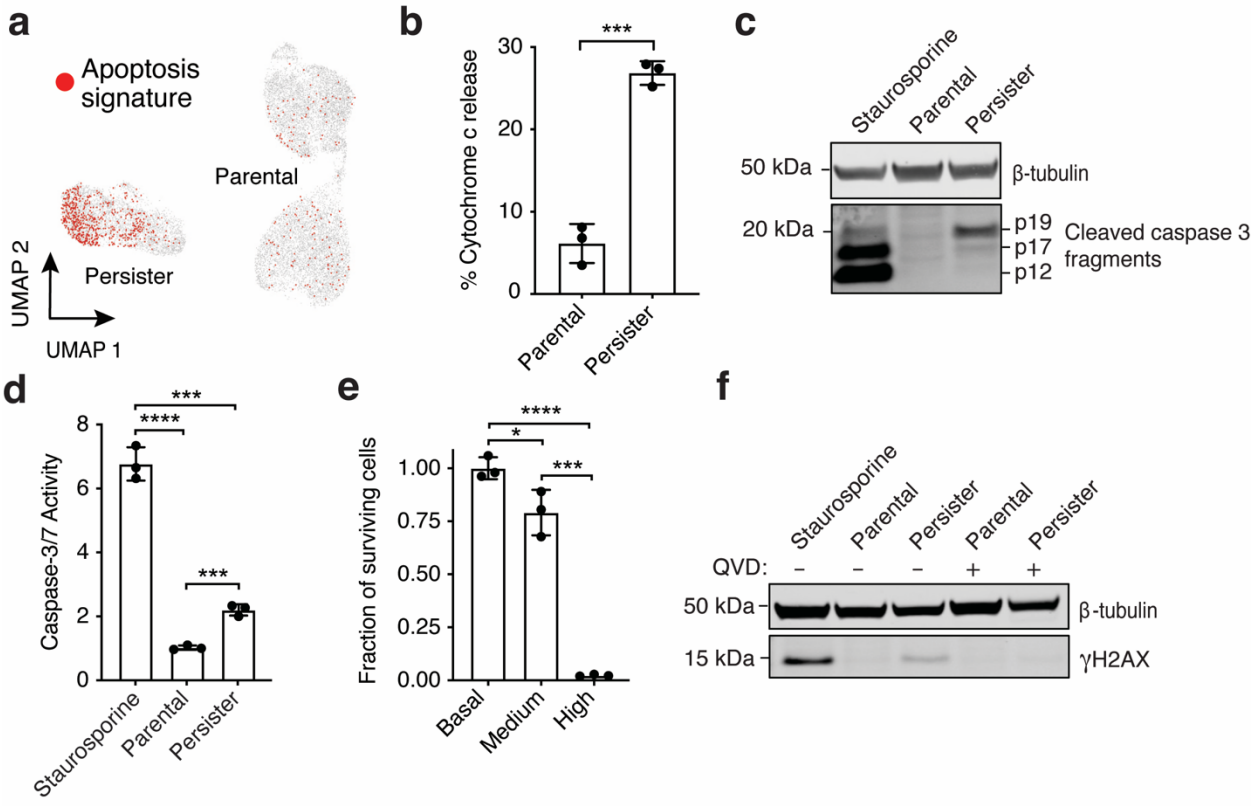

Figure. 3: Drug-tolerant persister cells undergo sublethal apoptotic signaling-induced DNA damage. a, ScRNAseq UMAP of A375 parental cells and persister cells derived from 2 weeks of treatment with 250 nM dabrafenib and 25 nM trametinib. Cells with enriched Hallmarks Apoptosis gene set are highlighted in red. **b**, A375 parental and persister cells assessed for mitochondrial release of cytosolic cytochrome c as a readout for mitochondrial outer membrane permeability (MOMP) with flow cytometry measurement of live-gated cells. **c**, Western blot of A375 persister cells and parental cells measuring cleaved caspase 3 fragments. **d**, Flow cytometry quantification of caspase 3/7 activity reporter geometric means. **e**, A375 persister cells were sorted for basal, medium (sublethal), and high (lethal) caspase 3/7 activity, replated in media without drug, and assessed for cell viability the following day. **f**, A375 parental and persister cells derived with 250 nM dabrafenib and 25 nM trametinib for 2 weeks assessed for DNA damage marker γH2AX with and without co-treatment of 10 μM caspase inhibitor QVD. For all experiments, persister cells were pre-derived with drug treatment and assayed while maintained in drug unless otherwise noted. **c**,**d**,**f**, Parental cells treated for 24 hours with 250 nM **(c,f)** or 4 hours with 1 μM **(d)** staurosporine were used as a positive control. **b**,**d**,**e**, n = 3 biological replicates; mean ± s.d. is shown; P values calculated with two-tailed Student's t-test, *P<0.05; ***P<0.001; ****P<0.0001.

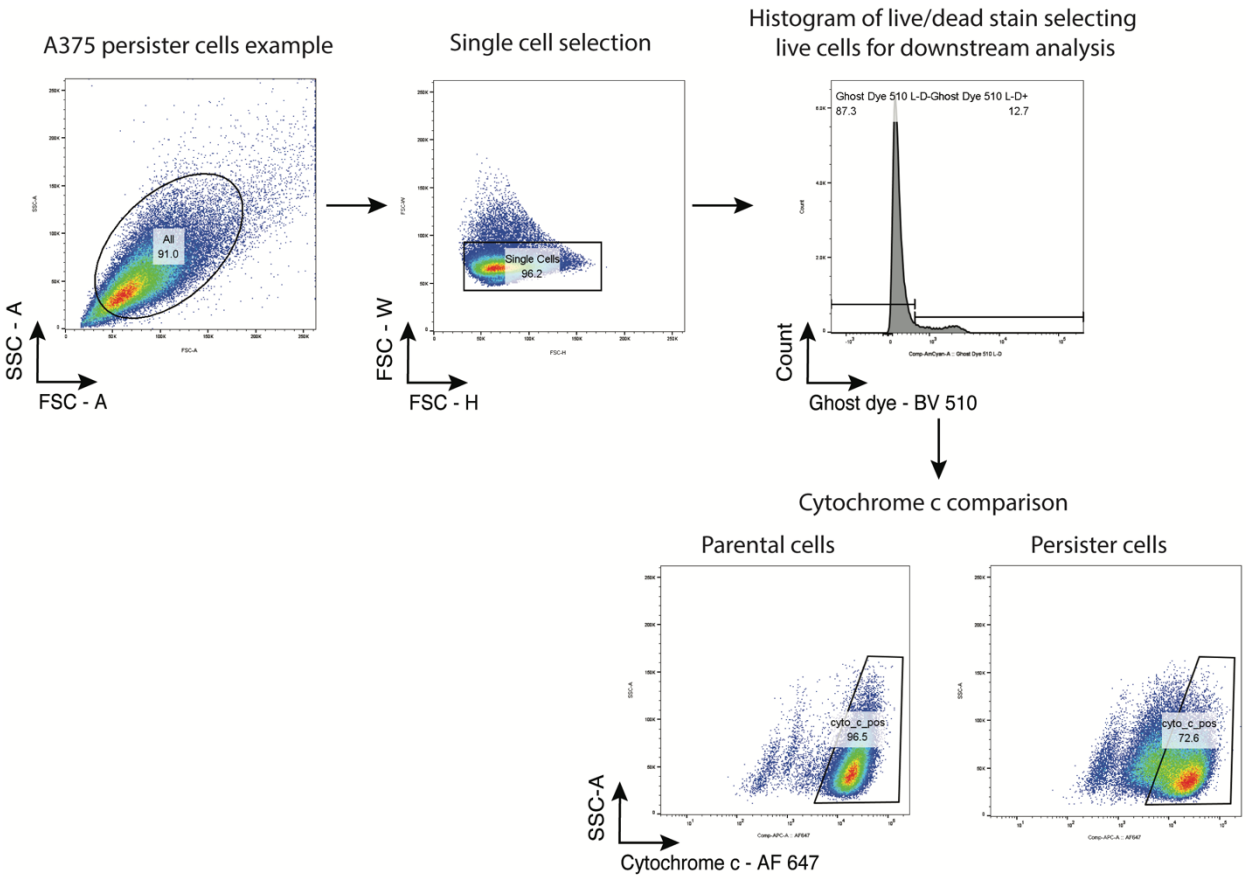

Figure 4: Mitochondrial release of cytochrome c flow cytometry assay schematic. Gating strategy used for A375 parental cells and persister cells derived from treatment with 250 nM dabrafenib and 25 nM trametinib in Figure 1b. See methods for details of this assay.

Figure 5: Persister cells survive drug induced sublethal apoptotic signaling that causes DNA damage. a, A375 parental and persister cells assessed for incomplete loss of mitochondrial (MT) potential using JC-1 indicator dye by flow cytometry measurement of live-gated cells. See Supplementary Fig. 3 for gating strategy. **b**, Quantification of cleaved caspase 3 geometric mean from flow cytometry of live-gated cells. See Supplementary Fig. 4 for gating strategy. **c**, Relative growth in drug-free media for 6 days of A375 persister cells after sorting for basal caspase 3/7 activity or medium (sublethal elevated) caspase 3/7 activity. See Supplementary Fig. 5 for gating and sorting strategy. **d**, A375 cells treated with 250 nM dabrafenib and 25 nM trametinib for 24 or 48 hours and assessed for cleaved caspase 3 or DNA damage marker γH2AX. 250 nM staurosporine treatment for 24 hours was used as a positive control. **e**, A375 persister cells derived from 2 weeks of treatment with 250 nM dabrafenib and 25 nM trametinib were assessed for cleaved caspase 3 or γH2AX following 1, 3, and 6 days of drug removal. 250 nM staurosporine treatment for 24 hours was used as a positive control. **f-h**, Parental and persister cells assessed by western blot for γH2AX with and without treatment with 10 μM caspase inhibitor QVD. Parental cells treated for 24 hours 500 nM staurosporine (PC9) or 750 nM staurosporine (BT474) were used as a positive control. **f,** PC9 cells treated with 2.5 μM erlotinib. **g,** PC9 cells treated with 500 nM osimertinib. **h,** BT474 cells treated with 500 nM lapatinib. **i**, A375 parental and persister cells assessed by flow cytometry of live-gated cells for γH2AX geometric mean fluorescence with and without 10 μM QVD. See Supplementary Fig. 6 for gating strategy. **j**, A375 persister cells exhibit caspase-dependent cleaved DFFA indicating DFFB activation. Conditions with caspase inhibitor were treated with 10 μM QVD for the duration of the experiment. For all experiments, persister cells were pre-derived with drug treatment and assayed while maintained in drug. For **a**, **b**, **c**, **i**, $n = 3$ biological replicates, mean ± s.d.; two-tailed Student's t-test; *P<0.05; **P<0.01; ns, not significant.

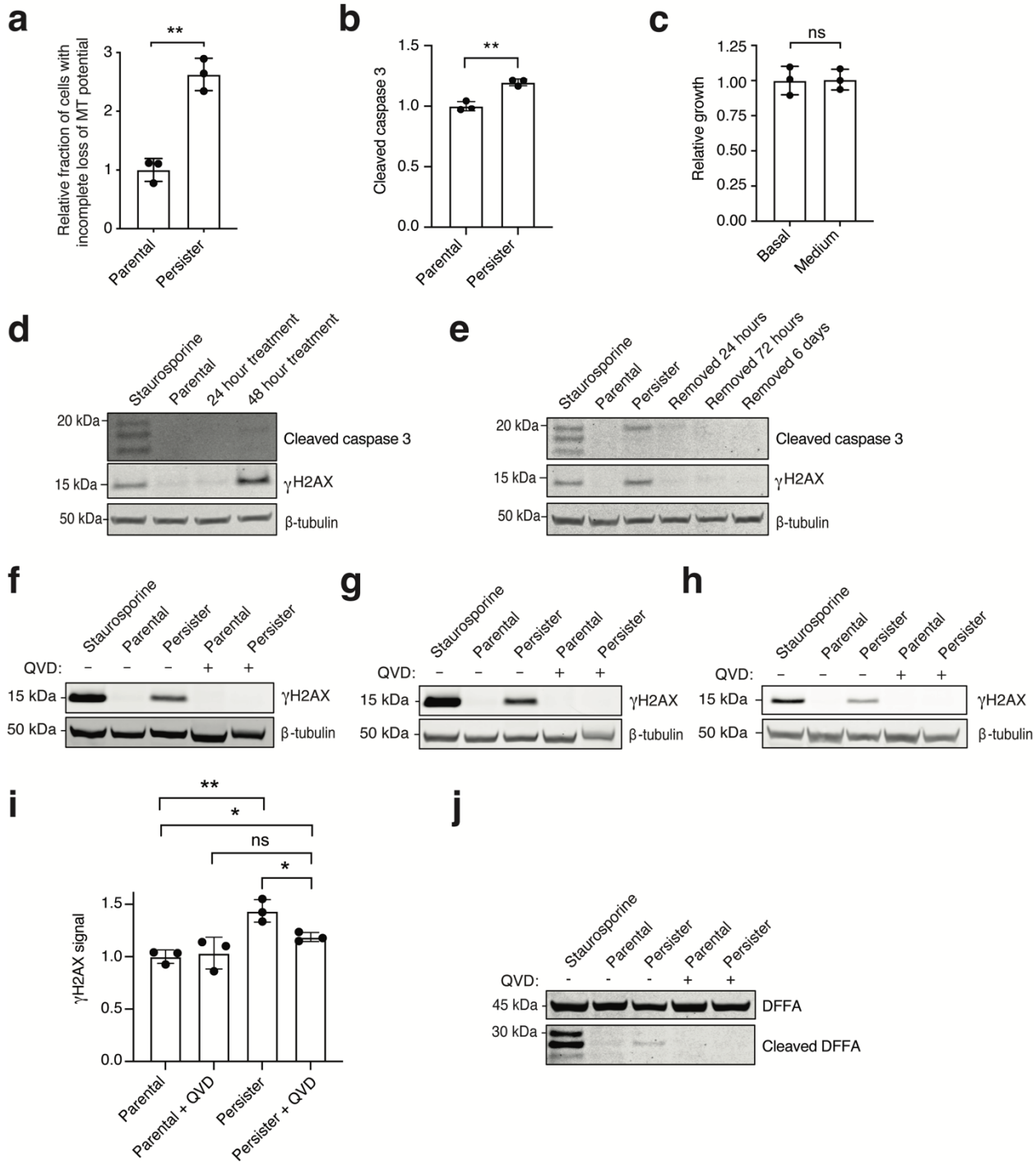
a
Relative fraction of cells with incomplete loss of MT potential
**
Parental
Persister
b
Cleaved caspase 3
**
Parental
Persister
c
Relative growth
ns
Basal
Medium
d
Staurosporine
Parental
24 hour treatment
48 hour treatment
20 kDa
Cleaved caspase 3
15 kDa
γH2AX
50 kDa
β-tubulin
e
Staurosporine
Parental
Persister
Removed 24 hours
Removed 72 hours
Removed 6 days
20 kDa
Cleaved caspase 3
15 kDa
γH2AX
50 kDa
β-tubulin
f
Staurosporine
Parental
Persister
Parental
Persister
QVD: − − − + +
15 kDa
γH2AX
50 kDa
β-tubulin
g
Staurosporine
Parental
Persister
Parental
Persister
QVD: − − − + +
15 kDa
γH2AX
50 kDa
β-tubulin
h
Staurosporine
Parental
Persister
Parental
Persister
QVD: − − − + +
15 kDa
γH2AX
50 kDa
β-tubulin
i
**
*
ns
*
γH2AX signal
Parental
Parental + QVD
Persister
Persister + QVD
j
Staurosporine
Parental
Persister
Parental
Persister
QVD: - - - + +
45 kDa
DFFA
30 kDa
Cleaved DFFA

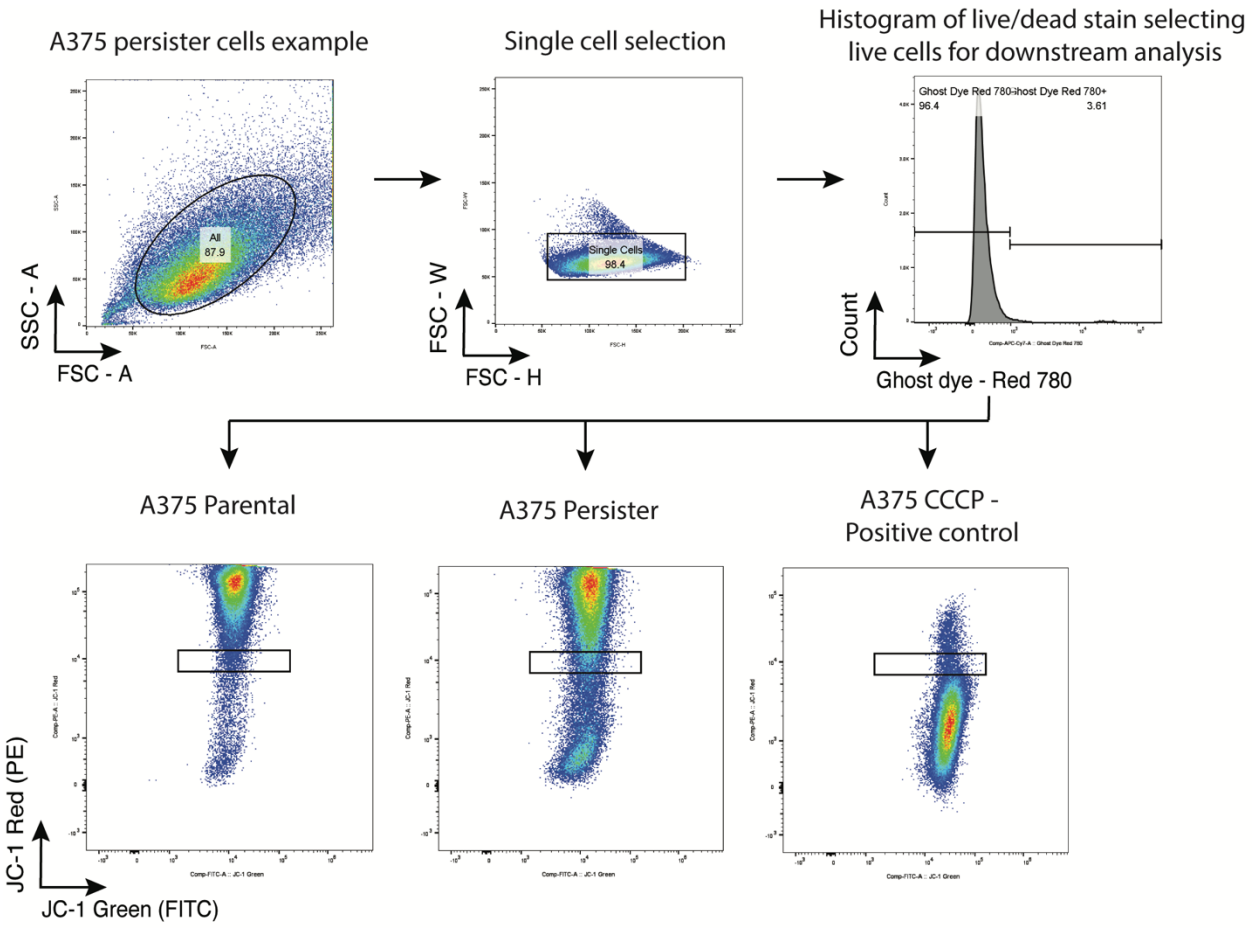

Figure 6: Flow cytometry schematic for JC-1 indicator dye-based assessment of loss of mitochondrial potential. Gating strategy used for Extended Data Figure 3a. Representative flow cytometry gating for loss of mitochondrial potential in A375 parental cells and persister cells treated with 250 nM dabrafenib and 25 nM trametinib. Results from triplicate biological replicates are presented in Extended Data Figure 3a. For the positive control, cells were treated with mitochondrial oxidative phosphorylation uncoupler carbonyl cyanide m-chlorophenylhydrazone (CCCP) (50 μM) for 5 minutes. Gating was set to compare relative levels of incomplete loss of mitochondrial potential, indicated by intermediate levels of loss of JC-1 red fluorescence, as illustrated.

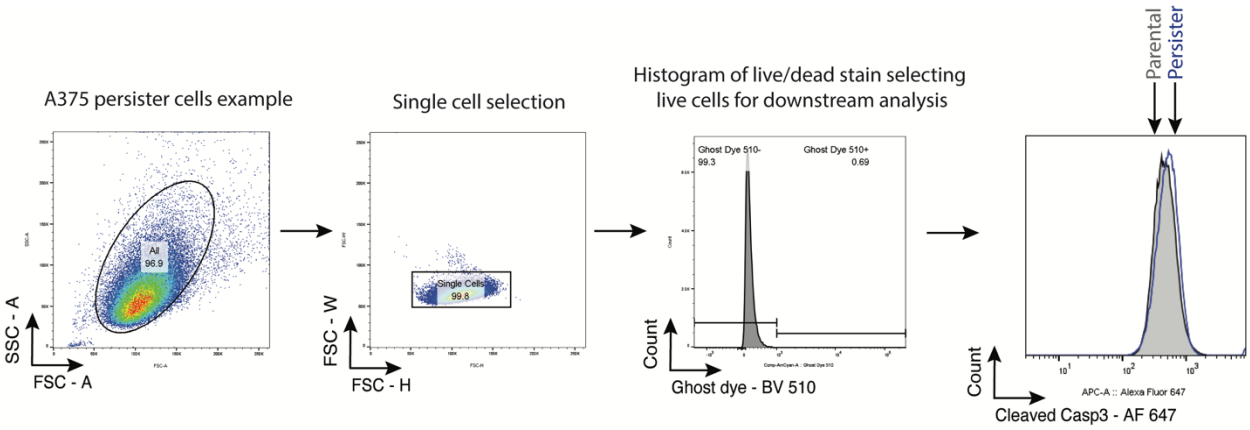

Figure 7: Cleaved caspase 3 flow cytometry schematic. Gating strategy used for A375 parental cells and persister cells derived from treatment with 250 nM dabrafenib and 25 nM trametinib in Extended Data Figure 3b.

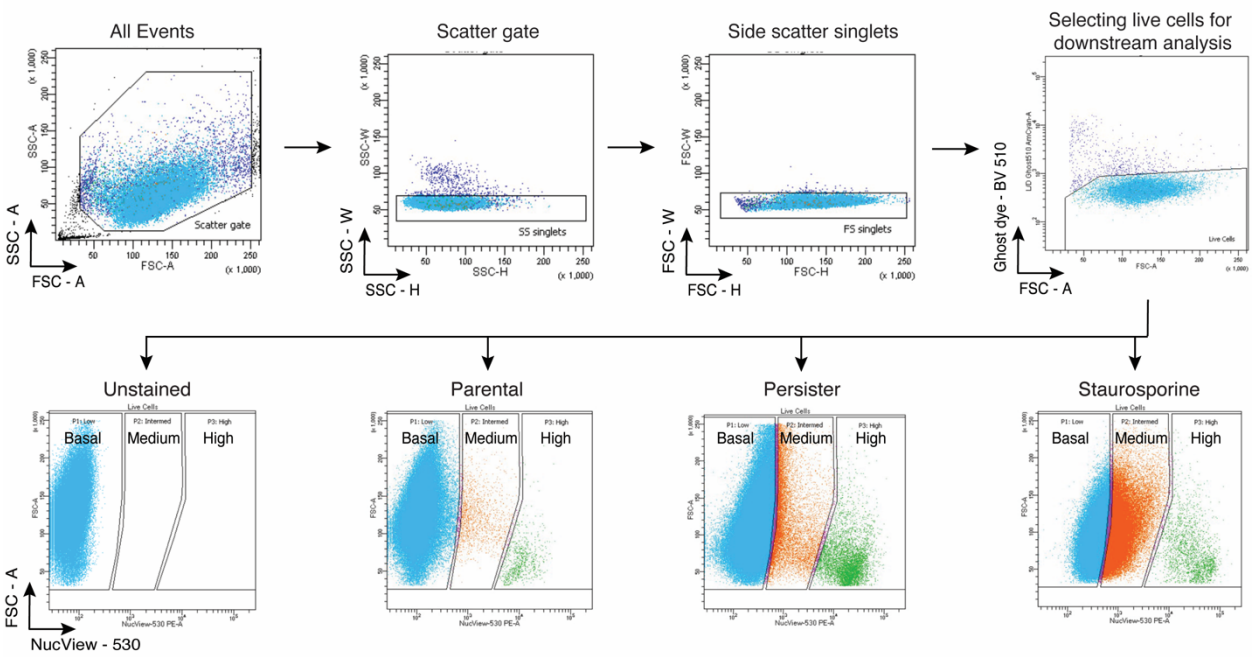

Figure 8: Caspase 3/7 activity reporter flow cytometry schematic. a, Representative gating strategy for sorting caspase 3/7 activity sensor levels in A375 parental cells, persister cells treated with 250 nM dabrafenib and 25 nM trametinib, and staurosporine- treated positive control cells. Representative caspase 3/7 activity sensor levels for each condition shown in bottom row. This gating strategy was used to sort the Basal, Medium and High Caspase 3/7 activity level persister cell populations for Figure 1d,e and Extended Data Figure 3c.

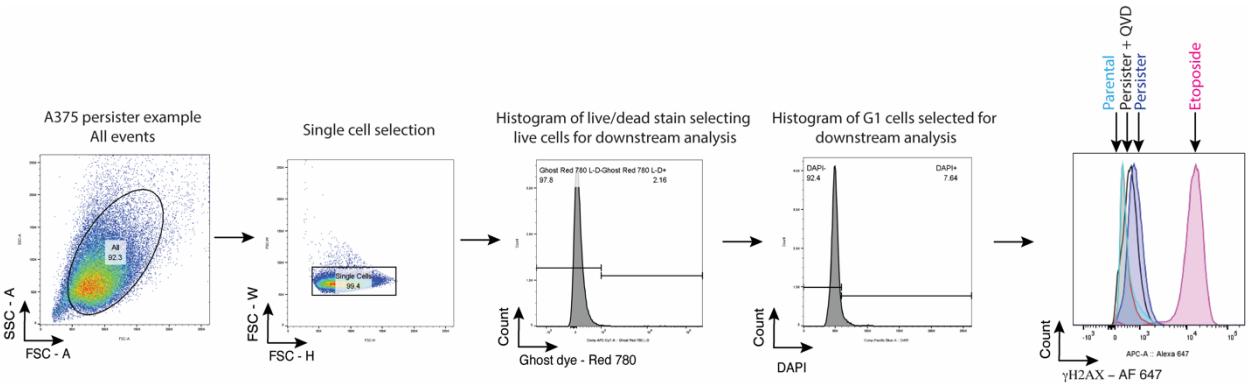

Figure 9: γH2AX DNA damage flow cytometry schematic. Representative flow cytometry gating for γH2AX in A375 parental cells, persister cells treated with 250 nM dabrafenib and 25 nM trametinib, and positive control etoposide-treated cells. 10 μM QVD co- treatment was present for the duration of the experiment for QVD treated cells. Parental cell treatment with 100 μM etoposide for 30 minutes was used as a positive control. This gating was used for Extended Data Fig. 3i.

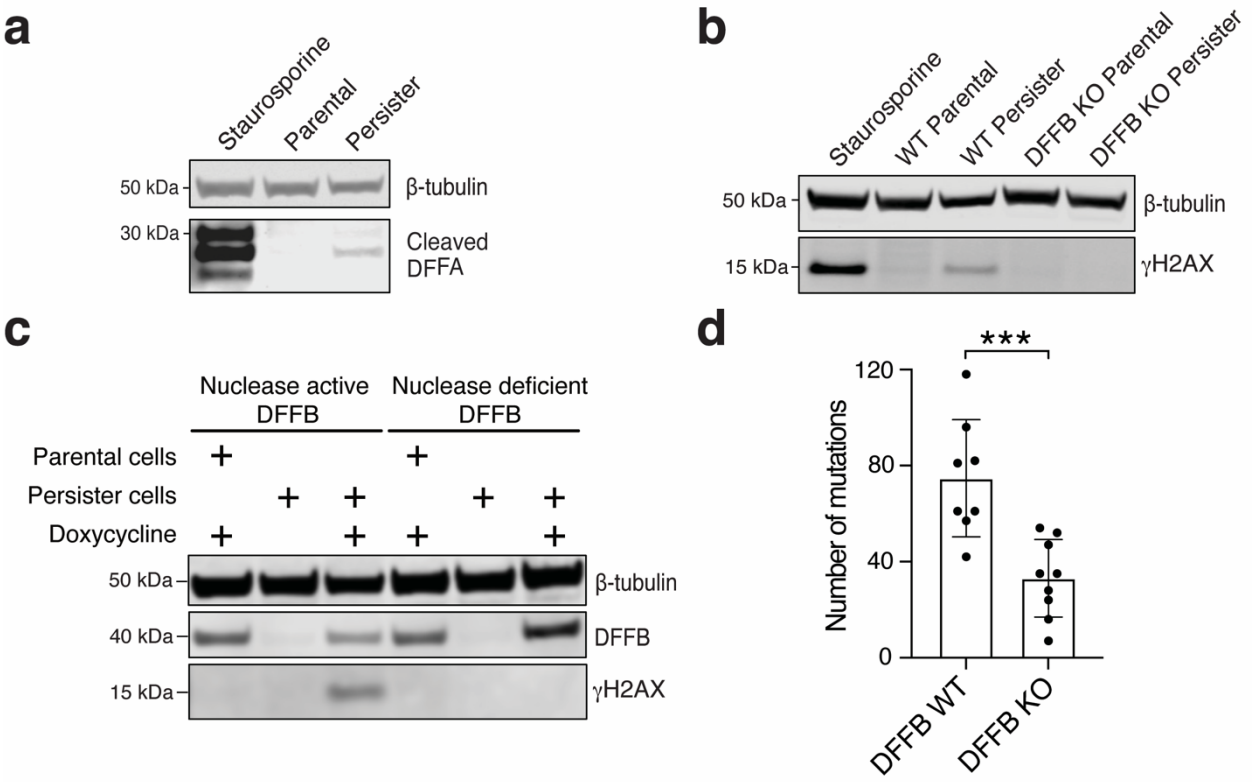

Figure 10: Apoptotic DNase DFFB mediates persister cell DNA damage and mutagenesis. a, A375 persister cells exhibit cleaved DFFA indicating DFFB activation. **b**, A375 persister cell DNA damage is absent in DFFB KO persister cells. In **a** and **b**, 250 nM staurosporine treatment for 24 hours was used as positive control. **c**, Doxycycline-inducible re-expression of nuclease active DFFB, but not nuclease dead DFFB in DFFB KO A375 persister cells restores drug-induced DNA damage. **d,** Whole exome sequencing analysis of mutations acquired by DFFB WT and KO #1 A375 cells during 7 weeks of dabrafenib and trametinib treatment. Data points represent genotypes of individual cells which were isolated following treatment, expanded without drug and whole exome sequenced. n = 8 WT biological replicates and 9 DFFB KO biological replicates; mean ± s.d.; two-tailed Student's t-test. **P<0.01; ***P<0.001. For all experiments, persister cells were pre-derived with drug treatment and assayed while maintained in drug unless otherwise noted.

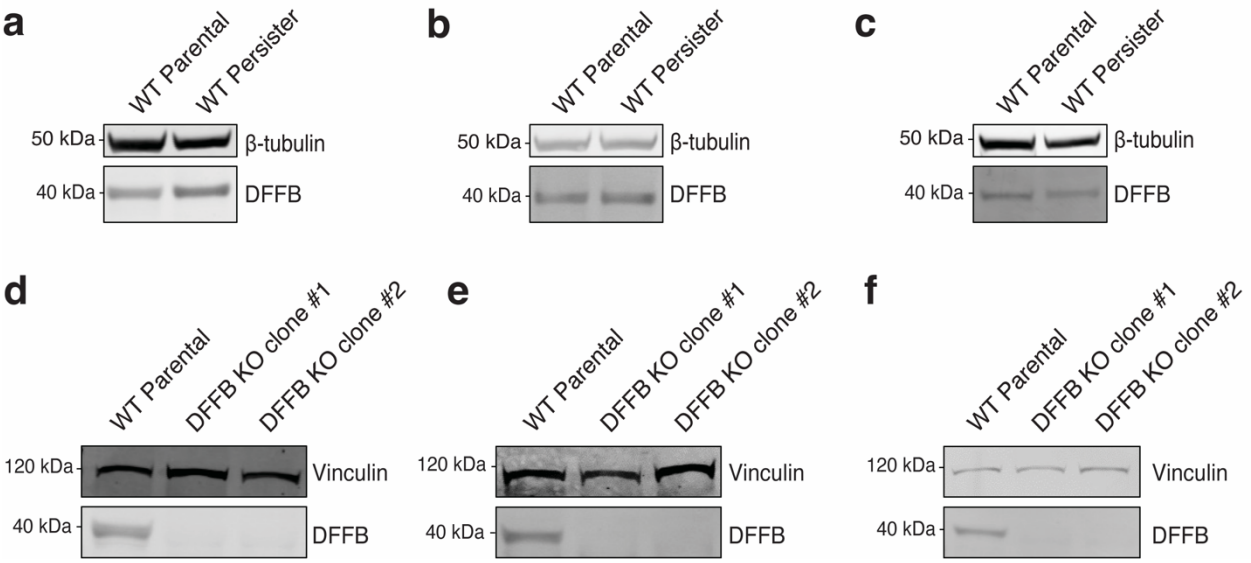

Figure 11: DFFB expression in persister cell models. a-c, DFFB expression in parental and persister cells. **a,** A375 cells treated with 250 nM dabrafenib and 25 nM trametinib. **b,** PC9 cells treated with 2.5 μM erlotinib. **c,** BT474 cells treated with 500 nM lapatinib. **d-f,** DFFB loss of expression in CRISPR KO clones. **d,** A375 DFFB KO clones. **e,** PC9 DFFB KO clones. **f,** BT474 DFFB KO clones. For all experiments, persister cells were pre-derived with drug treatment and assayed while maintained in drug.

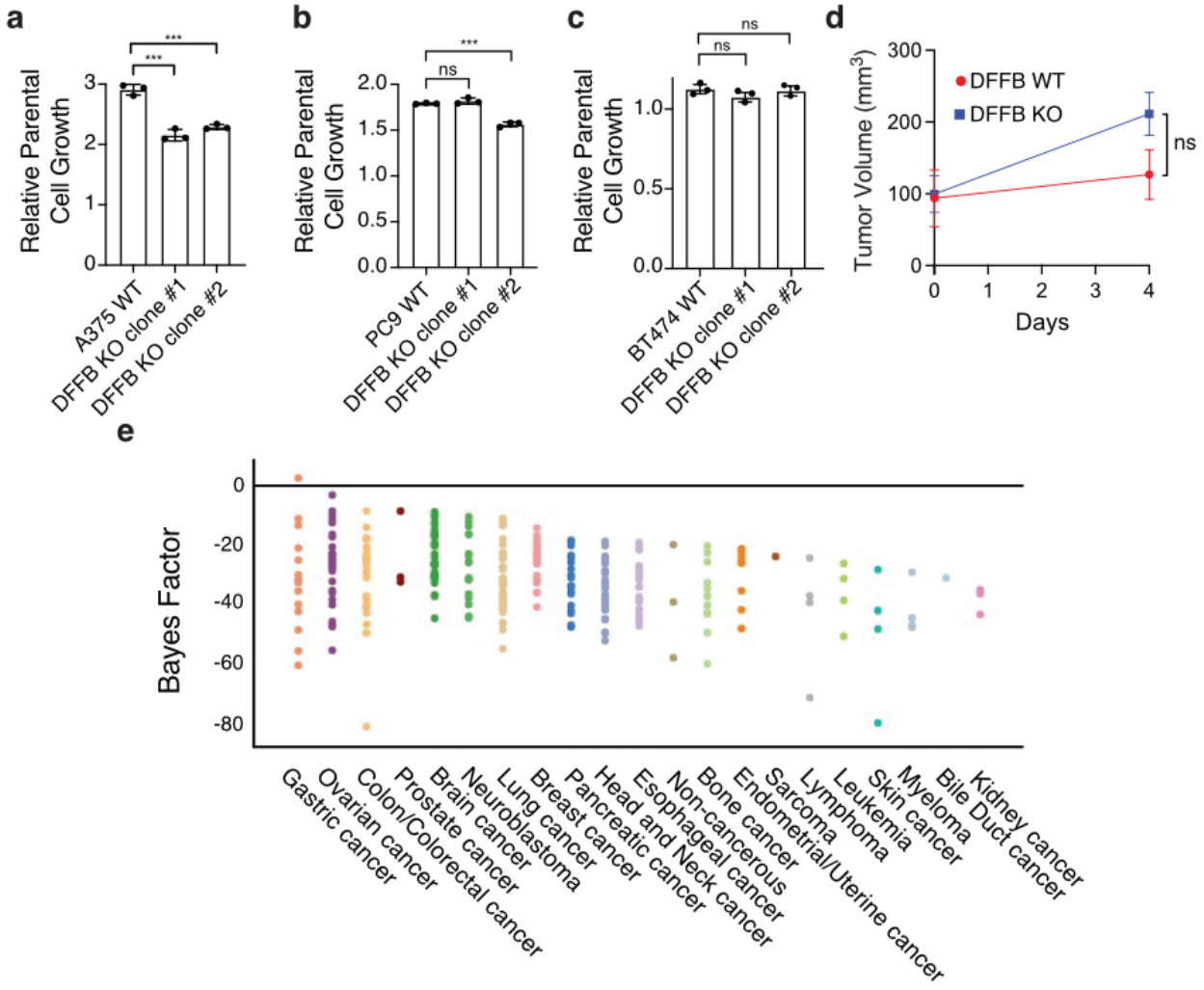

Figure 12: DFFB loss has minimal effect on parental cancer cell viability. a-c, Cell growth rates in cell culture for (**a**) A375, (**b**) PC9 and (**c**) BT474 parental DFFB WT cells and DFFB KO clones. *n* = 3 biological replicates; mean ± s.d. is shown; P values calculated with two-tailed Student's t-test; ***P<0.001; ns, not significant. **d,** A375 WT and DFFB KO growth rates when injected into mice. *n* = 6 biological replicates; mean ± s.d. is shown; P values calculated with two-tailed Student's t-test; ns, not significant. **e,** DFFB essentiality assessed using CRISPR screen data across many cell lines from the PICKLES database using the Score/Sanger dataset from the indicated cancer types. Negative scores reflect non-essentiality.[174]

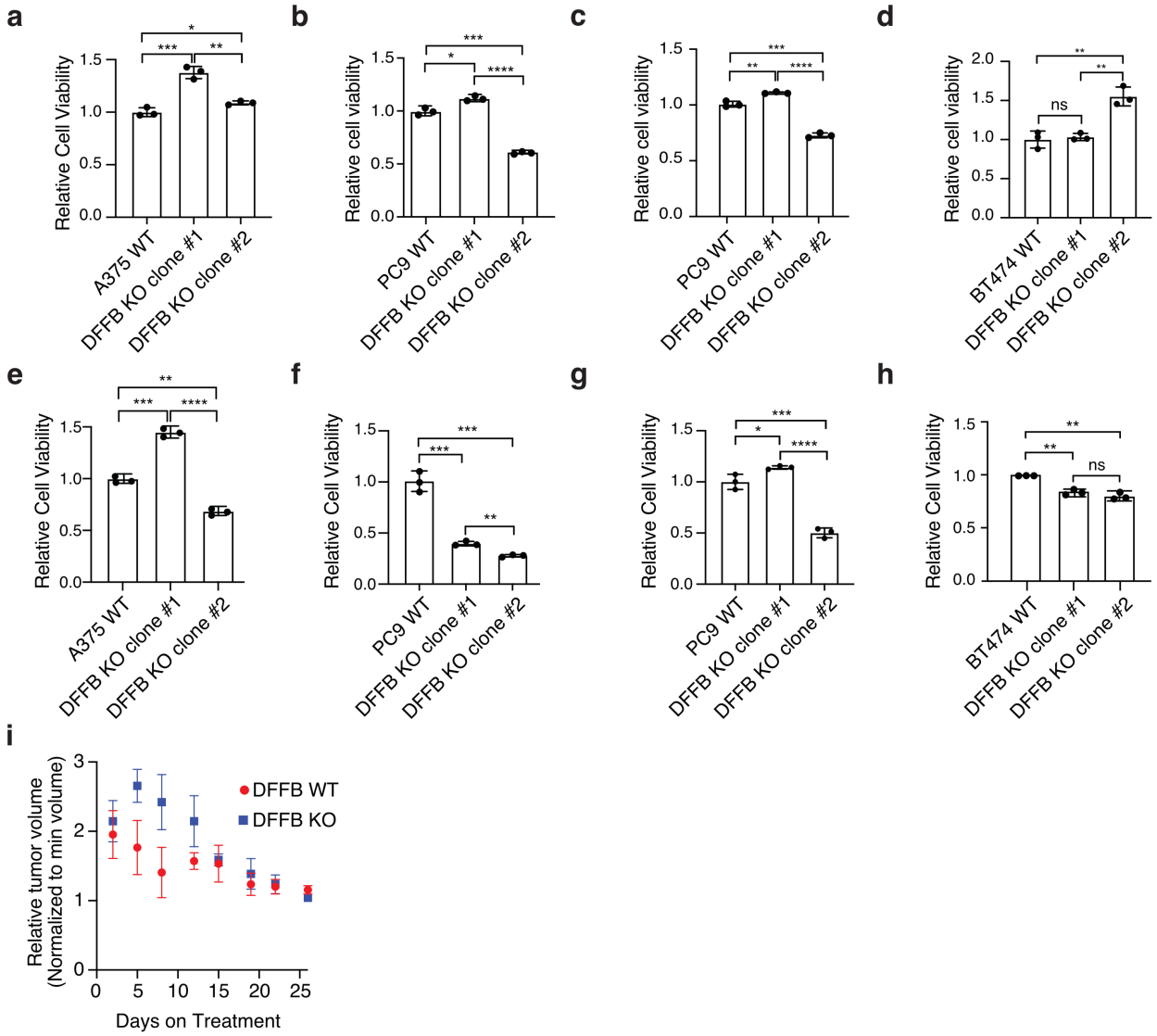

Figure 13: Initial drug response and persister cell formation is independent of DFFB. a-d, Quantification of WT and DFFB KO cell initial 3 day drug treatment response. **a,** A375 cells treated with 250 nM dabrafenib and 25 nM trametinib. **b,** PC9 cells treated with 2.5 μM erlotinib. **c,** PC9 cells treated with 500 nM osimertinib. **d,** BT474 cells treated with 2 μM lapatinib. **e-h,** Quantification of WT and DFFB KO persister cell formation. **e,** A375 cells treated with dabrafenib and trametinib. **f,** PC9 cells treated with erlotinib. **g,** PC9 cells treated with osimertinib. **h,** BT474 cells treated with lapatinib. For **a-h**, $n = 3$ biological replicates; mean ± s.d. is shown; P values calculated with two-tailed Student's t-test. *P<0.05; **P<0.01; ***P<0.001; ****P<0.0001; ns, not significant. **i**, A375 WT and DFFB KO xenograft models treated with dabrafenib and trametinib and monitored for tumor volume. $n = 6$ biological replicates; mean ± s.d. is shown.

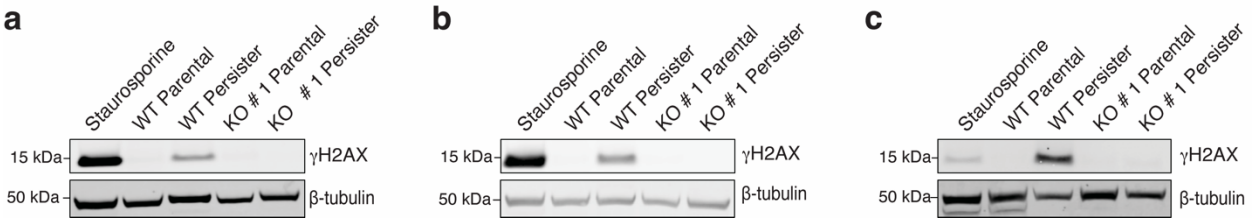

Figure 14: DFFB is required for drug-induced persister cell DNA damage. a-c, Cells were assessed for DNA damage marker γH2AX. Parental cells were treated for 24 hours with 500 nM staurosporine (PC9) or 750 nM staurosporine (BT474) as a positive control. **a,** PC9 persister cells were treated with 2.5 μM erlotinib. **b,** PC9 persister cells were treated with 500 nM osimertinib. **c,** BT474 persister cells were treated with 500 nM lapatinib. For all experiments, persister cells were pre-derived with drug treatment and assayed while maintained in drug.

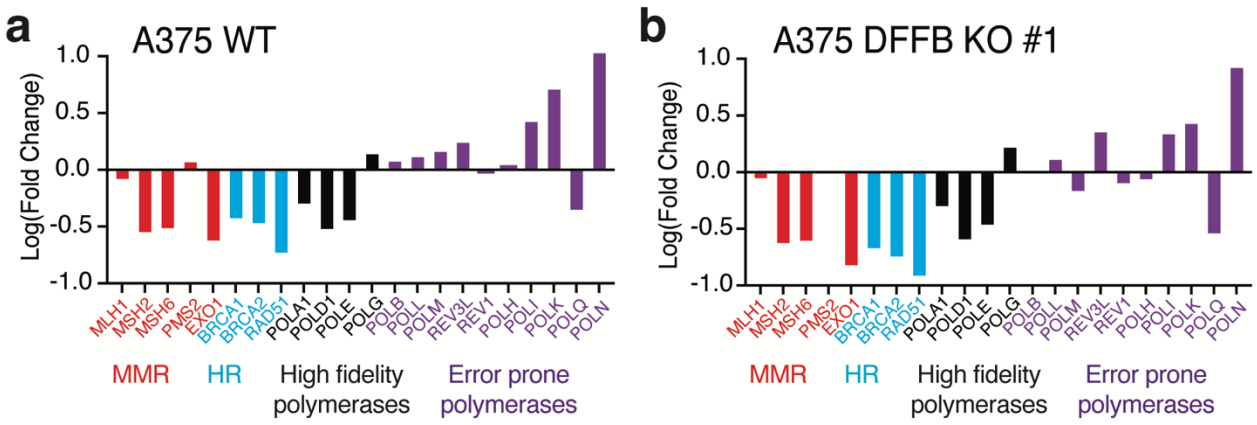

Figure 15: A375 DFFB WT and KO persister cells have similar differential expression of DNA repair genes. a-b, Log(Fold Change) of scRNAseq mean expression values in persister cells compared to parental cells are shown. **a,** A375 WT cells. **b,** A375 DFFB KO clone #1 cells. Mismatch repair (MMR); homology-directed repair (HR).

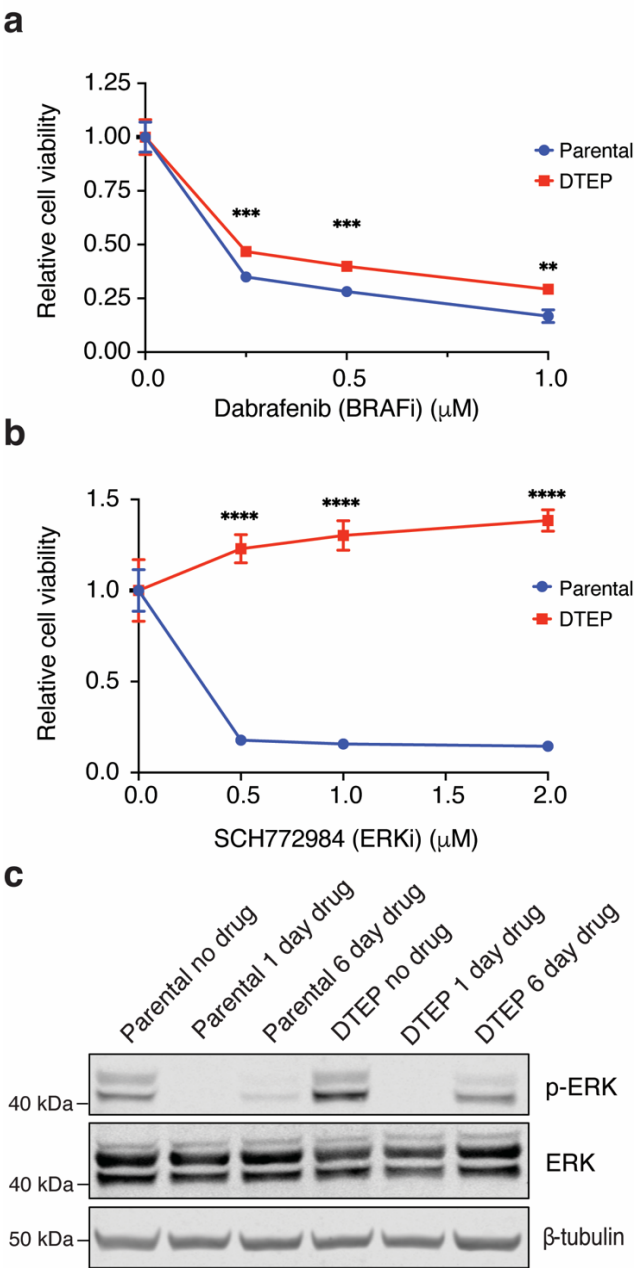

Figure 16: Acquired *BRAF* p.R252* mutation DTEP cells have altered drug response. a, A375 DTEP cells with an acquired *BRAF* p.R252* mutation (DTEP clone WT-4) were treated with dabrafenib for 3 days and compared to nonmutated A375 parental cells. Data are normalized to untreated cells. **b**, A375 *BRAF* p.R252* mutant DTEP cells and nonmutated parental cells were treated with 250 nM dabrafenib, 25 nM trametinib, and ERK inhibitor SCH772984 for 14 days. **c**, A375 *BRAF* p.R252* mutant DTEP cells and nonmutated parental cells were assessed for phosphorylated ERK (p-ERK) following treatment with 1 μM dabrafenib and 100 nM trametinib for 1 or 6 days. **a-c**, All cells were maintained in drug-free media prior to these experiments. For **a**,**b**, $n = 3$ biological replicates; mean ± s.d. is shown; P values calculated with two-tailed Student's t-test. **P<0.01; ***P<0.001; ****P<0.0001.

Figure 17: DFFB mediated DNA damage inhibits growth suppressive interferon signaling. **a**, ScRNAseq analysis of Hallmark enriched gene sets in A375 DFFB WT compared to DFFB KO clone #1 cells treated with 250 nM dabrafenib and 25 nM trametinib for 2 weeks. **b**, UMAP of A375 WT and DFFB KO cells treated for 2 weeks with 250 nM dabrafenib and 25 nM trametinib. Cells with enriched Hallmarks Interferon gamma response gene set are highlighted in red. **c**, ScRNAseq analysis of Hallmark enriched gene sets in A375 DFFB WT compared to DFFB KO clone #1 cells treated with 250 nM dabrafenib and 25 nM trametinib for 9 weeks. **a,c**; False discovery rate q value represents the Benjamini-Hochberg corrected P value. Negative normalized enrichment scores indicate relative depletion of the gene set in DFFB WT persister cells. **d**, UMAP of A375 WT and DFFB KO cells treated for 2 weeks with 250 nM dabrafenib and 25 nM trametinib. Cells with enriched Hallmarks Interferon gamma response gene set are highlighted in red. **e**, UMAPs of A735 WT and DFFB KO persister cells colored with indicated gene expression levels. **f-k**, Parental and persister cells were assessed for (**f-g**) STING or (**h-k**) STAT1. A375 persister cells were treated with 250 nM dabrafenib and 25 nM trametinib. PC9 persister cells were treated with 500 nM osimertinib. (**j**) 10 μM QVD or 50 μM LEHD were added to pre-derived persister cells for 3 days. (**k**) 10 μM QVD was added with osimertinib for the duration of the 10 day treatment. **l**, Effect of JAK inhibition on DTEP colony formation. A375 WT and DFFB KO cells were treated with 250 nM dabrafenib and 25 nM trametinib for 2 weeks to derive persister cells, then 1 μM JAK inhibitor ruxolitinib was added and all three drugs were maintained for the remaining 5 week duration of the experiment. DTEP fraction refers to the fraction of all surviving cells which regrew into DTEP colonies; $n = 3$ biological replicates; mean ± s.d. is shown; P values calculated with two-tailed Student's t-test. *P<0.05, **P<0.01; ***P<0.001.

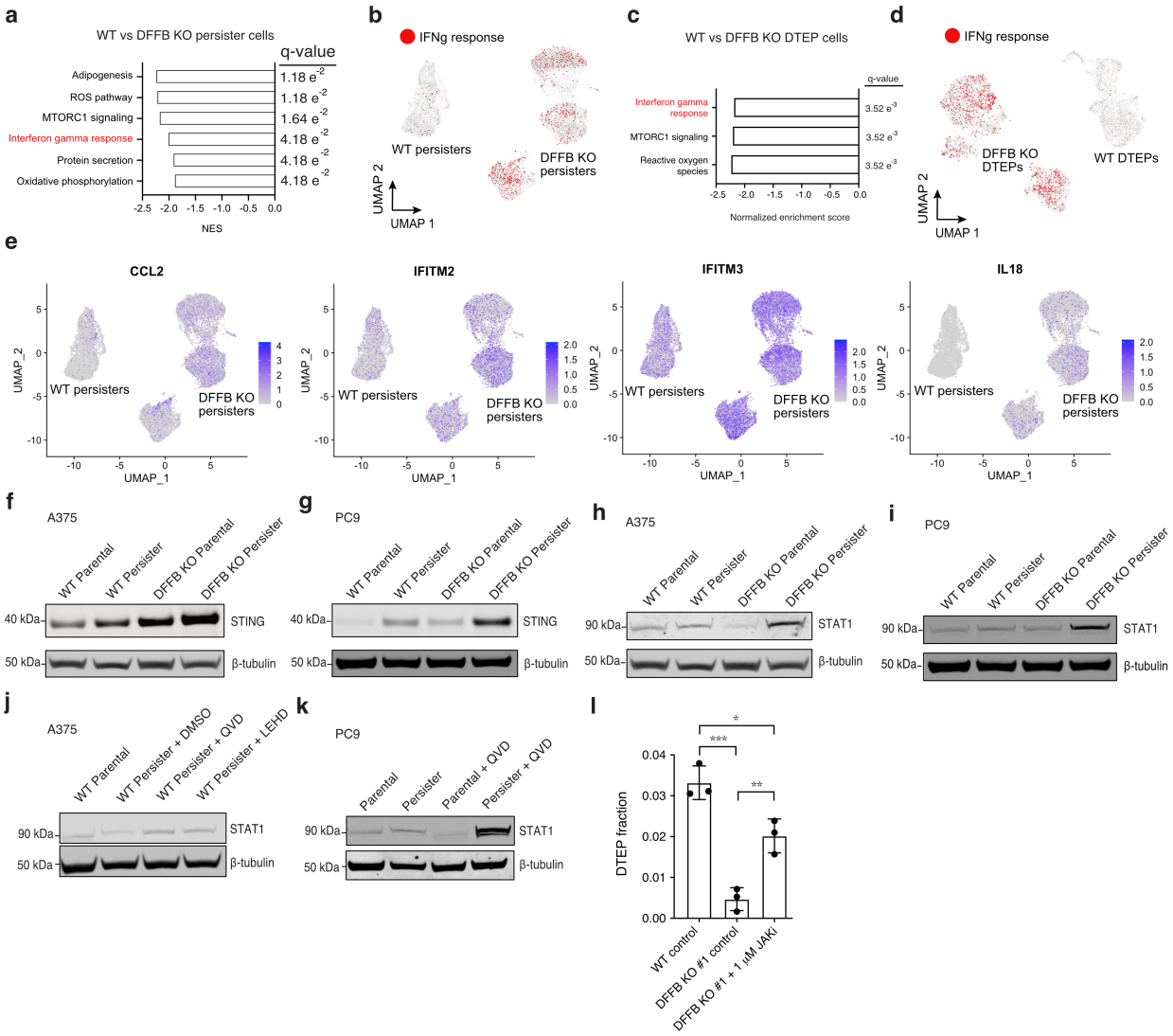
a
WT vs DFFB KO persister cells
q-value
Adipogenesis
ROS pathway
MTORC1 signaling
Interferon gamma response
Protein secretion
Oxidative phosphorylation
1.18 e-2
1.18 e-2
1.64 e-2
4.18 e-2
4.18 e-2
4.18 e-2
-2.5 -2.0 -1.5 -1.0 -0.5 0.0
NES
b
IFNg response
WT persisters
DFFB KO persisters
UMAP 2
UMAP 1
c
WT vs DFFB KO DTEP cells
q-value
Interferon gamma response
MTORC1 signaling
Reactive oxygen species
3.52 e-3
3.52 e-3
3.52 e-3
-2.5 -2.0 -1.5 -1.0 -0.5 0.0
Normalized enrichment score
d
IFNg response
DFFB KO DTEPs
WT DTEPs
UMAP 2
UMAP 1
e
CCL2
IFITM2
IFITM3
IL18
WT persisters
DFFB KO persisters
UMAP_2
UMAP_1
f
A375
WT Parental
WT Persister
DFFB KO Parental
DFFB KO Persister
40 kDa
STING
50 kDa
β-tubulin
g
PC9
WT Parental
WT Persister
DFFB KO Parental
DFFB KO Persister
40 kDa
STING
50 kDa
β-tubulin
h
A375
WT Parental
WT Persister
DFFB KO Parental
DFFB KO Persister
90 kDa
STAT1
50 kDa
β-tubulin
i
PC9
WT Parental
WT Persister
DFFB KO Parental
DFFB KO Persister
90 kDa
STAT1
50 kDa
β-tubulin
j
A375
WT Parental
WT Persister + DMSO
WT Persister + QVD
WT Persister + LEHD
90 kDa
STAT1
50 kDa
β-tubulin
k
PC9
Parental
Persister
Parental + QVD
Persister + QVD
90 kDa
STAT1
50 kDa
β-tubulin
l
DTEP fraction
0.04
0.03
0.02
0.01
0.00
*
***
**
WT control
DFFB KO #1 control
DFFB KO #1 + 1 μM JAKi

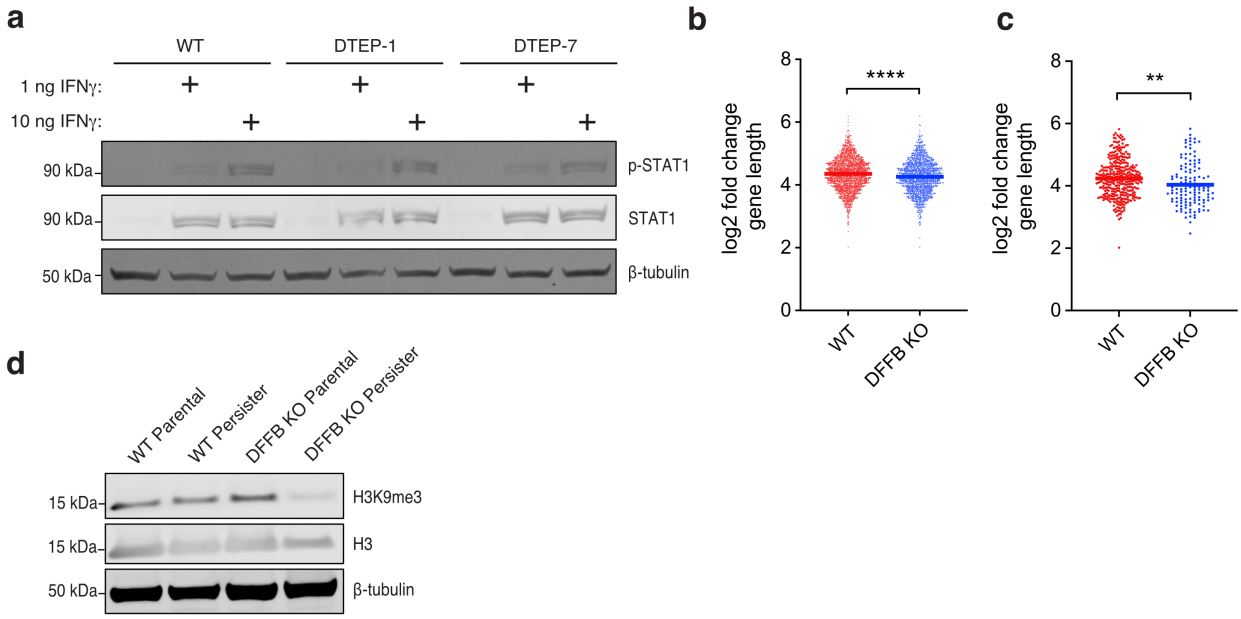

Figure 18: DFFB mediates gene repression through transcriptional silencing. a, A375 parental cells, *IFNGR1* mutant DTEP cells (clone WT-1), and *JAK1* mutant DTEP cells (clone WT-7) were assessed for phosphorylated STAT1 (p-STAT1) and STAT1 following treatment with 1 or 10 ng interferon-γ for 72 hours. **b,c**, Length of differentially expressed downregulated genes in A375 WT or DFFB KO (**b**) persister cells versus parental cells and (**c**) DTEP timepoint cells versus persister cells. Bar indicates average. **P<0.01, ****P<0.0001. **d**, A375 WT and DFFB KO parental and persister cells treated with 250 nM dabrafenib and 25 nM trametinib for 14 days were analyzed for H3K9me3.

Figure 19: Assessment of DNA damage response signaling in A375 DFFB WT persister cells. a-f, Western blots of A375 DFFB WT parental and persister cells assessed for (**a**) ATM, (**b**) ATR, (**c**) DNA-PK, (**d**) JNK, (**e**) STAT3, and (**f**) NF-κB phosphorylation. For (**d**) and (**f**), treatment with 20 ng TNFα for 10 minutes was used for a positive control. **g**,**h**, Identification of minimally toxic concentrations of DNA damage response inhibitors (**g**) KU-55933 (ATMi) and (**h**) NU7441 (DNA-PKi) in A375 parental cells to use for subsequent DTEP colony formation assays in **i**. **i,** Test of whether ATM or DNA-PK inhibition blocks DTEP colony formation. A375 WT cells were treated with 250 nM dabrafenib and 25 nM trametinib for 7 weeks to form DTEP colonies. During this treatment ATM or DNA-PK inhibitor was added at week 2 to pre-derived persister cells and was maintained for the remaining 5 week duration of the experiment. Control conditions were the same as in Extended Data Fig. 10b. DTEP fraction refers to the fraction of all surviving cells which regrew into DTEP colonies. For **g-i**, n=3 biological replicates; mean ± s.d. is shown; P values calculated with two-tailed Student's t-test. *P<0.05; **P<0.01; ***P<0.001; ns, not significant. **j**. A375 persister cells derived from 250 nM dabrafenib and 25 nM trametinib were allowed to regrow without drug for 48 hours and were analyzed for micronuclei. n=4 biological replicates; mean ± s.d. is shown; P values calculated with two-tailed Student's t-test. ns, not significant**.**

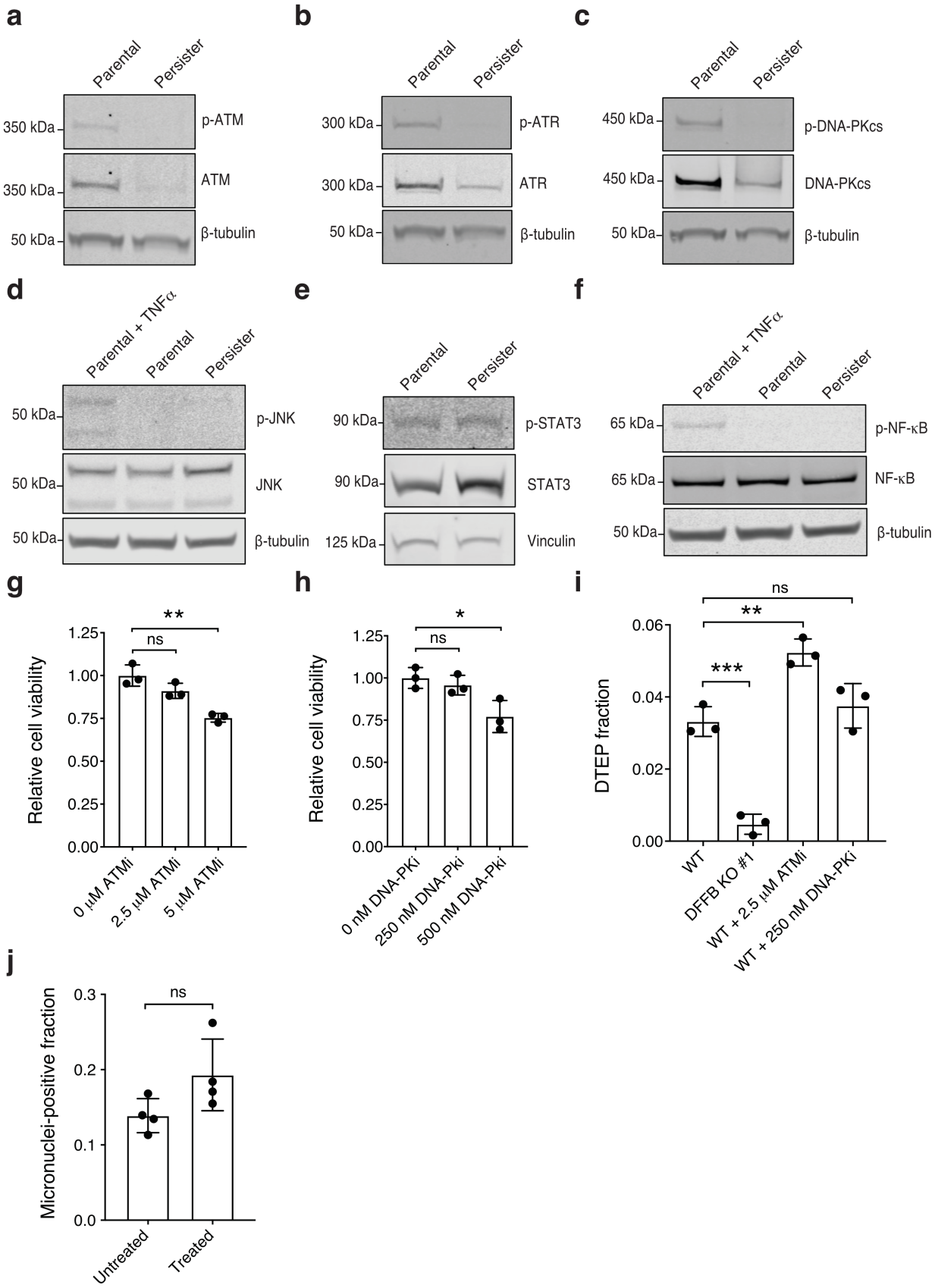
a
Parental
Persister
350 kDa
p-ATM
350 kDa
ATM
50 kDa
β-tubulin
b
Parental
Persister
300 kDa
p-ATR
300 kDa
ATR
50 kDa
β-tubulin
c
Parental
Persister
450 kDa
p-DNA-PKcs
450 kDa
DNA-PKcs
50 kDa
β-tubulin
d
Parental + TNFα
Parental
Persister
50 kDa
p-JNK
50 kDa
JNK
50 kDa
β-tubulin
e
Parental
Persister
90 kDa
p-STAT3
90 kDa
STAT3
125 kDa
Vinculin
f
Parental + TNFα
Parental
Persister
65 kDa
p-NF-κB
65 kDa
NF-κB
50 kDa
β-tubulin
g
Relative cell viability
1.25
1.00
0.75
0.50
0.25
0.00
**
ns
0 μM ATMi
2.5 μM ATMi
5 μM ATMi
h
Relative cell viability
1.25
1.00
0.75
0.50
0.25
0.00
*
ns
0 nM DNA-PKi
250 nM DNA-PKi
500 nM DNA-PKi
i
DTEP fraction
0.06
0.04
0.02
0.00
ns
**
***
WT
DFFB KO #1
WT + 2.5 μM ATMi
WT + 250 nM DNA-PKi
j
Micronuclei-positive fraction
0.3
0.2
0.1
0.0
ns
Untreated
Treated

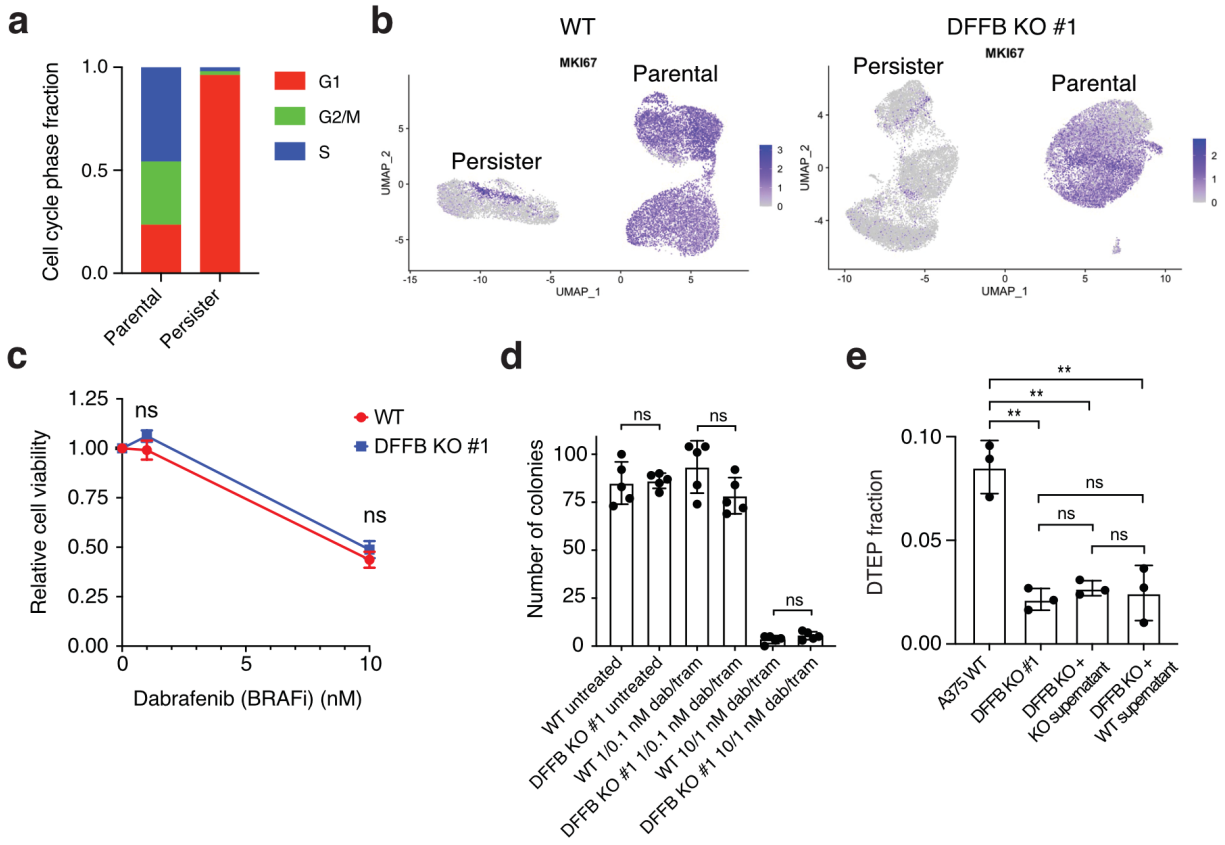

Figure 20: A375 DFFB KO cells exhibit persister cell G1 cell cycle arrest and clonogenic potential under drug stress similar to DFFB WT cells, and DFFB KO DTEP colony formation is not rescued by DFFB WT supernatant. a, A375 DFFB KO clone #1 parental and persister cells analyzed for cell cycle phase fractions with scRNAseq**.** Compare to A375 DFFB WT persister cell cycle phase fractions in Extended Data Fig. 2b. **b**, UMAP displays of expression values of the proliferation marker *Ki-67* for A375 WT and DFFB KO clone #1 cells. **c**, Identification of sub-cytostatic concentrations of dabrafenib to allow for assessment of clonogenic growth under drug stress in **d**. A375 WT and DFFB KO clone #1 parental cells were tested for cell viability at 10 nM dabrafenib and 1 nM trametinib or 1 nM dabrafenib and 0.1 nM trametinib for 3 days. Data are relative to untreated wells. **d,** A375 WT and DFFB KO clone #1 were assessed for clonogenic growth under sub-cytostatic concentrations of drug stress. 100 cells were plated in drug media at the concentrations indicated. Untreated and 1 nM/0.1 nM dabrafenib/trametinib conditions were fixed at day 9 when outgrowth had occurred whereas 10 nM/1 nM dabrafenib/trametinib were fixed at week 4 when outgrown colonies formed. For **c**, $n = 3$ biological replicates, **d,** n=5 biological replicates; mean ± s.d. is shown; P values were calculated with two-tailed Student's t-test. ns, not significant. **e**, A375 DFFB KO persister cells derived from treatment with 250 nM dabrafenib and 25 nM trametinib were cultured in conditioned media from drug-treated DFFB WT cells (WT Supernatant) or KO clone #1 cells (KO Supernatant), or without conditioned media. DTEP colony formation was measured following 7 total weeks of drug treatment. DTEP fraction refers to the fraction of all surviving cells which regrew into DTEP colonies. $n = 3$ biological replicates; mean ± s.d. is shown; P values were calculated with two-tailed Student's t-test. **P<0.01; ns, not significant.

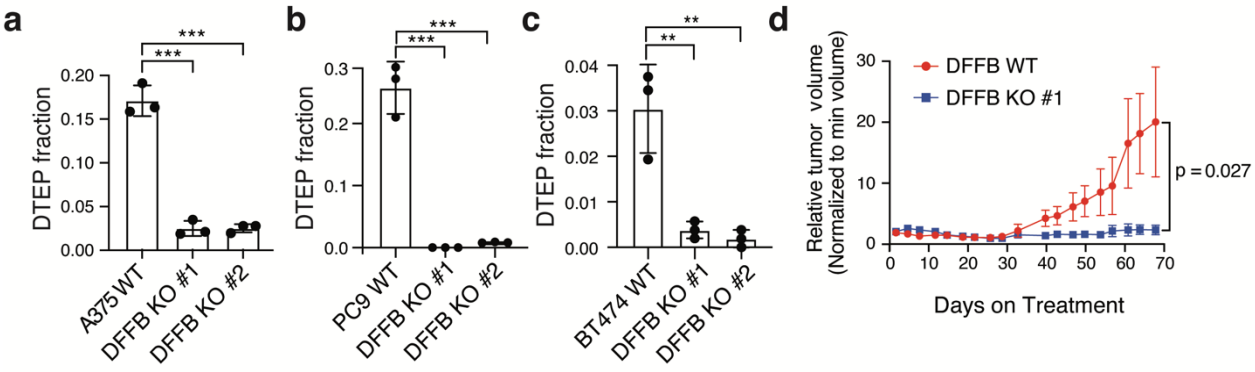

Figure 21: DFFB is necessary for acquired resistance. a-c, Fraction of all surviving cells which regrew into DTEP colonies during prolonged treatment with targeted therapies. *n* = 3 biological replicates; mean ± s.d.; two-tailed Student's t-test; **P<0.01, ***P<0.001, ****P<0.0001. **a**, A375 BRAF V600E melanoma cells treated with dabrafenib and trametinib. **b**, PC9 EGFR mutant lung cancer cells treated with osimertinib. **c**, BT474 HER2 amplified breast cancer cells treated with lapatinib. **d**, Response and acquired resistance of A375 DFFB WT and KO xenograft tumours in mice treated with dabrafenib and trametinib. To display fold change in tumour regrowth following initial treatment response, data are normalized to the minimum volume of each tumour during treatment; *n* = 3 biological replicates; mean ± s.d.; two-tailed Student's t-test.

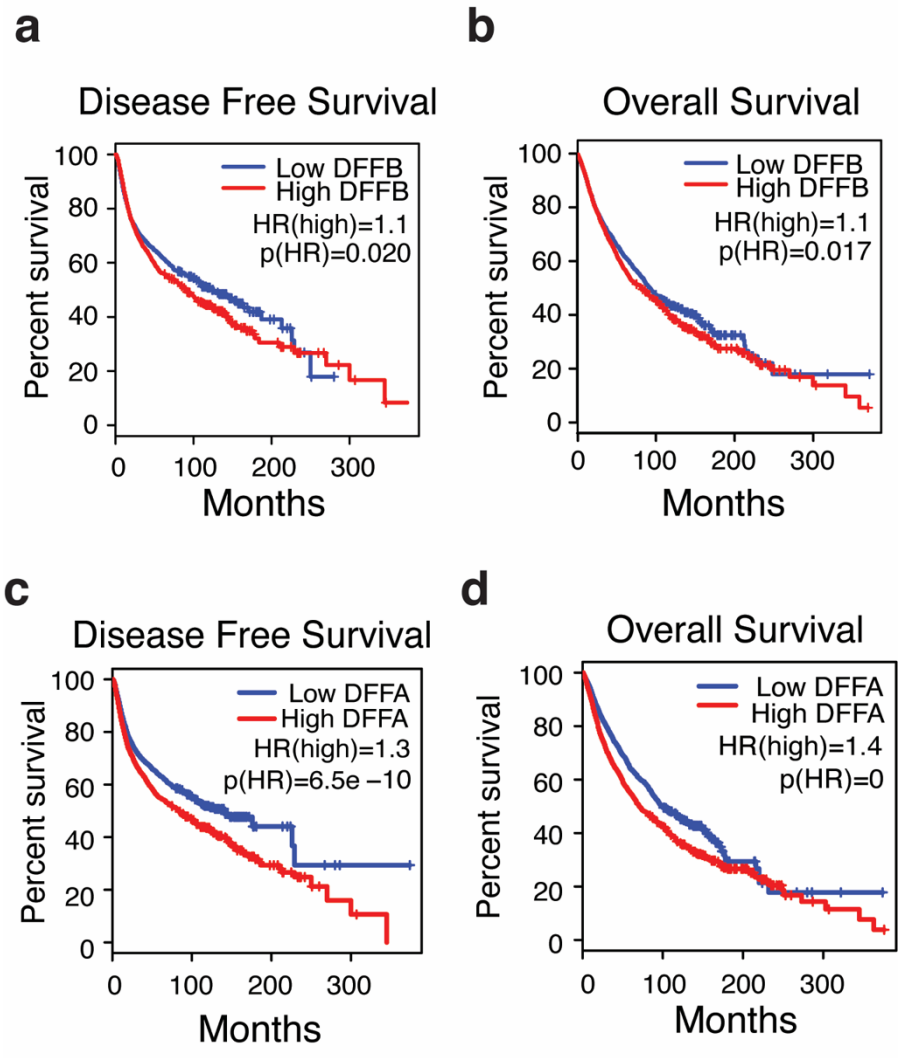

Figure 22: DFFA and DFFB expression correlate with worse patient survival outcomes. Correlation between (**a**,**b**) DFFB or (**c**,**d**) DFFA mRNA expression and (**a**,**c**) disease free survival or (**b**,**d**) overall survival across all tumours types using TCGA data. HR, Hazard Ratio; p(HR), P value of the Hazard Ratio. P value calculated with log-rank test.

CHAPTER 3

CONCLUSION

The ability for a subpopulation to survive, adapt, and regrow during stressful exposures ensures the continued existence of a population. Survival and adaptation strategies are evolutionarily conserved across biological systems including bacteria, vertebrate embryos, and cancer cells.[2,3,15,22] First described in the 1940's, persister cells were observed as a subpopulation of bacteria that survived penicillin treatment.[11,12] These cells entered a dormant or quiescent pro-survival cell state and were responsible for seeding disease relapse. A similar subpopulation of cancer persister cells has been observed and investigated throughout the past decade. The Darwinian selection of preexisting cells containing resistance mutations is one scenario by which drug resistance emerges. This fatalistic scenario is difficult to therapeutically combat given the myriad potential resistance mechanisms available to cells. However, persister cells survive through reversible, nongenetic mechanisms indicating that drug resistance is not a foregone conlusion.[4,12] In parallel with epigenetic changes, both bacterial and cancer persister cells increase their mutagenic rate to increase genetic diversity and adapt to drug treatment.[17,27,64,67] This process in the context of cancer acquired drug resistance remains poorly understood. Thus, investigating this residual surviving subpopulation is crucial to eliminate disease and increase cures by discovering targetable vulnerabilities.

The research in this dissertation reveals the role sublethal apoptosis signaling plays in mediating a stress response in cancer persister cells. First, we observed and characterized sublethal apoptotic signaling in persister cells. We then investigated one of the apoptotic signaling effector molecules responsible for DNA fragmentation, DFFB, for its role in persistence. Drug stress activates DFFB in persister cells and DFFB is the major source of DNA damage during

nongenotoxic drug treatments. This DNA damage resulted in both genetic and epigenetic changes that promoted persister cell regrowth under drug pressure. While we characterized important details concerning the sublethal apoptosis pathway in cancer persister cells, additional investigations into its activity in persister cells as well as expanding the scope of sublethal apoptotic signaling to other diseases is warranted.

Cells have the ability to survive apoptotic signaling when exposed to stressful environments.[85,88,89] A recent study proposed that sublethal apoptosis initiated by BH3 mimetics induces several persister cell characteristics including drug tolerance, EMT, and ferroptosis sensitivity.[36] This acutely-triggered phenotype depends on cytochrome C release from the mitochondria, is caspase independent, and causes translational reprogramming that ultimately activates the transcription factor ATF4. However, whether sublethal apoptotic signaling occurs in persister cells derived from prolonged drug treatment remains unknown. Importantly, we showed that cancer persister cells under chronic oncogene targeted therapy stress also display sublethal apoptosis characteristics including minority MOMP, cytochrome C release and caspase activation. We then focused on caspase-dependent phenotypes including DNA damage, mutagenesis and suppression of interferon signaling. It will be important for future studies to determine caspase-dependent and caspase-independent sublethal apoptotic signaling functions. Studies regarding mitochondrial dynamics in persister cells, for example, could illuminate other factors that promote persister cell survival.[175] Furthermore, the degree of MOMP persister cells can tolerate will be interesting to determine. Persister cells could either be resilient to MOMP or poised on the edge of death from further MOMP induction. We also observed a partial cleavage of caspase 3 to the p19 fragment. Factors mediating this partial cleavage, potentially the IAP family, should be investigated as a potential vulnerability, given that SMAC mimetics have already been shown to

kill persister cells.[9,31] Together, our data provide valuable insights into the sublethal apoptosis in persister cells, but more studies are required to fully characterize this pathway.

We then focused on the role the apoptotic nuclease DFFB plays in cancer persister cells given its dominant role in mediating DNA damage. While we found that DFFA is cleaved and DFFB is required for DNA damage in persister cells, indicating DFFB activation, more work is required to determine how DFFB is fully regulated in persister cells. A recent study discovered a novel DFFB regulation event modulated by DNA damage response signaling factors ATM and ATR. These kinases activate DFFB through DFFA phosphorylation to induce single strand DNA nicks that promote cell cycle checkpoints and cancer cell survival following radiation-induced DNA damage.[115] While we did not find evidence that DFFB influenced the cell cycle in our oncogene targeted therapy-derived persister cells, it could be that DFFB-induced DNA damage does affect cell cycle progression in other treatment contexts. Whether DFFA is phosphorylated to activate DFFB in our persister cell models should also be investigated. However, we did not observe ATM or ATR activation by phosphorylation in our A375 model, and therefore the full scope of this novel DFFB activation mechanism should be investigated. DFFB localization may be another important factor given the above study provided evidence for DFFB recruitment to chromatin fractions.[115] However, previous literature shows that DFFB/DFFA nuclear localization does not signal DFFB activity.[176,177] Whether there is a DFFB/DFFA localization change in persister cells remains unknown, but this could be important to determine as a strategy for therapeutically blocking DFFB activity. Therefore, understanding the spectrum of DFFB regulation in persister cells is an important next step from the research in this dissertation.

DNA damage is a crucial cellular event that can introduce mutations, impact gene expression, disrupt chromatin architecture, and initiate integral signaling cascades.[32,117,146,178]

Given recent literature focusing on the importance acquired mutations play in persister cells, we first focused on the mutagenic activity of DFFB.[27,64–67] While we identified approximately double the amount of mutations in WT cells versus KO cells, the impact these mutations play in facilitating persister regrowth requires further investigation. First, our early A375 DTEP colony cells remained reversibly drug tolerant, indicating that mutations alone do not fully confer drug resistance at this early DTEP formation timepoint. This finding is consistent with other reports showing that early DTEPs remain reversibly drug tolerant, suggesting that epigenetic factors play a more dominant role in initial persister regrowth.[4,26] It remains possible that mutations still promote DTEP formation since several identified mutations are in genes reported to play a role in cancer, including a *BRAF* mutation that increases MAPK signaling. Determining which mutations or combinations of mutations contribute to persister growth will require introducing these specific mutations into cells and observing their DTEP formation ability. Importantly, mutations responsible for robust drug resistance do emerge at later timepoints.[65,66] Thus, mutagenesis is an important event in DTEPs and blocking mutagenic DFFB activity remains a viable strategy to combat drug resistance.

Beyond mutations, DFFB mediates important epigenetic changes including the suppression of growth-inhibiting interferon signaling to promote DTEP formation. Two previous studies identified the important role caspase signaling plays in suppressing interferon signaling during hematopoietic development and viral infections.[140,141] The suppression of interferon production is integral for controlling the level of inflammatory cell death. These studies investigated caspase and MOMP signaling to show that these factors influence interferon suppression but the role of DFFB was not explored. Here, we showed that DFFB is indeed the apoptotic effector responsible for interferon suppression in the context of cancer acquired drug resistance across multiple models.

This is an important finding given the necessity for cancer persister cells to modulate STAT1 signaling levels.[50] There are multiple possibilities for how DFFB decreases interferon signaling. These include degrading mitochondrial DNA that leaks into the cytoplasm to decrease STING activation, dampening interferon gene expression through transcriptional interference or global chromatin changes, and disrupting interferon protein function through mutagenesis. We did observe that DFFB effects both transcriptional silencing as well as global chromatin architecture, but whether additional factors contribute to interferon signaling modulation should be investigated. Although we found that isolated DTEP samples with interferon gene mutations contained functional IFNγ signaling, it remains possible that this signaling is affected under drug treatment. Given this evidence, the ability for DFFB to mediate both genetic and epigenetic changes in persister cells makes it an attractive target to inhibit drug stress-adaptive processes.

DFFB mediated DNA damage and mutagenesis may be involved in additional physiological processes beyond cancer including aging and neurodegenerative diseases. The major cellular mutagenic source in human somatic and germ cells may not be mitotic activity but could instead be sublethal apoptotic signaling. A recent study showed that post-mitotic and proliferative primary human tissues accumulate somatic mutations throughout life at a constant rate.[156] This mutation rate has a strong association with aging across mammals, suggesting that mutational processes could be a contributing factor to aging.[179] Whether mutations are a major aging accelerator is controversial given that people with higher mutation rates from error prone polymerases do not always show signs of premature aging.[180] Indeed, a study showed that the loss of epigenetic information through DNA damage without mutagenesis drastically accelerated aging phenotypes in mice suggesting that DNA damage itself and consequent epigenetic reprogramming plays a greater role during aging than mutagenesis.[178] Whether mutagenesis or epigenetic

reprogramming is more important for aging, we showed that DFFB mediates both processes, revealing the nuclease as an important factor for future aging investigations. DFFB could also play a role in neurodegenerative diseases such as Alzheimer's disease. DNA damage accumulates in Alzheimer's disease brain astrocytes, decreasing their ability to provide neuronal support.[181] In an experimental rat model of Alzheimer's disease, decreased DFFB expression from glutamate antibody treatment promoted disease stabilization and a corresponding decrease in neuronal and glial cell death.[182] Furthermore, an unpublished study using Alzheimer's Disease Neuroimaging Initiative cohort data identified the neuronal apoptotic process and *DFFB* expression as highly enriched in Alzheimer's disease patients.[183] Therefore, sublethal apoptotic signaling and DFFB-mediated DNA damage should be investigated for its role in both aging and neurodegeneration.

In conclusion, sublethal apoptotic signaling and the apoptotic nuclease DFFB play important roles outside of cell death. We investigated the importance DFFB-mediated DNA damage plays in promoting cancer acquired drug resistance, implicating DFFB as a novel therapeutic target. Finally, further research into the role sublethal apoptotic signaling and DFFB play in other biological processes including aging and neurodegenerative disease is important to determine if targeting DFFB in these situations could improve patient's lives.

REFERENCES

1. Oxnard, G. R. The cellular origins of drug resistance in cancer. *Nat. Med.* **22,** 232–234 (2016).

2. Shen, S., Vagner, S. & Robert, C. Persistent Cancer Cells: The Deadly Survivors. *Cell* **183,** 860–874 (2020).

3. Cabanos, H. F. & Hata, A. N. Emerging Insights into Targeted Therapy-Tolerant Persister Cells in Cancer. *Cancers* **13,** 2666 (2021).

4. Sharma, S. V., Lee, D. Y., Li, B., Quinlan, M. P., Takahashi, F., Maheswaran, S., McDermott, U., Azizian, N., Zou, L., Fischbach, M. A., Wong, K.-K., Brandstetter, K., Wittner, B., Ramaswamy, S., Classon, M. & Settleman, J. A Chromatin-Mediated Reversible Drug-Tolerant State in Cancer Cell Subpopulations. *Cell* **141,** 69–80 (2010).

5. Holohan, C., Van Schaeybroeck, S., Longley, D. B. & Johnston, P. G. Cancer drug resistance: an evolving paradigm. *Nat. Rev. Cancer* **13,** 714–726 (2013).

6. Neel, D. S. & Bivona, T. G. Resistance is futile: overcoming resistance to targeted therapies in lung adenocarcinoma. *Npj Precis. Oncol.* **1,** 1–6 (2017).

7. Hanahan, D. Rethinking the war on cancer. *The Lancet* **383,** 558–563 (2014).

8. Gu, J., Mu, N., Jia, B., Guo, Q., Pan, L., Zhu, M., Zhang, W., Zhang, K., Li, W., Li, M., Wei, L., Xue, X., Zhang, Y. & Zhang, W. Targeting radiation-tolerant persister cells as a strategy for inhibiting radioresistance and recurrence in glioblastoma. *Neuro-Oncol.* **24,** 1056–1070 (2022).

9. Sehgal, K., Portell, A., Ivanova, E. V., Lizotte, P. H., Mahadevan, N. R., Greene, J. R., Vajdi, A., Gurjao, C., Teceno, T., Taus, L. J., Thai, T. C., Kitajima, S., Liu, D., Tani, T., Noureddine, M., Lau, C. J., Kirschmeier, P. T., Liu, D., Giannakis, M., Jenkins, R. W., Gokhale, P. C., Goldoni, S., Pinzon-Ortiz, M., Hastings, W. D., Hammerman, P. S., Miret, J. J., Paweletz, C. P. & Barbie, D. A. Dynamic single-cell RNA sequencing identifies immunotherapy persister cells following PD-1 blockade. *J. Clin. Invest.* **131,** (2021).

10. Oren, Y., Tsabar, M., Cuoco, M. S., Amir-Zilberstein, L., Cabanos, H. F., Hütter, J.-C., Hu, B., Thakore, P. I., Tabaka, M., Fulco, C. P., Colgan, W., Cuevas, B. M., Hurvitz, S. A., Slamon, D. J., Deik, A., Pierce, K. A., Clish, C., Hata, A. N., Zaganjor, E., Lahav, G., Politi, K., Brugge, J. S. & Regev, A. Cycling cancer persister cells arise from lineages with distinct programs. *Nature* **596,** 576–582 (2021).

11. Hobby, G. L., Meyer, K. & Chaffee, E. Observations on the Mechanism of Action of Penicillin. *Proc. Soc. Exp. Biol. Med.* **50,** 281–285 (1942).

12. Bigger, J. TREATMENT OF STAPHYLOCOCCAL INFECTIONS WITH PENICILLIN BY INTERMITTENT STERILISATION. *The Lancet* **244,** 497–500 (1944).

13. Balaban, N. Q., Merrin, J., Chait, R., Kowalik, L. & Leibler, S. Bacterial Persistence as a Phenotypic Switch. *Science* **305,** 1622–1625 (2004).

14. Fasani, R. A. & Savageau, M. A. Molecular mechanisms of multiple toxin–antitoxin systems are coordinated to govern the persister phenotype. *Proc. Natl. Acad. Sci.* **110,** E2528–E2537 (2013).

15. Fisher, R. A., Gollan, B. & Helaine, S. Persistent bacterial infections and persister cells. *Nat. Rev. Microbiol.* **15,** 453–464 (2017).

16. Layton, J. C. & Foster, P. L. Error-prone DNA polymerase IV is controlled by the stress-response sigma factor, RpoS, in Escherichia coli. *Mol. Microbiol.* **50,** 549–561 (2003).

17. Foster, P. L. Stress-Induced Mutagenesis in Bacteria. *Crit. Rev. Biochem. Mol. Biol.* **42,** 373–397 (2007).

18. Duy, C., Li, M., Teater, M., Meydan, C., Garrett-Bakelman, F. E., Lee, T. C., Chin, C. R., Durmaz, C., Kawabata, K. C., Dhimolea, E., Mitsiades, C. S., Doehner, H., D'Andrea, R. J., Becker, M. W., Paietta, E. M., Mason, C. E., Carroll, M. & Melnick, A. M. Chemotherapy Induces Senescence-Like Resilient Cells Capable of Initiating AML Recurrence. *Cancer Discov.* **11,** 1542–1561 (2021).

19. Dhimolea, E., de Matos Simoes, R., Kansara, D., Al'Khafaji, A., Bouyssou, J., Weng, X., Sharma, S., Raja, J., Awate, P., Shirasaki, R., Tang, H., Glassner, B. J., Liu, Z., Gao, D., Bryan, J., Bender, S., Roth, J., Scheffer, M., Jeselsohn, R., Gray, N. S., Georgakoudi, I., Vazquez, F., Tsherniak, A., Chen, Y., Welm, A., Duy, C., Melnick, A., Bartholdy, B., Brown, M., Culhane, A. C. & Mitsiades, C. S. An Embryonic Diapause-like Adaptation with Suppressed Myc Activity Enables Tumor Treatment Persistence. *Cancer Cell* **39,** 240-256.e11 (2021).

20. Rehman, S. K., Haynes, J., Collignon, E., Brown, K. R., Wang, Y., Nixon, A. M. L., Bruce, J. P., Wintersinger, J. A., Singh Mer, A., Lo, E. B. L., Leung, C., Lima-Fernandes, E., Pedley, N. M., Soares, F., McGibbon, S., He, H. H., Pollet, A., Pugh, T. J., Haibe-Kains, B., Morris, Q., Ramalho-Santos, M., Goyal, S., Moffat, J. & O'Brien, C. A. Colorectal Cancer Cells Enter a Diapause-like DTP State to Survive Chemotherapy. *Cell* **184,** 226-242.e21 (2021).

21. Chang, C. A., Jen, J., Jiang, S., Sayad, A., Mer, A. S., Brown, K. R., Nixon, A. M. L., Dhabaria, A., Tang, K. H., Venet, D., Sotiriou, C., Deng, J., Wong, K., Adams, S., Meyn, P., Heguy, A., Skok, J. A., Tsirigos, A., Ueberheide, B., Moffat, J., Singh, A., Haibe-Kains, B., Khodadadi-Jamayran, A. & Neel, B. G. Ontogeny and Vulnerabilities of Drug-Tolerant Persisters in HER2+ Breast Cancer. *Cancer Discov.* **12,** 1022–1045 (2022).

22. Renfree, M. B. & Fenelon, J. C. The enigma of embryonic diapause. *Development* **144,** 3199–3210 (2017).

23. Kuczynski, E. A., Sargent, D. J., Grothey, A. & Kerbel, R. S. Drug rechallenge and treatment beyond progression—implications for drug resistance. *Nat. Rev. Clin. Oncol.* **10,** 571–587 (2013).

24. Raha, D., Wilson, T. R., Peng, J., Peterson, D., Yue, P., Evangelista, M., Wilson, C., Merchant, M. & Settleman, J. The Cancer Stem Cell Marker Aldehyde Dehydrogenase Is Required to Maintain a Drug-Tolerant Tumor Cell Subpopulation. *Cancer Res.* **74,** 3579–3590 (2014).

25. Liau, B. B., Sievers, C., Donohue, L. K., Gillespie, S. M., Flavahan, W. A., Miller, T. E., Venteicher, A. S., Hebert, C. H., Carey, C. D., Rodig, S. J., Shareef, S. J., Najm, F. J., van Galen, P., Wakimoto, H., Cahill, D. P., Rich, J. N., Aster, J. C., Suvà, M. L., Patel, A. P. & Bernstein, B. E. Adaptive Chromatin Remodeling Drives Glioblastoma Stem Cell Plasticity and Drug Tolerance. *Cell Stem Cell* **20,** 233-246.e7 (2017).

26. Shaffer, S. M., Dunagin, M. C., Torborg, S. R., Torre, E. A., Emert, B., Krepler, C., Beqiri, M., Sproesser, K., Brafford, P. A., Xiao, M., Eggan, E., Anastopoulos, I. N., Vargas-Garcia, C. A., Singh, A., Nathanson, K. L., Herlyn, M. & Raj, A. Rare cell variability and drug-induced reprogramming as a mode of cancer drug resistance. *Nature* **546,** 431–435 (2017).

27. Russo, M., Pompei, S., Sogari, A., Corigliano, M., Crisafulli, G., Puliafito, A., Lamba, S., Erriquez, J., Bertotti, A., Gherardi, M., Di Nicolantonio, F., Bardelli, A. & Cosentino Lagomarsino, M. A modified fluctuation-test framework characterizes the population dynamics and mutation rate of colorectal cancer persister cells. *Nat. Genet.* **54,** 976–984 (2022).

28. Echeverria, G. V., Ge, Z., Seth, S., Zhang, X., Jeter-Jones, S., Zhou, X., Cai, S., Tu, Y., McCoy, A., Peoples, M., Sun, Y., Qiu, H., Chang, Q., Bristow, C., Carugo, A., Shao, J., Ma, X., Harris, A., Mundi, P., Lau, R., Ramamoorthy, V., Wu, Y., Alvarez, M. J., Califano, A., Moulder, S. L., Symmans, W. F., Marszalek, J. R., Heffernan, T. P., Chang, J. T. & Piwnica-Worms, H. Resistance to neoadjuvant chemotherapy in triple-negative breast cancer mediated by a reversible drug-tolerant state. *Sci. Transl. Med.* **11,** eaav0936 (2019).

29. Kurppa, K. J., Liu, Y., To, C., Zhang, T., Fan, M., Vajdi, A., Knelson, E. H., Xie, Y., Lim, K., Cejas, P., Portell, A., Lizotte, P. H., Ficarro, S. B., Li, S., Chen, T., Haikala, H. M., Wang, H., Bahcall, M., Gao, Y., Shalhout, S., Boettcher, S., Shin, B. H., Thai, T., Wilkens, M. K., Tillgren, M. L., Mushajiang, M., Xu, M., Choi, J., Bertram, A. A., Ebert, B. L., Beroukhim, R., Bandopadhayay, P., Awad, M. M., Gokhale, P. C., Kirschmeier, P. T., Marto, J. A., Camargo, F. D., Haq, R., Paweletz, C. P., Wong, K.-K., Barbie, D. A., Long, H. W., Gray, N. S. & Jänne, P. A. Treatment-Induced Tumor Dormancy through YAP-Mediated Transcriptional Reprogramming of the Apoptotic Pathway. *Cancer Cell* **37,** 104-122.e12 (2020).

30. Hangauer, M. J., Viswanathan, V. S., Ryan, M. J., Bole, D., Eaton, J. K., Matov, A., Galeas, J., Dhruv, H. D., Berens, M. E., Schreiber, S. L., McCormick, F. & McManus, M. T. Drug-tolerant persister cancer cells are vulnerable to GPX4 inhibition. *Nature* **551,** 247–250 (2017).

31. Martin, M. J., Floc'h, N., Pfeifer, M., Criscione, S., Delpuech, O., Gagrica, S., Yao, Y., McDermott, U. & Smith, P. D. Pharmaceutical Reactivation of Attenuated Apoptotic Pathways Leads to Elimination of Osimertinib Drug-Tolerant Cells. *Cancer Res. Commun.* **2,** 1312–1325 (2022).

32. Ali, M., Lu, M., Ang, H. X., Soderquist, R. S., Eyler, C. E., Hutchinson, H. M., Glass, C., Bassil, C. F., Lopez, O. M., Kerr, D. L., Falcon, C. J., Yu, H. A., Hata, A. N., Blakely, C. M., McCoach, C. E., Bivona, T. G. & Wood, K. C. Small-molecule targeted therapies induce dependence on DNA double-strand break repair in residual tumor cells. *Sci. Transl. Med.* **14,** eabc7480 (2022).

33. Risom, T., Langer, E. M., Chapman, M. P., Rantala, J., Fields, A. J., Boniface, C., Alvarez, M. J., Kendsersky, N. D., Pelz, C. R., Johnson-Camacho, K., Dobrolecki, L. E., Chin, K., Aswani, A. J., Wang, N. J., Califano, A., Lewis, M. T., Tomlin, C. J., Spellman, P. T., Adey, A., Gray, J. W. & Sears, R. C. Differentiation-state plasticity is a targetable resistance mechanism in basal-like breast cancer. *Nat. Commun.* **9,** 3815 (2018).

34. Zawistowski, J. S., Bevill, S. M., Goulet, D. R., Stuhlmiller, T. J., Beltran, A. S., Olivares-Quintero, J. F., Singh, D., Sciaky, N., Parker, J. S., Rashid, N. U., Chen, X., Duncan, J. S., Whittle, M. C., Angus, S. P., Velarde, S. H., Golitz, B. T., He, X., Santos, C., Darr, D. B., Gallagher, K., Graves, L. M., Perou, C. M., Carey, L. A., Earp, H. S. & Johnson, G. L. Enhancer Remodeling during Adaptive Bypass to MEK Inhibition Is Attenuated by Pharmacologic Targeting of the P-TEFb Complex. *Cancer Discov.* **7,** 302–321 (2017).

35. Jiang, X., Stockwell, B. R. & Conrad, M. Ferroptosis: mechanisms, biology and role in disease. *Nat. Rev. Mol. Cell Biol.* **22,** 266–282 (2021).

36. Kalkavan, H., Chen, M. J., Crawford, J. C., Quarato, G., Fitzgerald, P., Tait, S. W. G., Goding, C. R. & Green, D. R. Sublethal cytochrome c release generates drug-tolerant persister cells. *Cell* **185,** 3356-3374.e22 (2022).

37. Viswanathan, V. S., Ryan, M. J., Dhruv, H. D., Gill, S., Eichhoff, O. M., Seashore-Ludlow, B., Kaffenberger, S. D., Eaton, J. K., Shimada, K., Aguirre, A. J., Viswanathan, S. R., Chattopadhyay, S., Tamayo, P., Yang, W. S., Rees, M. G., Chen, S., Boskovic, Z. V., Javaid, S., Huang, C., Wu, X., Tseng, Y.-Y., Roider, E. M., Gao, D., Cleary, J. M., Wolpin, B. M., Mesirov, J. P., Haber, D. A., Engelman, J. A., Boehm, J. S., Kotz, J. D., Hon, C. S., Chen, Y., Hahn, W. C., Levesque, M. P., Doench, J. G., Berens, M. E., Shamji, A. F., Clemons, P. A., Stockwell, B. R. & Schreiber, S. L. Dependency of a therapy-resistant state of cancer cells on a lipid peroxidase pathway. *Nature* **547,** 453–457 (2017).

38. Wilson, T. R., Fridlyand, J., Yan, Y., Penuel, E., Burton, L., Chan, E., Peng, J., Lin, E., Wang, Y., Sosman, J., Ribas, A., Li, J., Moffat, J., Sutherlin, D. P., Koeppen, H., Merchant, M., Neve, R. & Settleman, J. Widespread potential for growth-factor-driven resistance to anticancer kinase inhibitors. *Nature* **487,** 505–509 (2012).

39. Straussman, R., Morikawa, T., Shee, K., Barzily-Rokni, M., Qian, Z. R., Du, J., Davis, A., Mongare, M. M., Gould, J., Frederick, D. T., Cooper, Z. A., Chapman, P. B., Solit, D. B., Ribas, A., Lo, R. S., Flaherty, K. T., Ogino, S., Wargo, J. A. & Golub, T. R. Tumour micro-environment elicits innate resistance to RAF inhibitors through HGF secretion. *Nature* **487,** 500–504 (2012).

40. Hirata, E., Girotti, M. R., Viros, A., Hooper, S., Spencer-Dene, B., Matsuda, M., Larkin, J., Marais, R. & Sahai, E. Intravital Imaging Reveals How BRAF Inhibition Generates Drug-Tolerant Microenvironments with High Integrin β1/FAK Signaling. *Cancer Cell* **27,** 574–588 (2015).

41. Glodde, N., Bald, T., van den Boorn-Konijnenberg, D., Nakamura, K., O'Donnell, J. S., Szczepanski, S., Brandes, M., Eickhoff, S., Das, I., Shridhar, N., Hinze, D., Rogava, M., van der Sluis, T. C., Ruotsalainen, J. J., Gaffal, E., Landsberg, J., Ludwig, K. U., Wilhelm, C., Riek-Burchardt, M., Müller, A. J., Gebhardt, C., Scolyer, R. A., Long, G. V., Janzen, V., Teng, M. W. L., Kastenmüller, W., Mazzone, M., Smyth, M. J., Tüting, T. & Hölzel, M. Reactive Neutrophil Responses Dependent on the Receptor Tyrosine Kinase c-MET Limit Cancer Immunotherapy. *Immunity* **47,** 789-802.e9 (2017).

42. Harada, H., Inoue, M., Itasaka, S., Hirota, K., Morinibu, A., Shinomiya, K., Zeng, L., Ou, G., Zhu, Y., Yoshimura, M., McKenna, W. G., Muschel, R. J. & Hiraoka, M. Cancer cells that survive radiation therapy acquire HIF-1 activity and translocate towards tumour blood vessels. *Nat. Commun.* **3,** 783 (2012).

43. Semenza, G. L. The hypoxic tumor microenvironment: A driving force for breast cancer progression. *Biochim. Biophys. Acta BBA - Mol. Cell Res.* **1863,** 382–391 (2016).

44. Endo, H., Okami, J., Okuyama, H., Nishizawa, Y., Imamura, F. & Inoue, M. The induction of MIG6 under hypoxic conditions is critical for dormancy in primary cultured lung cancer cells with activating EGFR mutations. *Oncogene* **36,** 2824–2834 (2017).

45. Yao, Z., Fenoglio, S., Gao, D. C., Camiolo, M., Stiles, B., Lindsted, T., Schlederer, M., Johns, C., Altorki, N., Mittal, V., Kenner, L. & Sordella, R. TGF-β IL-6 axis mediates selective and adaptive mechanisms of resistance to molecular targeted therapy in lung cancer. *Proc. Natl. Acad. Sci.* **107,** 15535–15540 (2010).

46. Lee, H.-J., Zhuang, G., Cao, Y., Du, P., Kim, H.-J. & Settleman, J. Drug Resistance via Feedback Activation of Stat3 in Oncogene-Addicted Cancer Cells. *Cancer Cell* **26,** 207–221 (2014).

47. Bivona, T. G., Hieronymus, H., Parker, J., Chang, K., Taron, M., Rosell, R., Moonsamy, P., Dahlman, K., Miller, V. A., Costa, C., Hannon, G. & Sawyers, C. L. FAS and NF-κB signalling modulate dependence of lung cancers on mutant EGFR. *Nature* **471,** 523–526 (2011).

48. Gong, K., Guo, G., Panchani, N., Bender, M. E., Gerber, D. E., Minna, J. D., Fattah, F., Gao, B., Peyton, M., Kernstine, K., Mukherjee, B., Burma, S., Chiang, C.-M., Zhang, S., Amod Sathe, A., Xing, C., Dao, K. H., Zhao, D., Akbay, E. A. & Habib, A. A. EGFR inhibition triggers an adaptive response by co-opting antiviral signaling pathways in lung cancer. *Nat. Cancer* **1,** 394–409 (2020).

49. Pal, D., Pertot, A., Shirole, N. H., Yao, Z., Anaparthy, N., Garvin, T., Cox, H., Chang, K., Rollins, F., Kendall, J., Edwards, L., Singh, V. A., Stone, G. C., Schatz, M. C., Hicks, J., Hannon, G. J. & Sordella, R. TGF-β reduces DNA ds-break repair mechanisms to heighten genetic diversity and adaptability of CD44+/CD24− cancer cells. *eLife* **6,** e21615 (2017).

50. Sun, X., Bieber, J. M., Hammerlindl, H., Chalkley, R. J., Li, K. H., Burlingame, A. L., Jacobson, M. P., Wu, L. F. & Altschuler, S. J. Modulating environmental signals to reveal mechanisms and vulnerabilities of cancer persisters. *Sci. Adv.* **8,** eabi7711 (2022).

51. Gerosa, L., Chidley, C., Fröhlich, F., Sanchez, G., Lim, S. K., Muhlich, J., Chen, J.-Y., Vallabhaneni, S., Baker, G. J., Schapiro, D., Atanasova, M. I., Chylek, L. A., Shi, T., Yi, L., Nicora, C. D., Claas, A., Ng, T. S. C., Kohler, R. H., Lauffenburger, D. A., Weissleder, R., Miller, M. A., Qian, W.-J., Wiley, H. S. & Sorger, P. K. Receptor-Driven ERK Pulses Reconfigure MAPK Signaling and Enable Persistence of Drug-Adapted BRAF-Mutant Melanoma Cells. *Cell Syst.* **11,** 478-494.e9 (2020).

52. Eskandari, E. & Eaves, C. J. Paradoxical roles of caspase-3 in regulating cell survival, proliferation, and tumorigenesis. *J. Cell Biol.* **221,** e202201159 (2022).

53. Cheng, J., He, S., Wang, M., Zhou, L., Zhang, Z., Feng, X., Yu, Y., Ma, J., Dai, C., Zhang, S., Sun, L., Gong, Y., Wang, Y., Zhao, M., Luo, Y., Liu, X., Tian, L., Li, C. & Huang, Q. The Caspase-3/PKCδ/Akt/VEGF-A Signaling Pathway Mediates Tumor Repopulation during Radiotherapy. *Clin. Cancer Res.* **25,** 3732–3743 (2019).

54. Feng, X., Yu, Y., He, S., Cheng, J., Gong, Y., Zhang, Z., Yang, X., Xu, B., Liu, X., Li, C.-Y., Tian, L. & Huang, Q. Dying glioma cells establish a proangiogenic microenvironment through a caspase 3 dependent mechanism. *Cancer Lett.* **385,** 12–20 (2017).

55. Kurtova, A. V., Xiao, J., Mo, Q., Pazhanisamy, S., Krasnow, R., Lerner, S. P., Chen, F., Roh, T. T., Lay, E., Ho, P. L. & Chan, K. S. Blocking PGE2-induced tumour repopulation abrogates bladder cancer chemoresistance. *Nature* **517,** 209–213 (2015).

56. Lin, M.-C., Chen, S.-Y., He, P.-L., Herschman, H. & Li, H.-J. PGE2/EP4 antagonism enhances tumor chemosensitivity by inducing extracellular vesicle-mediated clearance of cancer stem cells. *Int. J. Cancer* **143,** 1440–1455 (2018).

57. Tong, D., Liu, Q., Wang, L., Xie, Q., Pang, J., Huang, Y., Wang, L., Liu, G., Zhang, D., Lan, W. & Jiang, J. The roles of the COX2/PGE2/EP axis in therapeutic resistance. *Cancer Metastasis Rev.* **37,** 355–368 (2018).

58. Hu, J., Sánchez-Rivera, F. J., Wang, Z., Johnson, G. N., Ho, Y., Ganesh, K., Umeda, S., Gan, S., Mujal, A. M., Delconte, R. B., Hampton, J. P., Zhao, H., Kottapalli, S., de Stanchina, E., Iacobuzio-Donahue, C. A., Pe'er, D., Lowe, S. W., Sun, J. C. & Massagué, J. STING inhibits the reactivation of dormant metastasis in lung adenocarcinoma. *Nature* **616,** 806–813 (2023).

59. Yang, C., Tian, C., Hoffman, T. E., Jacobsen, N. K. & Spencer, S. L. Melanoma subpopulations that rapidly escape MAPK pathway inhibition incur DNA damage and rely on stress signalling. *Nat. Commun.* **12,** 1747 (2021).

60. Rambow, F., Rogiers, A., Marin-Bejar, O., Aibar, S., Femel, J., Dewaele, M., Karras, P., Brown, D., Chang, Y. H., Debiec-Rychter, M., Adriaens, C., Radaelli, E., Wolter, P., Bechter, O., Dummer, R., Levesque, M., Piris, A., Frederick, D. T., Boland, G., Flaherty, K. T., van den Oord, J., Voet, T., Aerts, S., Lund, A. W. & Marine, J.-C. Toward Minimal Residual Disease-Directed Therapy in Melanoma. *Cell* **174,** 843-855.e19 (2018).

61. Miao, Y., Yang, H., Levorse, J., Yuan, S., Polak, L., Sribour, M., Singh, B., Rosenblum, M. D. & Fuchs, E. Adaptive Immune Resistance Emerges from Tumor-Initiating Stem Cells. *Cell* **177,** 1172-1186.e14 (2019).

62. Davies, A. H., Beltran, H. & Zoubeidi, A. Cellular plasticity and the neuroendocrine phenotype in prostate cancer. *Nat. Rev. Urol.* **15,** 271–286 (2018).

63. Shaffer, S. M., Emert, B. L., Reyes Hueros, R. A., Cote, C., Harmange, G., Schaff, D. L., Sizemore, A. E., Gupte, R., Torre, E., Singh, A., Bassett, D. S. & Raj, A. Memory Sequencing Reveals Heritable Single-Cell Gene Expression Programs Associated with Distinct Cellular Behaviors. *Cell* **182,** 947-959.e17 (2020).

64. Cipponi, A., Goode, D. L., Bedo, J., McCabe, M. J., Pajic, M., Croucher, D. R., Rajal, A. G., Junankar, S. R., Saunders, D. N., Lobachevsky, P., Papenfuss, A. T., Nessem, D., Nobis, M., Warren, S. C., Timpson, P., Cowley, M., Vargas, A. C., Qiu, M. R., Generali, D. G., Keerthikumar, S., Nguyen, U., Corcoran, N. M., Long, G. V., Blay, J.-Y. & Thomas, D. M. MTOR signaling orchestrates stress-induced mutagenesis, facilitating adaptive evolution in cancer. *Science* **368,** 1127–1131 (2020).

65. Ramirez, M., Rajaram, S., Steininger, R. J., Osipchuk, D., Roth, M. A., Morinishi, L. S., Evans, L., Ji, W., Hsu, C.-H., Thurley, K., Wei, S., Zhou, A., Koduru, P. R., Posner, B. A., Wu, L. F. & Altschuler, S. J. Diverse drug-resistance mechanisms can emerge from drug-tolerant cancer persister cells. *Nat. Commun.* **7,** 10690 (2016).

66. Hata, A. N., Niederst, M. J., Archibald, H. L., Gomez-Caraballo, M., Siddiqui, F. M., Mulvey, H. E., Maruvka, Y. E., Ji, F., Bhang, H. C., Krishnamurthy Radhakrishna, V., Siravegna, G., Hu, H., Raoof, S., Lockerman, E., Kalsy, A., Lee, D., Keating, C. L., Ruddy, D. A., Damon, L. J., Crystal, A. S., Costa, C., Piotrowska, Z., Bardelli, A., Iafrate, A. J., Sadreyev, R. I., Stegmeier, F., Getz, G., Sequist, L. V., Faber, A. C. & Engelman, J. A. Tumor cells can follow distinct evolutionary paths to become resistant to epidermal growth factor receptor inhibition. *Nat. Med.* **22,** 262–269 (2016).

67. Russo, M., Crisafulli, G., Sogari, A., Reilly, N. M., Arena, S., Lamba, S., Bartolini, A., Amodio, V., Magrì, A., Novara, L., Sarotto, I., Nagel, Z. D., Piett, C. G., Amatu, A., Sartore-Bianchi, A., Siena, S., Bertotti, A., Trusolino, L., Corigliano, M., Gherardi, M., Lagomarsino, M. C., Nicolantonio, F. D. & Bardelli, A. Adaptive mutability of colorectal cancers in response to targeted therapies. *Science* **366,** 1473–1480 (2019).

68. Temprine, K., Campbell, N. R., Huang, R., Langdon, E. M., Simon-Vermot, T., Mehta, K., Clapp, A., Chipman, M. & White, R. M. Regulation of the error-prone DNA polymerase Polκ by oncogenic signaling and its contribution to drug resistance. *Sci. Signal.* **13,** (2020).

69. Pecori, R., Di Giorgio, S., Paulo Lorenzo, J. & Nina Papavasiliou, F. Functions and consequences of AID/APOBEC-mediated DNA and RNA deamination. *Nat. Rev. Genet.* **23,** 505–518 (2022).

70. Nik-Zainal, S., Alexandrov, L. B., Wedge, D. C., Van Loo, P., Greenman, C. D., Raine, K., Jones, D., Hinton, J., Marshall, J., Stebbings, L. A., Menzies, A., Martin, S., Leung, K., Chen, L., Leroy, C., Ramakrishna, M., Rance, R., Lau, K. W., Mudie, L. J., Varela, I., McBride, D. J., Bignell, G. R., Cooke, S. L., Shlien, A., Gamble, J., Whitmore, I., Maddison, M., Tarpey, P. S., Davies, H. R., Papaemmanuil, E., Stephens, P. J., McLaren, S., Butler, A. P., Teague, J. W., Jönsson, G., Garber, J. E., Silver, D., Miron, P., Fatima, A., Boyault, S., Langerød, A., Tutt, A., Martens, J. W. M., Aparicio, S. A. J. R., Borg, Å., Salomon, A. V., Thomas, G., Børresen-Dale, A.-L., Richardson, A. L., Neuberger, M. S., Futreal, P. A., Campbell, P. J. & Stratton, M. R. Mutational Processes Molding the Genomes of 21 Breast Cancers. *Cell* **149,** 979–993 (2012).

71. Isozaki, H., Abbasi, A., Nikpour, N., Langenbucher, A., Su, W., Stanzione, M., Cabanos, H. F., Siddiqui, F. M., Phan, N., Jalili, P., Oh, S., Timonina, D., Bilton, S., Gomez-Caraballo, M., Archibald, H. L., Nangia, V., Dionne, K., Riley, A., Lawlor, M., Banwait, M. K., Cobb, R. G., Zou, L., Dyson, N. J., Ott, C. J., Benes, C., Getz, G., Chan, C. S., Shaw, A. T., Lin, J. J., Sequist, L. V., Piotrowska, Z., Engelman, J. A., Lee, J. J.-K., Maruvka, Y., Buisson, R., Lawrence, M. S. & Hata, A. N. APOBEC3A drives acquired resistance to targeted therapies in non-small cell lung cancer. *bioRxiv* 2021.01.20.426852 (2021). doi:10.1101/2021.01.20.426852

72. Mayekar, M. K., Caswell, D. R., Vokes, N. I., Law, E. K., Wu, W., Hill, W., Gronroos, E., Rowan, A., Bakir, M. A., McCoach, C. E., Blakely, C. M., Temiz, N. A., Nagano, A., Kerr, D. L., Rotow, J. K., Haderk, F., Dietzen, M., Ruiz, C. M., Almeida, B., Cech, L., Gini, B., Przewrocka, J., Moore, C., Murillo, M., Bakker, B., Rule, B., Durfee, C., Nanjo, S., Tan, L., Larson, L. K., Argyris, P. P., Brown, W. L., Yu, J., Gomez, C., Gui, P., Vogel, R. I., Yu, E. A., Thomas, N. J., Venkatesan, S., Hobor, S., Chew, S. K., Kanu, N., McGranahan, N., Allen, E. M. V., Downward, J., Harris, R. S., Bivona, T. G. & Swanton, C. Targeted cancer therapy induces APOBEC fuelling the evolution of drug resistance. *bioRxiv* 2020.12.18.423280 (2020). doi:10.1101/2020.12.18.423280

73. Wörmann, S. M., Zhang, A., Thege, F. I., Cowan, R. W., Rupani, D. N., Wang, R., Manning, S. L., Gates, C., Wu, W., Levin-Klein, R., Rajapakshe, K. I., Yu, M., Multani, A. S., Kang, Y., Taniguchi, C. M., Schlacher, K., Bellin, M. D., Katz, M. H. G., Kim, M. P., Fleming, J. B., Gallinger, S., Maddipati, R., Harris, R. S., Notta, F., Ross, S. R., Maitra, A. & Rhim, A. D. APOBEC3A drives deaminase domain-independent chromosomal instability to promote pancreatic cancer metastasis. *Nat. Cancer* **2,** 1338–1356 (2021).

74. Channathodiyil, P., May, K., Segonds-Pichon, A., Smith, P. D., Cook, S. J. & Houseley, J. Escape from G1 arrest during acute MEK inhibition drives the acquisition of drug resistance. *NAR Cancer* **4,** zcac032 (2022).

75. Carneiro, B. A. & El-Deiry, W. S. Targeting apoptosis in cancer therapy. *Nat. Rev. Clin. Oncol.* **17,** 395–417 (2020).

76. Singh, R., Letai, A. & Sarosiek, K. Regulation of apoptosis in health and disease: the balancing act of BCL-2 family proteins. *Nat. Rev. Mol. Cell Biol.* **20,** 175–193 (2019).

77. Kalkavan, H. & Green, D. R. MOMP, cell suicide as a BCL-2 family business. *Cell Death Differ.* **25,** 46–55 (2018).

78. Yosefzon, Y., Soteriou, D., Feldman, A., Kostic, L., Koren, E., Brown, S., Ankawa, R., Sedov, E., Glaser, F. & Fuchs, Y. Caspase-3 Regulates YAP-Dependent Cell Proliferation and Organ Size. *Mol. Cell* **70,** 573-587.e4 (2018).

79. Li, F., He, Z., Shen, J., Huang, Q., Li, W., Liu, X., He, Y., Wolf, F. & Li, C.-Y. Apoptotic Caspases Regulate Induction of iPSCs from Human Fibroblasts. *Cell Stem Cell* **7,** 508–520 (2010).

80. Dick, S. A., Chang, N. C., Dumont, N. A., Bell, R. A. V., Putinski, C., Kawabe, Y., Litchfield, D. W., Rudnicki, M. A. & Megeney, L. A. Caspase 3 cleavage of Pax7 inhibits self-renewal of satellite cells. *Proc. Natl. Acad. Sci.* **112,** E5246–E5252 (2015).

81. Gabet, A.-S., Coulon, S., Fricot, A., Vandekerckhove, J., Chang, Y., Ribeil, J.-A., Lordier, L., Zermati, Y., Asnafi, V., Belaid, Z., Debili, N., Vainchenker, W., Varet, B., Hermine, O. & Courtois, G. Caspase-activated ROCK-1 allows erythroblast terminal maturation independently of cytokine-induced Rho signaling. *Cell Death Differ.* **18,** 678–689 (2011).

82. Larsen, B. D., Rampalli, S., Burns, L. E., Brunette, S., Dilworth, F. J. & Megeney, L. A. Caspase 3/caspase-activated DNase promote cell differentiation by inducing DNA strand breaks. *Proc. Natl. Acad. Sci.* **107,** 4230–4235 (2010).

83. Naarmann-de Vries, I. S., Urlaub, H., Ostareck, D. H. & Ostareck-Lederer, A. Caspase-3 cleaves hnRNP K in erythroid differentiation. *Cell Death Dis.* **4,** e548–e548 (2013).

84. Man, N., Tan, Y., Sun, X.-J., Liu, F., Cheng, G., Greenblatt, S. M., Martinez, C., Karl, D. L., Ando, K., Sun, M., Hou, D., Chen, B., Xu, M., Yang, F.-C., Chen, Z., Chen, S., Nimer, S. D. & Wang, L. Caspase-3 controls AML1-ETO–driven leukemogenesis via autophagy modulation in a ULK1-dependent manner. *Blood* **129,** 2782–2792 (2017).

85. Tang, H. L., Tang, H. M., Mak, K. H., Hu, S., Wang, S. S., Wong, K. M., Wong, C. S. T., Wu, H. Y., Law, H. T., Liu, K., Talbot, C. C., Lau, W. K., Montell, D. J. & Fung, M. C. Cell survival, DNA damage, and oncogenic transformation after a transient and reversible apoptotic response. *Mol. Biol. Cell* **23,** 2240–2252 (2012).

86. Sun, G., Guzman, E., Balasanyan, V., Conner, C. M., Wong, K., Zhou, H. R., Kosik, K. S. & Montell, D. J. A molecular signature for anastasis, recovery from the brink of apoptotic cell death. *J. Cell Biol.* **216,** 3355–3368 (2017).

87. Nano, M., Mondo, J. A., Harwood, J., Balasanyan, V. & Montell, D. J. Cell survival following direct executioner-caspase activation. *Proc. Natl. Acad. Sci.* **120,** e2216531120 (2023).

88. Ichim, G., Lopez, J., Ahmed, S. U., Muthalagu, N., Giampazolias, E., Delgado, M. E., Haller, M., Riley, J. S., Mason, S. M., Athineos, D., Parsons, M. J., van de Kooij, B., Bouchier-Hayes, L., Chalmers, A. J., Rooswinkel, R. W., Oberst, A., Blyth, K., Rehm, M., Murphy, D. J. & Tait, S. W. G. Limited Mitochondrial Permeabilization Causes DNA Damage and Genomic Instability in the Absence of Cell Death. *Mol. Cell* **57,** 860–872 (2015).

89. Berthenet, K., Castillo Ferrer, C., Fanfone, D., Popgeorgiev, N., Neves, D., Bertolino, P., Gibert, B., Hernandez-Vargas, H. & Ichim, G. Failed Apoptosis Enhances Melanoma Cancer Cell Aggressiveness. *Cell Rep.* **31,** 107731 (2020).

90. Liu, X., Li, F., Huang, Q., Zhang, Z., Zhou, L., Deng, Y., Zhou, M., Fleenor, D. E., Wang, H., Kastan, M. B. & Li, C.-Y. Self-inflicted DNA double-strand breaks sustain tumorigenicity and stemness of cancer cells. *Cell Res.* **27,** 764–783 (2017).

91. Sakahira, H., Enari, M. & Nagata, S. Cleavage of CAD inhibitor in CAD activation and DNA degradation during apoptosis. *Nature* **391,** 96–99 (1998).

92. Larsen, B. D. & Sørensen, C. S. The caspase-activated DNase: apoptosis and beyond. *FEBS J.* **284,** 1160–1170 (2017).

93. Kulbay, M., Bernier-Parker, N. & Bernier, J. The role of the DFF40/CAD endonuclease in genomic stability. *Apoptosis* **26,** 9–23 (2021).

94. Iglesias-Guimarais, V., Gil-Guiñon, E., Sánchez-Osuna, M., Casanelles, E., García-Belinchón, M., Comella, J. X. & Yuste, V. J. Chromatin Collapse during Caspase-dependent Apoptotic Cell Death Requires DNA Fragmentation Factor, 40-kDa Subunit-/Caspase-activated Deoxyribonuclease-mediated 3′-OH Single-strand DNA Breaks*. *J. Biol. Chem.* **288,** 9200–9215 (2013).

95. Widlak, P. & Garrard, W. T. Ionic and cofactor requirements for the activity of the apoptotic endonuclease DFF40/CAD. *Mol. Cell. Biochem.* **218,** 125–130 (2001).

96. Widłak, P. The DFF40/CAD endonuclease and its role in apoptosis. *Acta Biochim. Pol.* **47,** 1037–1044 (2000).

97. Widlak, P., Li, P., Wang, X. & Garrard, W. T. Cleavage Preferences of the Apoptotic Endonuclease DFF40 (Caspase-activated DNase or Nuclease) on Naked DNA and Chromatin Substrates *. *J. Biol. Chem.* **275,** 8226–8232 (2000).

98. Enari, M., Sakahira, H., Yokoyama, H., Okawa, K., Iwamatsu, A. & Nagata, S. A caspase-activated DNase that degrades DNA during apoptosis, and its inhibitor ICAD. *Nature* **391,** 43–50 (1998).

99. Zhang, J., Liu, X., Scherer, D. C., Kaer, L. van, Wang, X. & Xu, M. Resistance to DNA fragmentation and chromatin condensation in mice lacking the DNA fragmentation factor 45. *Proc. Natl. Acad. Sci.* **95,** 12480–12485 (1998).

100. Kawane, K., Fukuyama, H., Yoshida, H., Nagase, H., Ohsawa, Y., Uchiyama, Y., Okada, K., Iida, T. & Nagata, S. Impaired thymic development in mouse embryos deficient in apoptotic DNA degradation. *Nat. Immunol.* **4,** 138–144 (2003).

101. Yan, B., Wang, H., Peng, Y., Hu, Y., Wang, H., Zhang, X., Chen, Q., Bedford, J. S., Dewhirst, M. W. & Li, C.-Y. A unique role of the DNA fragmentation factor in maintaining genomic stability. *Proc. Natl. Acad. Sci.* **103,** 1504–1509 (2006).

102. Yan, B., Wang, H., Xie, D., Wakamatsu, N., Anscher, M. S., Dewhirst, M. W., Mitchel, R. E. J., Chen, B. J. & Li, C.-Y. Increased skin carcinogenesis in caspase-activated DNase knockout mice. *Carcinogenesis* **30,** 1776–1780 (2009).

103. Konishi, S., Ishiguro, H., Shibata, Y., Kudo, J., Terashita, Y., Sugiura, H., Koyama, H., Kimura, M., Sato, A., Shinoda, N., Kuwabara, Y. & Fujii, Y. Decreased expression of DFF45/ICAD is correlated with a poor prognosis in patients with esophageal carcinoma. *Cancer* **95,** 2473–2478 (2002).

104. Errami, Y., Brim, H., Oumouna-Benachour, K., Oumouna, M., Naura, A. S., Kim, H., Ju, J., Davis, C. J., Kim, J. G., Ashktorab, H., Fallon, K., Xu, M., Zhang, J., Valle, L. D. & Boulares, A. H. ICAD Deficiency in Human Colon Cancer and Predisposition to Colon Tumorigenesis: Linkage to Apoptosis Resistance and Genomic Instability. *PLOS ONE* **8,** e57871 (2013).

105. Rajandram, R., Razack, A. H. A., Ng, K. L. & Gobe, G. C. Decreased Expression of Inhibitor of Caspase-Activated DNase (ICAD) in Renal Cell Carcinoma –Tissue Microarray of Human Samples. *J. Kidney Cancer VHL* **3,** 1–11 (2016).

106.Banas, T., Pitynski, K., Okon, K. & Czerw, A. DNA fragmentation factors 40 and 45 (DFF40/DFF45) and B-cell lymphoma 2 (Bcl-2) protein are underexpressed in uterine leiomyosarcomas and may predict survival. *OncoTargets Ther.* **10,** 4579–4589 (2017).

107.Sánchez-Osuna, M., Martínez-Escardó, L., Granados-Colomina, C., Martínez-Soler, F., Pascual-Guiral, S., Iglesias-Guimarais, V., Velasco, R., Plans, G., Vidal, N., Tortosa, A., Barcia, C., Bruna, J. & Yuste, V. J. An intrinsic DFF40/CAD endonuclease deficiency impairs oligonucleosomal DNA hydrolysis during caspase-dependent cell death: a common trait in human glioblastoma cells. *Neuro-Oncol.* **18,** 950–961 (2016).

108.Jong, J. E., Jeong, K. W., Shin, H., Hwang, L. R., Lee, D. & Seo, T. Human papillomavirus type 16 E6 protein inhibits DNA fragmentation via interaction with DNA fragmentation factor 40. *Cancer Lett.* **324,** 109–117 (2012).

109.Cortazar, A. R., Torrano, V., Martín-Martín, N., Caro-Maldonado, A., Camacho, L., Hermanova, I., Guruceaga, E., Lorenzo-Martín, L. F., Caloto, R., Gomis, R. R., Apaolaza, I., Quesada, V., Trka, J., Gomez-Muñoz, A., Vincent, S., Bustelo, X. R., Planes, F. J., Aransay, A. M. & Carracedo, A. CANCERTOOL: A Visualization and Representation Interface to Exploit Cancer Datasets. *Cancer Res.* **78,** 6320–6328 (2018).

110.Haimovici, A., Höfer, C., Badr, M. T., Bavafaye Haghighi, E., Amer, T., Boerries, M., Bronsert, P., Glavynskyi, I., Fanfone, D., Ichim, G., Thilmany, N., Weber, A., Brummer, T., Spohr, C., Öllinger, R., Janssen, K.-P., Rad, R. & Häcker, G. Spontaneous activity of the mitochondrial apoptosis pathway drives chromosomal defects, the appearance of micronuclei and cancer metastasis through the Caspase-Activated DNAse. *Cell Death Dis.* **13,** 315 (2022).

111.Brustmann, H. Poly(ADP-ribose) polymerase (PARP) and DNA-fragmentation factor (DFF45): Expression and correlation in normal, hyperplastic and neoplastic endometrial tissues. *Pathol. - Res. Pract.* **203,** 65–72 (2007).

112.Brustmann, H. DNA fragmentation factor (DFF45): Expression and prognostic value in serous ovarian cancer. *Pathol. - Res. Pract.* **202,** 713–720 (2006).

113.Kulbay, M., Johnson, B., Fiola, S., Diaz, R. J. & Bernier, J. DFF40 deficiency in cancerous T cells is implicated in chemotherapy drug sensitivity and resistance through the regulation of the apoptotic pathway. *Biochem. Pharmacol.* **194,** 114801 (2021).

114.Song, J. H., Kandasamy, K., Zemskova, M., Lin, Y.-W. & Kraft, A. S. The BH3 Mimetic ABT-737 Induces Cancer Cell Senescence. *Cancer Res.* **71,** 506–515 (2011).

115.Larsen, B. D., Benada, J., Yung, P. Y. K., Bell, R. A. V., Pappas, G., Urban, V., Ahlskog, J. K., Kuo, T. T., Janscak, P., Megeney, L. A., Elsässer, S. J., Bartek, J. & Sørensen, C. S. Cancer cells use self-inflicted DNA breaks to evade growth limits imposed by genotoxic stress. *Science* **376,** 476–483 (2022).

116.Hawkins, C. J. & Miles, M. A. Mutagenic Consequences of Sublethal Cell Death Signaling. *Int. J. Mol. Sci.* **22,** 6144 (2021).

117.O'Hagan, H. M., Mohammad, H. P. & Baylin, S. B. Double Strand Breaks Can Initiate Gene Silencing and SIRT1-Dependent Onset of DNA Methylation in an Exogenous Promoter CpG Island. *PLOS Genet.* **4,** e1000155 (2008).

118.Lovric, M. M. & Hawkins, C. J. TRAIL treatment provokes mutations in surviving cells. *Oncogene* **29,** 5048–5060 (2010).

119.Miles, M. A. & Hawkins, C. J. Executioner caspases and CAD are essential for mutagenesis induced by TRAIL or vincristine. *Cell Death Dis.* **8,** e3062–e3062 (2017).

120.Miles, M. A., Harris, M. A. & Hawkins, C. J. Proteasome inhibitors trigger mutations via activation of caspases and CAD, but mutagenesis provoked by the HDAC inhibitors vorinostat and romidepsin is caspase/CAD-independent. *Apoptosis* **24,** 404–413 (2019).

121.Miles, M. A. & Hawkins, C. J. In vitro analysis reveals necroptotic signaling does not provoke DNA damage or HPRT mutations. *Cell Death Dis.* **11,** 1–13 (2020).

122.Shekhar, T. M., Green, M. M., Rayner, D. M., Miles, M. A., Cutts, S. M. & Hawkins, C. J. Inhibition of Bcl-2 or IAP proteins does not provoke mutations in surviving cells. *Mutat. Res. Mol. Mech. Mutagen.* **777,** 23–32 (2015).

123.Jackman, D., Pao, W., Riely, G. J., Engelman, J. A., Kris, M. G., Jänne, P. A., Lynch, T., Johnson, B. E. & Miller, V. A. Clinical Definition of Acquired Resistance to Epidermal Growth Factor Receptor Tyrosine Kinase Inhibitors in Non–Small-Cell Lung Cancer. *J. Clin. Oncol.* **28,** 357–360 (2010).

124.Wagle, N., Van Allen, E. M., Treacy, D. J., Frederick, D. T., Cooper, Z. A., Taylor-Weiner, A., Rosenberg, M., Goetz, E. M., Sullivan, R. J., Farlow, D. N., Friedrich, D. C., Anderka, K., Perrin, D., Johannessen, C. M., McKenna, A., Cibulskis, K., Kryukov, G., Hodis, E., Lawrence, D. P., Fisher, S., Getz, G., Gabriel, S. B., Carter, S. L., Flaherty, K. T., Wargo, J. A. & Garraway, L. A. MAP Kinase Pathway Alterations in BRAF-Mutant Melanoma Patients with Acquired Resistance to Combined RAF/MEK Inhibition. *Cancer Discov.* **4,** 61–68 (2014).

125.Long, G. V., Fung, C., Menzies, A. M., Pupo, G. M., Carlino, M. S., Hyman, J., Shahheydari, H., Tembe, V., Thompson, J. F., Saw, R. P., Howle, J., Hayward, N. K., Johansson, P., Scolyer, R. A., Kefford, R. F. & Rizos, H. Increased MAPK reactivation in early resistance to dabrafenib/trametinib combination therapy of BRAF-mutant metastatic melanoma. *Nat. Commun.* **5,** 5694 (2014).

126.Aissa, A. F., Islam, A. B. M. M. K., Ariss, M. M., Go, C. C., Rader, A. E., Conrardy, R. D., Gajda, A. M., Rubio-Perez, C., Valyi-Nagy, K., Pasquinelli, M., Feldman, L. E., Green, S. J., Lopez-Bigas, N., Frolov, M. V. & Benevolenskaya, E. V. Single-cell transcriptional changes associated with drug tolerance and response to combination therapies in cancer. *Nat. Commun.* **12,** 1628 (2021).

127.Miles, M. A. & Hawkins, C. J. Mutagenic assessment of chemotherapy and Smac mimetic drugs in cells with defective DNA damage response pathways. *Sci. Rep.* **8,** 14421 (2018).

128.Liu, X., Zou, H., Widlak, P., Garrard, W. & Wang, X. Activation of the Apoptotic Endonuclease DFF40 (Caspase-activated DNase or Nuclease): OLIGOMERIZATION AND DIRECT INTERACTION WITH HISTONE H1*. *J. Biol. Chem.* **274,** 13836–13840 (1999).

129.Meiss, G., Scholz, S. R., Korn, C., Gimadutdinow, O. & Pingoud, A. Identification of functionally relevant histidine residues in the apoptotic nuclease CAD. *Nucleic Acids Res.* **29,** 3901–3909 (2001).

130.Bonilla, X., Parmentier, L., King, B., Bezrukov, F., Kaya, G., Zoete, V., Seplyarskiy, V. B., Sharpe, H. J., McKee, T., Letourneau, A., Ribaux, P. G., Popadin, K., Basset-Seguin, N., Chaabene, R. B., Santoni, F. A., Andrianova, M. A., Guipponi, M., Garieri, M., Verdan, C., Grosdemange, K., Sumara, O., Eilers, M., Aifantis, I., Michielin, O., de Sauvage, F. J., Antonarakis, S. E. & Nikolaev, S. I. Genomic analysis identifies new drivers and progression pathways in skin basal cell carcinoma. *Nat. Genet.* **48,** 398–406 (2016).

131.Negrao, M. V., Raymond, V. M., Lanman, R. B., Robichaux, J. P., He, J., Nilsson, M. B., Ng, P. K. S., Amador, B. E., Roarty, E. B., Nagy, R. J., Banks, K. C., Zhu, V. W., Ng, C., Chae, Y. K., Clarke, J. M., Crawford, J. A., Meric-Bernstam, F., Ignatius Ou, S.-H., Gandara, D. R., Heymach, J. V., Bivona, T. G. & McCoach, C. E. Molecular Landscape of BRAF-Mutant NSCLC Reveals an Association Between Clonality and Driver Mutations and Identifies Targetable Non-V600 Driver Mutations. *J. Thorac. Oncol.* **15,** 1611–1623 (2020).

132.Capparelli, C., Purwin, T. J., Heilman, S. A., Chervoneva, I., McCue, P. A., Berger, A. C., Davies, M. A., Gershenwald, J. E., Krepler, C. & Aplin, A. E. ErbB3 Targeting Enhances the Effects of MEK Inhibitor in Wild-Type BRAF/NRAS Melanoma. *Cancer Res.* **78,** 5680–5693 (2018).

133.Kim, M.H., Kim, J., Hong, H., Lee, S., Lee, J., Jung, E., Kim, J. Actin remodeling confers BRAF inhibitor resistance to melanoma cells through YAP/TAZ activation. *EMBO J.* **35,** 462–478 (2016).

134.Kauko, O., O'Connor, C. M., Kulesskiy, E., Sangodkar, J., Aakula, A., Izadmehr, S., Yetukuri, L., Yadav, B., Padzik, A., Laajala, T. D., Haapaniemi, P., Momeny, M., Varila, T., Ohlmeyer, M., Aittokallio, T., Wennerberg, K., Narla, G. & Westermarck, J. PP2A inhibition is a druggable MEK inhibitor resistance mechanism in KRAS-mutant lung cancer cells. *Sci. Transl. Med.* **10,** eaaq1093 (2018).

135. Lin, A., Giuliano, C. J., Palladino, A., John, K. M., Abramowicz, C., Yuan, M. L., Sausville, E. L., Lukow, D. A., Liu, L., Chait, A. R., Galluzzo, Z. C., Tucker, C. & Sheltzer, J. M. Off-target toxicity is a common mechanism of action of cancer drugs undergoing clinical trials. *Sci. Transl. Med.* **11,** eaaw8412 (2019).

136. Shattuck-Brandt, R. L., Chen, S.-C., Murray, E., Johnson, C. A., Crandall, H., O'Neal, J. F., Al-Rohil, R. N., Nebhan, C. A., Bharti, V., Dahlman, K. B., Ayers, G. D., Yan, C., Kelley, M. C., Kauffmann, R. M., Hooks, M., Grau, A., Johnson, D. B., Vilgelm, A. E. & Richmond, A. Metastatic Melanoma Patient–Derived Xenografts Respond to MDM2 Inhibition as a Single Agent or in Combination with BRAF/MEK Inhibition. *Clin. Cancer Res.* **26,** 3803–3818 (2020).

137. Hu, X., Li, J., Fu, M., Zhao, X. & Wang, W. The JAK/STAT signaling pathway: from bench to clinic. *Signal Transduct. Target. Ther.* **6,** 1–33 (2021).

138. Motwani, M., Pesiridis, S. & Fitzgerald, K. A. DNA sensing by the cGAS–STING pathway in health and disease. *Nat. Rev. Genet.* **20,** 657–674 (2019).

139. Kitajima, S., Ivanova, E., Guo, S., Yoshida, R., Campisi, M., Sundararaman, S. K., Tange, S., Mitsuishi, Y., Thai, T. C., Masuda, S., Piel, B. P., Sholl, L. M., Kirschmeier, P. T., Paweletz, C. P., Watanabe, H., Yajima, M. & Barbie, D. A. Suppression of STING Associated with LKB1 Loss in KRAS-Driven Lung Cancer. *Cancer Discov.* **9,** 34–45 (2019).

140. White, M. J., McArthur, K., Metcalf, D., Lane, R. M., Cambier, J. C., Herold, M. J., van Delft, M. F., Bedoui, S., Lessene, G., Ritchie, M. E., Huang, D. C. S. & Kile, B. T. Apoptotic Caspases Suppress mtDNA-Induced STING-Mediated Type I IFN Production. *Cell* **159,** 1549–1562 (2014).

141. Rongvaux, A., Jackson, R., Harman, C. C. D., Li, T., West, A. P., de Zoete, M. R., Wu, Y., Yordy, B., Lakhani, S. A., Kuan, C.-Y., Taniguchi, T., Shadel, G. S., Chen, Z. J., Iwasaki, A. & Flavell, R. A. Apoptotic Caspases Prevent the Induction of Type I Interferons by Mitochondrial DNA. *Cell* **159,** 1563–1577 (2014).

142. McArthur, K., Whitehead, L. W., Heddleston, J. M., Li, L., Padman, B. S., Oorschot, V., Geoghegan, N. D., Chappaz, S., Davidson, S., San Chin, H., Lane, R. M., Dramicanin, M., Saunders, T. L., Sugiana, C., Lessene, R., Osellame, L. D., Chew, T.-L., Dewson, G., Lazarou, M., Ramm, G., Lessene, G., Ryan, M. T., Rogers, K. L., van Delft, M. F. & Kile, B. T. BAK/BAX macropores facilitate mitochondrial herniation and mtDNA efflux during apoptosis. *Science* **359,** eaao6047 (2018).

143. Bai, X., Fisher, D. E. & Flaherty, K. T. Cell-state dynamics and therapeutic resistance in melanoma from the perspective of MITF and IFNγ pathways. *Nat. Rev. Clin. Oncol.* **16,** 549–562 (2019).

144. Lu, H., Yang, M. & Zhou, Q. Reprogramming transcription after DNA damage: recognition, response, repair, and restart. *Trends Cell Biol.* (2022). doi:10.1016/j.tcb.2022.11.010

145. Andrade-Lima, L. C., Veloso, A., Paulsen, M. T., Menck, C. F. M. & Ljungman, M. DNA repair and recovery of RNA synthesis following exposure to ultraviolet light are delayed in long genes. *Nucleic Acids Res.* **43,** 2744–2756 (2015).

146. Oberdoerffer, P., Michan, S., McVay, M., Mostoslavsky, R., Vann, J., Park, S.-K., Hartlerode, A., Stegmuller, J., Hafner, A., Loerch, P., Wright, S. M., Mills, K. D., Bonni, A., Yankner, B. A., Scully, R., Prolla, T. A., Alt, F. W. & Sinclair, D. A. SIRT1 Redistribution on Chromatin Promotes Genomic Stability but Alters Gene Expression during Aging. *Cell* **135,** 907–918 (2008).

147. Guler, G. D., Tindell, C. A., Pitti, R., Wilson, C., Nichols, K., KaiWai Cheung, T., Kim, H.-J., Wongchenko, M., Yan, Y., Haley, B., Cuellar, T., Webster, J., Alag, N., Hegde, G., Jackson, E., Nance, T. L., Giresi, P. G., Chen, K.-B., Liu, J., Jhunjhunwala, S., Settleman, J., Stephan, J.-P., Arnott, D. & Classon, M. Repression of Stress-Induced LINE-1 Expression Protects Cancer Cell Subpopulations from Lethal Drug Exposure. *Cancer Cell* **32,** 221-237.e13 (2017).

148. Ren, W., Fan, H., Grimm, S. A., Guo, Y., Kim, J. J., Yin, J., Li, L., Petell, C. J., Tan, X.-F., Zhang, Z.-M., Coan, J. P., Gao, L., Cai, L., Detrick, B., Çetin, B., Cui, Q., Strahl, B. D., Gozani, O., Wang, Y., Miller, K. M., O'Leary, S. E., Wade, P. A., Patel, D. J., Wang, G. G. & Song, J. Direct readout of heterochromatic H3K9me3 regulates DNMT1-mediated maintenance DNA methylation. *Proc. Natl. Acad. Sci.* **117,** 18439–18447 (2020).

149. Orth, J. D., Loewer, A., Lahav, G. & Mitchison, T. J. Prolonged mitotic arrest triggers partial activation of apoptosis, resulting in DNA damage and p53 induction. *Mol. Biol. Cell* **23,** 567–576 (2012).

150. Behan, F. M., Iorio, F., Picco, G., Gonçalves, E., Beaver, C. M., Migliardi, G., Santos, R., Rao, Y., Sassi, F., Pinnelli, M., Ansari, R., Harper, S., Jackson, D. A., McRae, R., Pooley, R., Wilkinson, P., van der Meer, D., Dow, D., Buser-Doepner, C., Bertotti, A., Trusolino, L., Stronach, E. A., Saez-Rodriguez, J., Yusa, K. & Garnett, M. J. Prioritization of cancer therapeutic targets using CRISPR–Cas9 screens. *Nature* **568,** 511–516 (2019).

151. Lenoir, W. F., Lim, T. L. & Hart, T. PICKLES: the database of pooled in-vitro CRISPR knockout library essentiality screens. *Nucleic Acids Res.* **46,** D776–D780 (2018).

152. Liu, X., He, Y., Li, F., Huang, Q., Kato, T. A., Hall, R. P. & Li, C.-Y. Caspase-3 Promotes Genetic Instability and Carcinogenesis. *Mol. Cell* **58,** 284–296 (2015).

153. Woo, E.-J., Kim, Y.-G., Kim, M.-S., Han, W.-D., Shin, S., Robinson, H., Park, S.-Y. & Oh, B.-H. Structural Mechanism for Inactivation and Activation of CAD/DFF40 in the Apoptotic Pathway. *Mol. Cell* **14,** 531–539 (2004).

154. Ding, A. X., Sun, G., Argaw, Y. G., Wong, J. O., Easwaran, S. & Montell, D. J. CasExpress reveals widespread and diverse patterns of cell survival of caspase-3 activation during development in vivo. *eLife* **5,** e10936 (2016).

155.Li, F., Huang, Q., Chen, J., Peng, Y., Roop, D., Bedford, J. S. & Li, C.-Y. Apoptotic Cells Activate the "Phoenix Rising" Pathway to Promote Wound Healing and Tissue Regeneration. *Sci. Signal.* **3,** ra13 (2010).

156.Abascal, F., Harvey, L. M. R., Mitchell, E., Lawson, A. R. J., Lensing, S. V., Ellis, P., Russell, A. J. C., Alcantara, R. E., Baez-Ortega, A., Wang, Y., Kwa, E. J., Lee-Six, H., Cagan, A., Coorens, T. H. H., Chapman, M. S., Olafsson, S., Leonard, S., Jones, D., Machado, H. E., Davies, M., Øbro, N. F., Mahubani, K. T., Allinson, K., Gerstung, M., Saeb-Parsy, K., Kent, D. G., Laurenti, E., Stratton, M. R., Rahbari, R., Campbell, P. J., Osborne, R. J. & Martincorena, I. Somatic mutation landscapes at single-molecule resolution. *Nature* **593,** 405–410 (2021).

157.Franken, N. A. P., Rodermond, H. M., Stap, J., Haveman, J. & van Bree, C. Clonogenic assay of cells in vitro. *Nat. Protoc.* **1,** 2315–2319 (2006).

158.Zheng, G. X. Y., Terry, J. M., Belgrader, P., Ryvkin, P., Bent, Z. W., Wilson, R., Ziraldo, S. B., Wheeler, T. D., McDermott, G. P., Zhu, J., Gregory, M. T., Shuga, J., Montesclaros, L., Underwood, J. G., Masquelier, D. A., Nishimura, S. Y., Schnall-Levin, M., Wyatt, P. W., Hindson, C. M., Bharadwaj, R., Wong, A., Ness, K. D., Beppu, L. W., Deeg, H. J., McFarland, C., Loeb, K. R., Valente, W. J., Ericson, N. G., Stevens, E. A., Radich, J. P., Mikkelsen, T. S., Hindson, B. J. & Bielas, J. H. Massively parallel digital transcriptional profiling of single cells. *Nat. Commun.* **8,** 14049 (2017).

159.Satija, R., Farrell, J. A., Gennert, D., Schier, A. F. & Regev, A. Spatial reconstruction of single-cell gene expression data. *Nat. Biotechnol.* **33,** 495–502 (2015).

160.Butler, A., Hoffman, P., Smibert, P., Papalexi, E. & Satija, R. Integrating single-cell transcriptomic data across different conditions, technologies, and species. *Nat. Biotechnol.* **36,** 411–420 (2018).

161.Stuart, T., Butler, A., Hoffman, P., Hafemeister, C., Papalexi, E., Mauck, W. M., Hao, Y., Stoeckius, M., Smibert, P. & Satija, R. Comprehensive Integration of Single-Cell Data. *Cell* **177,** 1888-1902.e21 (2019).

162.Kowalczyk, M. S., Tirosh, I., Heckl, D., Rao, T. N., Dixit, A., Haas, B. J., Schneider, R. K., Wagers, A. J., Ebert, B. L. & Regev, A. Single-cell RNA-seq reveals changes in cell cycle and differentiation programs upon aging of hematopoietic stem cells. *Genome Res.* **25,** 1860–1872 (2015).

163.Aibar, S., González-Blas, C. B., Moerman, T., Huynh-Thu, V. A., Imrichova, H., Hulselmans, G., Rambow, F., Marine, J.-C., Geurts, P., Aerts, J., van den Oord, J., Atak, Z. K., Wouters, J. & Aerts, S. SCENIC: single-cell regulatory network inference and clustering. *Nat. Methods* **14,** 1083–1086 (2017).

164.Yu, G., Wang, L.-G., Han, Y. & He, Q.-Y. clusterProfiler: an R Package for Comparing Biological Themes Among Gene Clusters. *OMICS J. Integr. Biol.* **16,** 284–287 (2012).

165. Villalobos-Ortiz, M., Ryan, J., Mashaka, T. N., Opferman, J. T. & Letai, A. BH3 profiling discriminates on-target small molecule BH3 mimetics from putative mimetics. *Cell Death Differ.* **27,** 999–1007 (2020).

166. McKenna, A., Hanna, M., Banks, E., Sivachenko, A., Cibulskis, K., Kernytsky, A., Garimella, K., Altshuler, D., Gabriel, S., Daly, M. & DePristo, M. A. The Genome Analysis Toolkit: A MapReduce framework for analyzing next-generation DNA sequencing data. *Genome Res.* **20,** 1297–1303 (2010).

167. DePristo, M. A., Banks, E., Poplin, R., Garimella, K. V., Maguire, J. R., Hartl, C., Philippakis, A. A., del Angel, G., Rivas, M. A., Hanna, M., McKenna, A., Fennell, T. J., Kernytsky, A. M., Sivachenko, A. Y., Cibulskis, K., Gabriel, S. B., Altshuler, D. & Daly, M. J. A framework for variation discovery and genotyping using next-generation DNA sequencing data. *Nat. Genet.* **43,** 491–498 (2011).

168. Auwera, G. A. V. der & O'Connor, B. D. *Genomics in the Cloud: Using Docker, GATK, and WDL in Terra*. (O'Reilly Media, Inc., 2020).

169. Li, H. & Durbin, R. Fast and accurate short read alignment with Burrows–Wheeler transform. *Bioinformatics* **25,** 1754–1760 (2009).

170. Mayakonda, A., Lin, D.-C., Assenov, Y., Plass, C. & Koeffler, H. P. Maftools: efficient and comprehensive analysis of somatic variants in cancer. *Genome Res.* **28,** 1747–1756 (2018).

171. Fenech, M. Cytokinesis-block micronucleus cytome assay. *Nat. Protoc.* **2,** 1084–1104 (2007).

172. Tang, Z., Li, C., Kang, B., Gao, G., Li, C. & Zhang, Z. GEPIA: a web server for cancer and normal gene expression profiling and interactive analyses. *Nucleic Acids Res.* **45,** W98–W102 (2017).

173. Hart, T. & Moffat, J. BAGEL: a computational framework for identifying essential genes from pooled library screens. *BMC Bioinformatics* **17,** 164 (2016).

174. Kim, E. & Hart, T. Improved analysis of CRISPR fitness screens and reduced off-target effects with the BAGEL2 gene essentiality classifier. *Genome Med.* **13,** 2 (2021).

175. Cao, K., Riley, J. S., Heilig, R., Montes-Gómez, A. E., Vringer, E., Berthenet, K., Cloix, C., Elmasry, Y., Spiller, D. G., Ichim, G., Campbell, K. J., Gilmore, A. P. & Tait, S. W. G. Mitochondrial dynamics regulate genome stability via control of caspase-dependent DNA damage. *Dev. Cell* **57,** 1211-1225.e6 (2022).

176. Lechardeur, D., Drzymala, L., Sharma, M., Zylka, D., Kinach, R., Pacia, J., Hicks, C., Usmani, N., Rommens, J. M. & Lukacs, G. L. Determinants of the Nuclear Localization of the Heterodimeric DNA Fragmentation Factor (Icad/Cad). *J. Cell Biol.* **150,** 321–334 (2000).

177. Samejima, K. & Earnshaw, W. C. Differential Localization of ICAD-L and ICAD-S in Cells Due to Removal of a C-Terminal NLS from ICAD-L by Alternative Splicing. *Exp. Cell Res.* **255,** 314–320 (2000).

178. Yang, J.-H., Hayano, M., Griffin, P. T., Amorim, J. A., Bonkowski, M. S., Apostolides, J. K., Salfati, E. L., Blanchette, M., Munding, E. M., Bhakta, M., Chew, Y. C., Guo, W., Yang, X., Maybury-Lewis, S., Tian, X., Ross, J. M., Coppotelli, G., Meer, M. V., Rogers-Hammond, R., Vera, D. L., Lu, Y. R., Pippin, J. W., Creswell, M. L., Dou, Z., Xu, C., Mitchell, S. J., Das, A., O'Connell, B. L., Thakur, S., Kane, A. E., Su, Q., Mohri, Y., Nishimura, E. K., Schaevitz, L., Garg, N., Balta, A.-M., Rego, M. A., Gregory-Ksander, M., Jakobs, T. C., Zhong, L., Wakimoto, H., El Andari, J., Grimm, D., Mostoslavsky, R., Wagers, A. J., Tsubota, K., Bonasera, S. J., Palmeira, C. M., Seidman, J. G., Seidman, C. E., Wolf, N. S., Kreiling, J. A., Sedivy, J. M., Murphy, G. F., Green, R. E., Garcia, B. A., Berger, S. L., Oberdoerffer, P., Shankland, S. J., Gladyshev, V. N., Ksander, B. R., Pfenning, A. R., Rajman, L. A. & Sinclair, D. A. Loss of epigenetic information as a cause of mammalian aging. *Cell* **186,** 305-326.e27 (2023).

179. Cagan, A., Baez-Ortega, A., Brzozowska, N., Abascal, F., Coorens, T. H. H., Sanders, M. A., Lawson, A. R. J., Harvey, L. M. R., Bhosle, S., Jones, D., Alcantara, R. E., Butler, T. M., Hooks, Y., Roberts, K., Anderson, E., Lunn, S., Flach, E., Spiro, S., Januszczak, I., Wrigglesworth, E., Jenkins, H., Dallas, T., Masters, N., Perkins, M. W., Deaville, R., Druce, M., Bogeska, R., Milsom, M. D., Neumann, B., Gorman, F., Constantino-Casas, F., Peachey, L., Bochynska, D., Smith, E. S. J., Gerstung, M., Campbell, P. J., Murchison, E. P., Stratton, M. R. & Martincorena, I. Somatic mutation rates scale with lifespan across mammals. *Nature* **604,** 517–524 (2022).

180. Robinson, P. S., Coorens, T. H. H., Palles, C., Mitchell, E., Abascal, F., Olafsson, S., Lee, B. C. H., Lawson, A. R. J., Lee-Six, H., Moore, L., Sanders, M. A., Hewinson, J., Martin, L., Pinna, C. M. A., Galavotti, S., Rahbari, R., Campbell, P. J., Martincorena, I., Tomlinson, I. & Stratton, M. R. Increased somatic mutation burdens in normal human cells due to defective DNA polymerases. *Nat. Genet.* **53,** 1434–1442 (2021).

181. Myung, N.-H., Zhu, X., Kruman, I. I., Castellani, R. J., Petersen, R. B., Siedlak, S. L., Perry, G., Smith, M. A. & Lee, H. Evidence of DNA damage in Alzheimer disease: phosphorylation of histone H2AX in astrocytes. *AGE* **30,** 209–215 (2008).

182. Kolobov, V. V., Davydova, T. V., Zakharova, I. A., Gorbatov, V. Yu. & Fomina, V. G. Glutamate antibodies repress expression of Dffb gene in brain of rats in experimental Alzheimer's disease. *Mol. Biol.* **46,** 678–686 (2012).

183. Ni, A., Sethi, A. & Initiative, for the A. D. N. Functional Genetic Biomarkers of Alzheimer's Disease and Gene Expression from Peripheral Blood. 2021.01.15.426891 Preprint at https://doi.org/10.1101/2021.01.15.426891 (2021)